

UNCLASSIFIED

AD NUMBER
AD813407
NEW LIMITATION CHANGE
TO Approved for public release, distribution unlimited
FROM Distribution authorized to U.S. Gov't. agencies and their contractors; Critical Technology; APR 1967. Other requests shall be referred to Physical Research Lab., Edgewood Arsenal, MD.
AUTHORITY
USAEA ltr, 22 Dec 1971

THIS PAGE IS UNCLASSIFIED

AD 813407

AD

SRI Project PAU-4900

# DEVELOPMENT OF AEROSOL CHARGE ANALYZER

Special Technical Report No. 11

By

C. E. LAPPLE, D. E. BLAKE, AND G. L. PRESSMAN

APRIL 1967



DDC  
RECEIVED  
MAY 9 1967  
B

Dissemination Research Department  
PHYSICAL RESEARCH LABORATORY  
Edgewood Arsenal  
Edgewood Arsenal, Maryland 21010

Contract DA-18-035-AMC-122(A)

STANFORD RESEARCH INSTITUTE  
Menlo Park, California

#### DISTRIBUTION STATEMENT

This document is subject to special export controls and each transmittal to foreign governments or foreign nationals may be made only with prior approval of the CO, Edgewood Arsenal, ATTN: SMUEA-TSTI-T, Edgewood Arsenal, Maryland, 21010.

#### DISCLAIMER

The findings in this report are not to be construed as an official Department of the Army position unless so designated by other authorized documents.

#### DISPOSITION

Destroy this report when no longer needed. Do not return it to the originator.

SRI Project PAU-4900

## DEVELOPMENT OF AEROSOL CHARGE ANALYZER

Special Technical Report No. 11

By

C. E. LAPPLE, D. E. BLAKE, AND G. L. PRESSMAN

APRIL 1967

Dissemination Research Department  
PHYSICAL RESEARCH LABORATORY  
Edgewood Arsenal  
Edgewood Arsenal, Maryland 21010

Contract DA-18-035-AMC-122(A)  
Task 1B522301A08101

STANFORD RESEARCH INSTITUTE  
Menlo Park, California

### Distribution Statement

This document is subject to special export controls and each transmittal to foreign governments or foreign nationals may be made only with prior approval of the CO, Edgewood Arsenal, ATTN: SMUEA-TSTI-T, Edgewood Arsenal, Maryland, 21010.

## FOREWORD

The work described in this report was authorized under Task 1B522301A08101, "Dissemination Investigations of Liquid and Solid Agents (U)." The work was started in July 1965 and completed in September 1966.

Reproduction of this document in whole or in part is prohibited except with permission of the CO, Edgewood Arsenal, ATTN: SMUEA-RPR, Edgewood Arsenal, Maryland 21010; however, Defense Documentation Center is authorized to reproduce the document for US Government purposes.

The information in this document has not been cleared for release to the general public.

The authors wish to acknowledge the able assistance of P. M. Newgard, who developed the mechanical design details of the probe assembly, and of B. A. Wolfe, for his prompt and capable handling of most of the mechanical fabrication used in this study.

## DIGEST

---

A technique has been developed for measuring both the electrical mobility distribution of an aerosol and the average effective size at each mobility level. With this technique, an aerosol is passed through a purifier and a narrow mobility channel (1.5 in. spacing between collection electrodes, 10 in. wide and 15 in. long). The purifier removes charged particles from all but a thin central stream that enters the mobility chamber halfway between the electrodes. Particles are deposited on an insulating surface according to their mobility. The total charge distribution on the walls is determined by a special scanning probe. The mass distribution is determined by chemical or colorimetric analysis. Tests carried out to determine the mobility distribution of a uranine aerosol generated by atomizing and evaporating a dilute water solution yielded reasonably consistent results. Although no absolute basis of assessment was available, the results were consistent with expected magnitudes. Average particle diameter (volume-to-diameter mean) was 0.8 micron, and particle charge levels ranged from 0.05 to 1 volt/micron specific particle surface gradient. Remaining problem areas are listed and suggestions are given for improving the technique and extending its usefulness.

## CONTENTS

<u>SECTION</u>	<u>PAGE</u>
I INTRODUCTION. . . . .	9
II SUMMARY AND CONCLUSIONS . . . . .	11
III RECOMMENDATIONS FOR FURTHER DEVELOPMENT . . . . .	13
IV DESCRIPTION OF MEASUREMENT TECHNIQUE. . . . .	15
V REPRESENTATION OF DISTRIBUTION DATA . . . . .	19
VI EXPERIMENTAL EQUIPMENT AND PROCEDURES . . . . .	23
A. Aerosol Generation System . . . . .	23
B. Mobility Channel System . . . . .	24
C. Operating Procedures. . . . .	30
D. Preliminary Evaluation. . . . .	34
VII EXPERIMENTAL RESULTS. . . . .	37
A. Material Balances . . . . .	38
B. Aerosol Characteristics . . . . .	42
VIII DISCUSSION OF RESULTS . . . . .	47
REFERENCES. . . . .	101
NOMENCLATURE. . . . .	103
APPENDIX A SIGNIFICANCE OF AVERAGE DIAMETER MEASURED BY MOBILITY CHANNEL. . . . .	109
APPENDIX B DEFINITION OF AND INTERRELATIONSHIP BETWEEN MEAN DIAMETERS. . . . .	113
APPENDIX C BASIC PERFORMANCE RELATIONSHIPS . . . . .	117
APPENDIX D FIELD INTENSITY FOR IDEAL MOBILITY CHANNEL. . . . .	133

CONTENTS (Concluded)

<u>SECTION</u>	<u>PAGE</u>
APPENDIX E CAPACITANCE OF CHARGE ANALYZER . . . . .	137
DISTRIBUTION LIST. . . . .	143
DOCUMENT CONTROL DATA - R&D (DD FORM 1473) . . . . .	145

LIST OF ILLUSTRATIONS

<u>FIGURE</u>	<u>PAGE</u>
1 Form of a Complete Curve for Expressing Both Size and Electrical Mobility (or Charge) Distribution of Aerosols or Powders . . . . .	55
2 Principle of Operation of Mobility Channel . . . . .	56
3 Schematic Arrangement of Experimental Equipment. . . . .	57
4 Photographs of Equipment . . . . .	59
5 Equipment Details. . . . .	71
6 Analysis of Tape Deposits. . . . .	79
7 Mobility Distribution of Aerosol . . . . .	83
8 Illustrative Probe Scan Record . . . . .	87
C-1 Diagram Illustrating Mobility Channel Operation. . . . .	127
C-2 Details of Apparatus Arrangements Evaluated for Field Distribution . . . . .	128
C-3 Relationship between Mobility and Position on Electrode . . . . .	129
C-4 Relationship between Mobility and Position on Electrode for Arrangement III . . . . .	130
D-1 Diagram Illustrating Geometry of and Electrical Conditions in Mobility Channel. . . . .	136
E-1 Diagram of Probe Measurement System. . . . .	142
E-2 Generalized Capacitance Diagram. . . . .	142
E-3 Modified Circuit . . . . .	142
E-4 Final Reduced Circuit. . . . .	142

LIST OF TABLES

<u>TABLE</u>	<u>PAGE</u>
I Summary of Mobilities Used in Analysis of Tape Deposits. . . . .	89
II Summary of Experimental Data . . . . .	91
III Details of Tape Deposits for Runs A1-A3 and B1-B3. . . . .	95
IV Specifications for Major Units of Commercial Equipment Used. . . . .	97
V Evaluation of Tape Deposit Data. . . . .	98
VI Summary of Aerosol Mobility Distribution Data . . . . .	99
B-I Value of $e\gamma \ln^2 \sigma$ as a Function of $J$ and $\gamma$ . . . . .	115
B-II Types and Definitions of Various Mean Diameters . . . . .	115
C-I Calculated Trajectories of Particles for Cases IIIa and IIIb from Graphical Evaluations. . . . .	131

## I INTRODUCTION

To assess the role of electrostatics in aerosol dissemination, it is necessary to have a means for characterizing the electrostatic properties of aerosols. To describe those properties completely calls for the evaluation of a distribution function of the form shown in Fig. 1, or its equivalent. The literature is replete with techniques for measuring electrostatic properties; however, all provide only a portion of the data necessary for formulating a complete distribution and most are either difficult to apply or involve intrinsic uncertainties or limitations. The available techniques are summarized and discussed in a previous report (Lapple, 1965), in which the development of a rapid and reliable technique is recommended.

The purpose of this investigation was to evaluate the concept for a new instrument to characterize electrostatic properties of aerosols. This concept would (1) incorporate the best features of available techniques, (2) incorporate novel features to extend the scope of the assessment without undue complexity, and (3) be readily adaptable as a tool for field assessment.

## II SUMMARY AND CONCLUSIONS

An instrument and technique was developed for measuring both the electrical mobility distribution of an aerosol and the average particle diameter (volume-to-diameter mean;  $\bar{D}_{31}$ ) at each mobility level. The aerosol is first passed through a "purifier" in which the charged particles from all but a thin central stream are removed by an electrostatic field. The particles in the central stream are then classified by sign and deposited according to mobility along two polystyrene electrodes in a mobility channel. The deposited particles are first scanned by a novel probe device to establish their charge level and then analyzed chemically or optically to establish mass distribution. These two sets of data in conjunction with the known mobility-position relationship are used to establish the average diameter at each mobility level.

To assess the usefulness of the technique, it was used to measure the charge distribution in an aerosol generated by atomizing and evaporating a 2 wt% solution of uranine dye in water. It was found that positive and negative particles were present in nominally equal amounts with about the same mobility distribution and had an average effective diameter (volume-to-diameter mean size) of 0.8 micron. The size was consistent with expectations from previous work with a similar aerosol. The measured charge levels, expressed as specific particle surface gradients, ranged from 0.05 to 1 volt/ $\mu$ , which corresponds to a charge level in the atomized drop before evaporation of 0.002 to 0.05 volt/ $\mu$ . This corresponds to the range of values reported in the literature for charge levels produced by atomization.

Although intrinsic measurements were considerably better, the data showed spreads averaging  $\pm 20\%$ . Negatively charged particles were slightly more prevalent than the positive charged ones and had a 50% greater charge. Correspondingly, the average diameter of the negative particles was some 15% smaller than for the positive particles. A few

anomalous results were also found. Unfortunately, there are no absolute means available for assessing the present techniques. The spread in the data could reflect reproducibility limitations of the present equipment or actual variations in the test aerosol. There are shortcomings in the purifier performance, and some obvious steps are presented for alleviating them. Actual variations in the test aerosol may have been due to variation of some conditions during generation. Thus, although the technique and equipment for measuring aerosol charge distribution are shown to be operational, certain obvious modifications should be made and proved to improve and extend its usefulness, indicated in Section III.

### III RECOMMENDATIONS FOR FURTHER DEVELOPMENT

Although the general usefulness of the aerosol charge measuring technique has been demonstrated, certain improvements in the technique are indicated. A few other measurements are suggested to better bracket the limitations and to extend the usefulness of the technique. These are discussed below.

1. The collection efficiency of the purifier should be increased. This can be done both (a) by lengthening the purifier plates threefold, and (b) by providing for corona charging by shortening the charged electrodes 1 in. and installing a 50-micron diameter wire about 1/2-in. downstream from the edge of the grounded electrodes but in the plane of the charged electrodes. This would call for a total of six such wires. It is also suggested that the purifier plates be coated with a thin film of nonconductive plastic. This may not be necessary with adhesive aerosol particles but could be with coarser conductive dry aerosol particles. It might also raise the purifier collection efficiency by permitting operation at higher potential differences.
2. The calibration capacitance of the probe system should be checked by direct measurements of a known charge. The known charge can be obtained by scribing vertical insulating lines on a metal-vapor coated electrode that can then be charged at a known spacing from a grounded electrode by means of a battery. This electrode would then be used in place of the polystyrene collection electrode and scanned with the probe.
3. The mobility channel should be operated without aerosol, to obtain a measure of stray charges that can be picked up from the compressed air stream. This has never been done.
4. The channel should be operated at higher capacities to minimize disturbing convective stream influences. It is indicated that the present channel could be operated at capacities up to 6 cfm before disruptive turbulence would ensue. Present tests have only gone as high as 1.2 cfm. At the higher capacities, the channel could handle aerosol particles up to 30 microns diameter, where at present capacities it is restricted to the range under 15 microns.

5. The reproducibility of the technique should be established more definitely and the question of whether the present scatter is in the technique or in the aerosol itself should be resolved. Any further operations with an aerosol generated by spraying uranine solution should be made at lower spray rates to minimize any aerosol variation problems associated with temperature and humidity changes. The spray head should also be grounded to avoid spurious induced electrostatic charges.
6. If a chart readout of the probe traverse is desired, the traverse speed should be adjusted to accommodate the response time of the electrometer. In the present system, the traverse speed used (16 in./min), was somewhat too great and because of meter overshoot, the probe had to be stopped to ensure a reliable reading at a specific location.

#### IV DESCRIPTION OF MEASUREMENT TECHNIQUE

If an aerosol flowing in a channel is exposed to a lateral electrostatic field, the aerosol particles will receive lateral velocity components proportional to their electrostatic mobility. These lateral velocity components will cause the particles to migrate toward the channel walls and deposit on them. The point on the wall where a given particle deposits will depend on its initial position in the channel and its electrostatic mobility. If the channel wall is a conductor, the particle may not only lose its charge on being deposited but may acquire a reverse charge due to the impressed field intensity at the collection surface. This reverse sign can cause the particle to leave the surface again and migrate toward the opposite wall. The extent to which this can happen depends on the electrical conductivity of the aerosol particle and the magnitude of the adhesive force between the particle and the surface. By covering the conductive channel walls with an insulator, however, the aerosol particles can be exposed to an electrostatic field but cannot lose their charge on being deposited.

The essential details of the proposed techniques for recovering mobility of aerosol particles are illustrated by Fig. 2. By confining the entering aerosol to a narrow central stream, all the aerosol particles start at essentially the same distance from the electrode walls. The negatively charged particles will then migrate toward the positive electrodes while the positive particles migrate toward the negative electrodes. If the electrode is covered with an insulating surface, a particle will deposit and remain deposited at a downstream position that is inversely proportional to the electrostatic mobility of the particle. The aerosol particles will, therefore, be classified not only by sign of charge but by magnitude of their mobility.

To achieve quantitative classification, it is necessary for the entire flow across the channel width to be laminar and of known (preferably uniform) velocity profile. To avoid mixing or turbulence, it is necessary

for the central narrow aerosol stream to be surrounded by clean gas entering at substantially the same velocity as the aerosol stream. The achievement of this velocity balancing poses a major problem. Because of the possible effect on the aerosol particles and alteration of them, the usual type of meter cannot be used to meter the aerosol stream. The need for metering and balancing two stream velocities can be avoided by admitting the aerosol stream over the entire channel width and removing all aerosol particles from the outer portion of the stream before the stream reaches the active mobility channel electrodes. This can be done by passing the aerosol through a passage containing a large number of vertical, equally spaced partitions, with the two central partitions grounded and all other partitions alternately charged and grounded. If such a channel is made long enough, charged aerosol particles in all but the central channel will be caused to deposit on the vertical partitions. To guard against redispersion of nonadhesive conductive particles, the charged partition plates should be covered with an insulating surface. The technique is basically equivalent to that used by Sergiyeva (1958) to maintain a constant moisture saturation in the clean shielding air.

In this report, the device for removing aerosol particles from the outer portions of the aerosol stream has been termed a "purifier." This combination of purifier and mobility channel represents essentially a combination of techniques previously reported by Gillespie and Langstroth (1952) and modified by Sergiyeva (1958). This combination represents a means for measuring mobility distribution of an aerosol. This distribution is determined by measuring the quantity of deposit as a function of position on the wall. The full theory involved in the operation of the mobility channel is discussed in Appendixes A, C, and D.

Since mobility is a function of both particle size and charge (in addition to ambient and operating conditions), such a measurement will not yield any information regarding either of these characteristics alone. However, if the total charge of the wall deposit is measured as a function of position in addition to total mass, additional information can be obtained regarding the average properties of the deposit. This is obtained from the average measured charge of the deposit and the known

mobility corresponding to the position of the deposit. Thus, by this separate charge measurement a measure of the average size and charge level of material can be obtained at each mobility level.

In the present development, a probe device has been designed and developed to measure the charge distribution on the channel walls. The probe consisted of two long, narrow, flat metal electrodes. The two electrodes were mounted back to back with a grounded wall between them and surrounded on the sides by a grounded shield. The outer exposed faces of each electrode faced the two mobility channel walls. The probe was inserted into the mobility channel after a run and mechanically allowed to traverse the entire length of the mobility channel. During the charge measurement, the metal mobility channel electrodes behind each plastic collection electrode were grounded. The probes were grounded while surrounded by grounded surfaces just before a traverse commenced to ensure that they were electrically neutral. During the traverse each probe was floating electrically and connected to an electrometer. It read, therefore, the potential induced on it by the presence of charges on the plastic collection electrode it faced. The full theory of the probe performance characteristics is discussed in Appendix E.

If, instead of using the purifier, the aerosol stream were admitted over the entire width of the mobility channel, a classification of particles by electrical mobility would still take place. However, at each position on the wall there would be an overlap of particles of different mobility. Particles of low mobility starting close to the wall would deposit at the same point as particles of higher mobility starting at a greater distance from the wall. It can be shown mathematically that it is possible to obtain a mobility distribution from such overlapping deposits. To do so, however, requires a process of differentiation (or curve-tangent intercepts) similar to the procedure necessary in interpreting results from size analysis techniques, such as the Oden sedimentation balance. It would, however, be much more difficult to assign any physical significance to the average effective particle size obtained at each position from the charge probe data. In fact, the average effective size so measured would be a function of the overall aerosol distribution, not just of the distribution within a given mobility range.

## V REPRESENTATION OF DISTRIBUTION DATA

Figure 1 shows a format for presenting a complete description of both size and charge distribution data on both a cumulative and a frequency basis. Charge has been expressed in terms of electrical mobility (a combined function of charge and size). However, other functions of charge (charge alone, specific particle surface gradient, specific particle surface potential, etc.) could be used in place of the mobility coordinate to yield an alternative method of presentation. Any of these forms would be derivable from the format shown in the figure, or vice versa. To obtain a complete description, the complete family of curves (or a surface) is required as shown.

The conventional size distribution curve ignores charge distribution. In Fig. 1, the conventional cumulative size distribution curve would be given by the intercept of the surface with the plane corresponding to infinite positive electrical particle mobility. This intercept is so labeled in the figure. The conventional frequency distribution cannot be shown directly in this figure. The conventional frequency curve corresponds to a plot of  $(d\varphi/dD_p)_{\beta=\infty}$  vs  $D_p$  (or involving any other function of  $D_p$ ). It can be obtained by differentiating the intercept corresponding to the conventional cumulative size distribution curve at various size levels or by integrating the frequency curve in Fig. 1 at several given size levels,

$$(d\varphi/dD_p)_{\beta=\infty} = \int_{-\infty}^{+\infty} (\partial^2 \varphi / \partial D_p \partial \beta_{pe})_{D_p} d\beta_{pe} \quad (1)$$

This will give the frequency at the given size level. Repeat integrations will give the frequency at other size levels. To convert the frequency curve in Fig. 1 to the conventional cumulative size distribution curve would require a double integration,

$$(\varphi)_{\beta=\infty} = \int_0^{D_p} dD_p \int_{-\infty}^{+\infty} (\partial^2 \varphi / \partial D_p \partial \beta_{pe})_{D_p} d\beta_{pe} \quad (2)$$

This mobility (or charge) distribution curve is given by the intercept of the surface with the plane corresponding to infinite particle size. The corresponding frequency distribution for charge alone could be obtained by differentiating this curve to obtain  $(d\varphi/d\beta_{pe})_{D_p=\infty}$  at various mobility levels or by integrating the general frequency curve at several given mobility levels.

$$(d\varphi/d\beta_{pe})_{D_p=\infty} = \int_0^{\infty} (\partial^2 \varphi / \partial D_p \partial \beta_{pe})_{\beta_{pe}} dD_p \quad (3)$$

The measurement device developed in this study will not by itself give the complete distribution depicted in Fig. 1. It will give the mobility distribution (the intercept of the plane corresponding to  $D_p = \infty$  with the surface). This is obtained directly from the measured mass distribution along the collection electrodes. In addition, the measured values of charge distribution along the electrode will yield a measure of the average charge-to-mass ratio,  $R_{cav}$ , at each mobility level. Alternatively, this can also be expressed as an average effective particle diameter at each mobility level. As proved in Appendix A, this average particle diameter at each mobility level is the average defined by

$$D_{pae} = \left[ \frac{\sum_0^{n_{p\beta}} D_p^3 dn_{p\beta}}{\sum_0^{n_{p\beta}} D_p (k_{Cae}/k_C) dn_{p\beta}} \right]^{1/2} \quad (4)$$

For particles large compared to the mean free path of the gas molecules (i.e.,  $D_p \gg 0.1 \mu$  at atmospheric conditions),  $D_{pae}$  is identical with  $\bar{D}_{31}$  (see Appendix B for conventions in defining mean diameters). For particles that are small compared to the mean free path ( $D_p \ll 0.1 \mu$  at

atmospheric condition),  $D_{pae}$  is identical with  $\bar{D}_{32}$  or the Sauter diameter. In general the Sauter diameter is finer than the mass median diameter but coarser than the volume-to-diameter mean,  $\bar{D}_{31}$ . Appendix B gives bases for relating these various mean diameters to each other and to both the number and mass median diameters.

If the complete form of Fig. 1 were desired, it would be necessary to measure the size distribution of the material collected at each mobility level (i.e., collected on each tape) instead of simply an average size at each level.

## VI EXPERIMENTAL EQUIPMENT AND PROCEDURES

This section describes the arrangement and use of all major pieces of equipment. A schematic arrangement of all the experimental equipment is shown in Fig. 3. Figure 4 presents photographs of the various assemblies and elements, while Fig. 5 presents details. Table IV gives specifications of the major units of commercial equipment employed.

Changes were made to the equipment during the program. Altogether there were three significantly different arrangements of the experimental apparatus. These are all illustrated in Fig. 4. The subsequent sections will point out the nature and reason for the differences. The final arrangement is illustrated by Figs. 3 and 4d.

### A. Aerosol Generation System

To assess the performance characteristics of the charge analyzing equipment, it was necessary to provide a source of charged aerosol. This was done by pneumatically spraying a dilute dye solution into a large aerosol (2-ft x 2-ft x 8-ft-high) chamber, as shown in Figs. 3 and 4a. The chamber served as a holdup device (1) in which the water could evaporate from the droplets, (2) in which the droplets could mix with air to give a uniform aerosol cloud, and (3) from which aerosol samples could be withdrawn through the charge analyzing equipment once equilibrium conditions were established in the aerosol chamber.

From the aerosol chamber the aerosol was exhausted to the atmosphere at the bottom of the chamber through a water scrubber that minimized contamination of the room with aerosol and provided material-balance data. The scrubber originally consisted of a high-pressure (40 psig) water jet pointed into a 2-in. pipe equipped with a gate valve downstream. Because of subsequent problems with material balances, the water ejector was replaced with a compressed air ejector to provide more intensive scrubbing contact. The air nozzle was directed into a 1/2-in. pipe and water was admitted with the induced air. Although never

established in detail it is likely that the original water scrubber was over 90 percent effective in removing aerosol, since early material balance problems were subsequently traced to another factor. The compressed-air-jet scrubber efficiency was measured as 95 to 97%. In either case, the jet on the scrubber would put the aerosol chamber under vacuum unless the gate valve in the discharge line was throttled. In all runs, the pressure in the aerosol chamber was maintained above atmospheric by adjustment of that valve and the air or water rate. The aerosol chamber pressure never exceeded atmospheric pressure by more than 1 cm xylene during a run and normally was maintained at 2 to 3 mm xylene.

Although, as shown in Fig. 4a, the aerosol chamber was equipped to permit admission of additional dilution air from the room, this was never done during normal operation. The only air entering the aerosol chamber was the 8.5 scfm used for atomization.

The aerosol was generated by pumping a 2.00-weight-percent water solution of uranine dye (technical grade of disodium fluorescein) through a rotameter into a pneumatic atomizing nozzle. In all runs, the rotameter was operated at the same flow meter reading, with a nominal flow rate of 3 cc/min. Because the flow meter was sensitive to ambient temperature the actual flow rate was taken from a calibration curve that showed a flow rate variation with temperature of  $1.5\%/^{\circ}\text{C}$ , the rate increasing with temperature. Details of this liquid feed system are shown in Figs 4j, 4k, 5a, and 5b.

It was normal practice to maintain liquid and air feed to the aerosol chamber at constant conditions for a period of at least 30 minutes before making any measurements in the mobility channel system. This was to ensure that equilibrium was established in the aerosol chamber.

#### B. Mobility Channel System

The outlet from the aerosol chamber to the mobility channel system was a 6-in. x 15-in. opening in the side of the aerosol chamber. On the inside of the aerosol chamber this opening was covered by a hood as shown in Fig. 4j, to minimize the possibility of impinging high velocity

air jets on portions of the opening and to prevent aerosol chamber wash water from entering the mobility channel system. This hood was installed in the last two equipment arrangements used.

The original arrangement of the mobility channel system is shown in Figs. 4a and 4b. The hooded aerosol chamber outlet port was connected to the mobility channel through a duct of 6-in. X 15-in. cross section, containing a honeycomb-type flow straightener at the inlet end. The purifier shown in Fig. 4e was mounted between the mobility channel and this aerosol chamber exhaust duct with the upstream flared end of the purifier projecting into the exhaust duct.

The mobility chamber discharged into a plenum chamber containing a bag filter. From here, the gases were led in turn through a control valve, a critical flow metering orifice, and a vacuum pump.

After early operating experiences, this arrangement underwent two stages of significant change. In the first stage, shown in Fig. 4c, a horizontal wooden channel 1 in. wide, 15 in. high, and 3 ft long was placed between the aerosol chamber exhaust port and the 6-in. X 15-in. duct. This was added to provide a means for bringing the sampled gas up to room temperature and to thermally insulate the aerosol chamber walls (which become cold due to water evaporation) from the mobility channel walls to minimize the thermal convection currents that had been observed previously. In addition the bag filter was replaced with two bubblers in series (1/10-in. and 1/8-in. nozzle diameter and operated at a combined pressure drop of some 9 in. Hg), and the mobility channel was thermally insulated during any runs with a covering of B-glass fiber.

The aerosol was observed with a strong collimated light beam as it traveled down the mobility channel with the purifier energized and the mobility channel electrodes grounded. Once all the system leaks were eliminated, a thin aerosol stream could be seen clearly moving down the center of the mobility channel. This stream was almost undisturbed at the inlet end of the mobility channel, but by the time it reached the downstream end of the channel the top one-third to half the aerosol had

disappeared. There was also some wavering of the stream that could be exaggerated by touching or tapping the channel walls. This would indicate the presence of a convective cell circulating upward at the mobility channel walls and downward at the center. Although there were times when the aerosol stream remained confined as a narrow central stream, its behavior was often erratic, and the disappearance of the top of the stream toward the downstream end was always present.

This led to the decision to go to the final modification shown in Fig. 4d. The major change was to replace the horizontal wooden channel with a vertical wooden channel. This vertical channel first directed the gases downward, then upward, as illustrated in Fig. 3, so that the mobility channel could be located at a reasonably accessible height. The vertical channel had a 1-1/2-in. by 15-in. cross section where it was connected to the aerosol chamber. The subsequent cross sections were 1-1/2 in. by 11 in., and two curved splitters were located at each turning point to minimize flow distortion. In this modification, the purifier was connected directly to the wooden channel.

In this final arrangement, a guard plate assembly (discussed later) was also added to the inlet of the mobility channel and required an additional 4-in. length of 1-1/2-in. x 10-in. aluminum channel to be installed between the purifier and the mobility channel as shown in Fig. 4k. Also a filter-paper holder followed by a cleanup bubbler was used downstream of the mobility channel in place of the two bubblers previously used. In this final arrangement, the air-operated scrubber was used on the aerosol chamber exhaust gases. All quantitative data reported in Tables II and III were taken with this final equipment arrangement.

This vertical orientation of the mobility channel was observed in operation with a light beam when the purifier potential was turned on but when no potential was on the mobility channel electrodes. A narrow sheet of aerosol was observed with more of the wavering or distortion previously observed.

Details of the purifier are shown in Figs. 4e and 5c. This consisted essentially of 13 vertical channels, 0.105 in. wide by 10 in. high, with 0.010-in.-thick X 3-in.-long stainless steel partitions electrically insulated from each other. The two central partitions and every alternate partition were grounded, while the remaining partitions were raised to a high negative potential. Although a potential of as much as 3000 volts could be applied across the plates without arcing, this was not consistently possible, especially when operating with aerosol. It was found that a potential of up to 1500 volts could be used consistently without arcing. In these tests, the purifier plates were not covered with an electrical insulating coating. Since the aerosol particles were probably at least tacky, it was unlikely that there was any redispersion.

Details of the mobility channel are shown in Figs. 4f, 4g, 5d, and 5e. The inside dimensions of the mobility channel were 1-1/2 in. wide by 10 in. high by 25 in. long. While the top and bottom of the channel were made of Lucite, the ends were aluminum. The sides at the center of the channel were composed of two removable electrodes mounted to fit flush with the inside channel walls. Each electrode consisted of a polystyrene sheet (1/8 in. thick, 14-23/32 in. long, and 9-23/32 in. high) supported 1/8 in. away from an aluminum electrode. Polystyrene was chosen for its low dielectric constant and high resistivity and served as the collection electrode for the aerosol.

During early operation of the system, it was observed that considerable aerosol was depositing upstream of the energized mobility channel electrodes. At that time, one metal side electrode was grounded, as were the aluminum walls on the upstream and downstream ends of the channel; the other metal side electrode was at a high potential. Because of these observations, a study was made of the magnitude and effect of fringe electrostatic fields as reported in Appendix C. It was concluded that very intense fields could exist upstream of the mobility channel electrode. These could be largely avoided by the use of grounded guard plates and by operating the mobility channel electrodes at equal and opposite potentials, rather than having one grounded. Both steps were used in the final equipment arrangement. These guard plates consisted of two vertical stainless

steel panels spaced equally apart from each other and the channel walls. These panels (0.040 in. thick, 10 in. high, and 9 in. long) were mounted with spacers in a separate section of 4-in.-long aluminum duct. The panels started 1 in. downstream from the inlet end of this duct and protruded out of the rear of this duct. When assembled with the mobility channel, the protruding portion projected into the mobility channel to a point  $3/8$  in. beyond the beginning of the polystyrene collection electrodes.

In actual use, plastic tapes ( $3/4$ -in.-wide Minnesota Mining and Manufacturing Co. No. 810 "Scotch Magic Transparent Tape") were mounted in predetermined positions (indicated by scribe marks on the polystyrene electrodes) along the length of the electrode as shown in Fig. 4g. These tapes were used to permit easy removal of aerosol deposit for subsequent analysis. These tapes were marked to an exact length of  $7-3/4$  in. corresponding to the height seen by the probe-electrode and the excess ends of the tapes were cut off before analysis.

In the original equipment arrangement, the air leaving the mobility channel was allowed to pass through two bubblers in series, each consisting of a glass nozzle submerged in water. These were replaced in the final arrangement with a filter holder designed to use 12.5-cm-diameter sheets of Whatman No. 1 filter paper. A bypass line around the filter was provided for use at the start of a run, as will be described later. The filter was followed by a bubbler that collected substantially no aerosol when the filter was used but served to protect the vacuum system in the event of a filter failure and during a filter bypass.

From the bubbler, the air passed through a critical-flow orifice before going to the vacuum pump. This orifice consisted of a square-edged hole, one hole diameter thick. A series of such orifices with hole diameters ranging from  $3/64$  to  $1/8$  in. were provided and calibrated by a water displacement technique. The flow rate was essentially proportional to the absolute pressure measured with a mercury manometer just upstream of the orifice, since the pressure at the pump was much less than half the absolute upstream pressure in all cases. The critical flow discharge coefficients calculated from these calibration data were within 2%

of the expected value of 0.83, which is within the corresponding precision with which the orifice diameter could be measured.

The probe assembly used for scanning the charge accumulated on the polystyrene electrodes is shown in Figs. 4h, 4i, and 5f. Each probe electrode was aluminum ( $1/16$  in. thick,  $3/4$  in. wide, and  $7-5/8$  in. high). It was surrounded by, but insulated from, an aluminum plate  $1/8$  in. away on all sides, except the surface facing the outside. This electrode assembly was mounted in a frame and on a screw shaft in such a way that it could be moved from one end of the frame to the other by means of a motor. The shaft contained a threaded section with 18 threads per inch and was connected directly to a 300 rpm output motor. The shaft was also coupled to a linear displacement indicator that could be adjusted to electrically read out the position of the probe electrode with respect to the mobility channel electrode. While the probe electrode was insulated from the carriage, it was connected to an electrometer by means of a sliding contact on a shielded cable shaft.

To use the probe, the probe assembly was inserted into the mobility channel along guide grooves cut into the center of the top and bottom plastic surfaces of the mobility channel. When the probe assembly had been completely inserted into the mobility channel, the motor was switched on and the probe electrode was driven to either end of the channel, at which point clips mounted in the aluminum walls of the channel automatically grounded the probe electrode to remove any stray charge. The carriage was then allowed to traverse the channel electrode at a rate of 16 in./min. In all cases, the electrode readings were recorded when the carriage position indicator corresponded to predetermined locations corresponding to the positions of the plastic tapes. The carriage travel was actually stopped at these locations and the electrometer reading allowed to reach equilibrium. Each collection electrode was scanned at least twice with the probe moving in both the upstream and downstream direction.

During early runs, a few electrometer readings were recorded on a strip recorder chart. A typical readout is shown in Fig. 8. This chart was obtained at a time when bad field-fringing conditions existed at

the ends of the electrode. It does illustrate, however, the nature of the traces obtained. In the final runs with guard electrodes, the peak was shifted further downstream at the same channel flow velocity.

### C. Operating Procedures

The volumes of the various elements of the system were appreciable compared to the flow rates, as shown by the following:

	<u>Aerosol Generation System</u>	<u>Mobility Channel System</u>
Total volume, cu ft (nominal)	32	1
Nominal flow rate, cfm	8	1
Nominal hold-up time, min	4	1

Consequently, unsteady state periods during starting and stopping operation could constitute appreciable portions of the total operating time during a run. Due allowances were made in the operating procedures to either eliminate errors due to such periods or to compensate for them. The following will present a step-by-step procedure of the manner in which the system was operated.

#### 1. Preliminary Procedures

- a. Check all components of the system to be sure that they are clean and dry, especially the mobility channel electrode plates.
- b. Process the mobility channel electrodes.
  - (1) Wash the surface of the electrodes with alcohol to remove any tape or glue residues from previous runs.
  - (2) Remove any electrostatic charges on the plates and strips of Scotch tape by waving the polonium deionizer strips (see Table IV for details) over the surface.
  - (3) Carefully mount the strips of plastic (Scotch) tape in proper positions on the electrode.
  - (4) Insert the electrodes in the mobility channel assembly and clamp in place.

- (5) Remove any electrostatic charge from the electrode surfaces by inserting the polonium deionizer strip and traversing the length of the channel.
  - (6) Insert probe assembly and check to see that electrometer reading is less than 100 millivolts at all positions.
- c. Assemble all the components of the mobility channel system (wood channel, purifier, guard plate duct, mobility channel, filter, and scrubber)
  - d. Run a leak test on the total system by pressurizing to 1 to 2 cm xylene and observing rate of pressure decay. Check system if leak rate is greater than 0.02 cfm at 1 cm xylene pressure. (It was never necessary to do this.)
  - e. Temporarily turn on electrical system to be sure that there are no shorts in the high potential circuits.
2. Start Up Aerosol Generation System
- a. Start pumping dye through rotometer, but discharging to drain. Adjust rate to desired value.
  - b. Open vent valve in the bottom of aerosol chamber.
  - c. Connect supply hose from spray nozzle to beaker of water and turn on and adjust atomizing air. This will suck up and atomize water from the beaker.
  - d. Turn on exhaust scrubber system.
  - e. Close vent valve and adjust scrubber water rate so that pressure in aerosol chamber is 1 to 2 mm xylene.
  - f. Rapidly disconnect water beaker hose from spray nozzle and connect hose from dye rotometer. Dye is now being sprayed into the aerosol chamber at the prescribed rate.
  - g. Allow the aerosol chamber to operate for 30 minutes to reach equilibrium conditions, all the time maintaining pressure, flow rate, etc., constant.
3. Preliminary Operation of Mobility Channel System (usually required 20 minutes)
- a. With filter holder bypassed, start vacuum pump and adjust flow rate to desired value. Allow 5 minutes for conditions in mobility channel system to equalize.
  - b. Turn on and adjust the power to purifier and wait 1 minute.

- c. Make two 1-minute filter paper tests. These are made by inserting two filter papers in the filter holder. The flow is then passed through the filter holder for exactly 1 minute by adjusting the bypass valves.
4. Mobility Channel Run (normally required 20-35 minutes)
  - a. Put four filter papers into the filter holder.
  - b. Turn on and adjust the mobility channel electrode power at the same time the gas flow is admitted to the filter holder. The mobility channel run is now in progress.
  - c. During the run make a timed collection of the aerosol chamber exhaust scrubber water effluent, which normally goes to the drain.
  - d. Turn off power on mobility channel electrodes and bypass the filter simultaneously. This terminates the mobility channel run.
5. Shutdown Procedure (required a total of about 30 minutes)
  - a. Create a vacuum of 1 cm xylene in aerosol chamber by adjustment of the exhaust scrubber water rate.
  - b. Simultaneously disconnect the dye hose from the atomizing nozzle, turn off the purifier power, and open the downstream end of the mobility channel to the atmosphere. This allows air to be sucked into the mobility channel system and sweeps out all suspended aerosol in that system.
  - c. Shut down the entire system after the aerosol suspended in the aerosol chamber is displaced (shut off atomizing air, scrubber water, and dye pump).
6. Mobility Channel Electrode Analysis
  - a. Unbolt mobility channel, taking flanges off both ends, and remove channel to laboratory bench.
  - b. Insert probe assembly and scan each electrode separately and at least twice, recording electrometer reading when position indicator shows probe electrode is over a tape.

c. Make mass determinations on tapes (usually not done until after Step 7)

- (1) Remove tapes one at a time and place on paper backing
- (2) Cut tapes to proper premarked length
- (3) Drop tapes into known volume of water previously adjusted to pH  $\approx$  11
- (4) Dilute as necessary and analyze on Turner fluorometer.

d. Wipe off each electrode with separate damp cloth, place cloth in water, and analyze leachings on Turner fluorometer, diluting if necessary.

7. Disassemble the system, washing down each component and recording quantity and analysis of each washing.

In the above procedures, distilled water was used in leaching the tapes and filter papers, but tap water was used in all washings of components, aerosol chamber washdown spray, and scrubber. Critical times were recorded as follows:

1. For purposes of assessing deposition in the wood channel, the time was taken as the total time that the mobility channel system gas flow was on.
2. For deposition on unenergized walls (guard duct and mobility channel), the time was taken as the length of time the mobility channel electrode was energized on the grounds that most of these deposits resulted from fringing electrostatic fields.
3. For deposition rates in the purifier and on the mobility channel walls, the effective time was taken as the length of time the power was on each respective unit.
4. For the filters, the time was taken as the actual length of time that the filter was exposed to gas flow.
5. For deposition on the aerosol chamber walls, the time was taken as the time during which uranine was being fed to the spray nozzle, on the grounds that the initial unsteady state after spraying starts would be compensated for by the final unsteady state period after the spray is stopped.

All the fluorescence measurements were carried out on a Turner fluorometer (see Table IV for details).

The primary filter used was an Eastman Kodak Wratten No. 47; three secondary filters were used--Wratten No. 58, Corning No. 1-60, and Wratten ND 1.00. With this filter arrangement, the sensitivity of the instrument was approximately  $10^{-10}$  g uranine/cc (i.e., at most sensitive instrument setting, a concentration of  $10^{-10}$  g/cc would cause the instrument dial to deflect 1 division out of a total scale of 100 divisions). Most measurements were made at a sample dilution corresponding to a uranine concentration of  $10^{-8}$  to  $10^{-7}$  g/cc.

#### D. Preliminary Evaluation

Early in the program, a considerable problem was experienced with air leakage. This was most serious at the mobility channel, because a small leakage jet could create a circulation. In the final arrangement, several leakage checks were made on each equipment component, and it was established that leakage was less than 0.5% of the minimum air flow rate that would normally be handled by that component. At a pressure of 1 cm xylene above atmosphere, the leakage rate for the aerosol chamber was 0.017 cfm; for the entire mobility channel system, it was 0.0026 cfm. These leakage rates were calculated from the calculated volume of the component by pressurizing the component and measuring the rate at which the pressure decayed.

Charge retention on the polystyrene electrode was measured by charging a portion of the electrode and, with both electrode and probe in place in the mobility channel, noting the rate at which the indicated probe potential decreased. Over a 50-hour period, the potential decreased 0.2% per hour (corresponding to a relaxation time of 21 days).

The effective capacitance of the probe electrode was established as 163 picofarads (Appendix E). The accuracy of this value is limited primarily by the ability to establish the average clearance between the probe electrode face and the polystyrene electrode face. The polystyrene sheet showed significant variation in thickness ( $\pm 0.01$  in.). Attempts were made to compensate for such variation by adjusting the thickness of the spacers between the polystyrene and the aluminum electrode. It is estimated that the measured effective capacitance is good to better

than 10%, and probably 5%. A better way to establish the capacitance would be to plate the polystyrene electrode with a very thin conductive layer and with narrow vertical separations at, say, 1/8-in. intervals. This surface could then be charged to a known charge density by placing it parallel to a grounded surface and simultaneously exposing each strip to a given battery potential. This surface could then be scanned by the probe. An attempt to do this was made by painting the polystyrene surface with an aluminum paint and scribing vertical breaks by means of a razor used as a stylus. It was concluded, however, that the paint film was too thick (of the order of 0.01 in.), and that there was too much capacitance coupling between adjacent strips to make it possible to establish a known and fixed charge density.

In early attempts at material balances, only a third to a half of the uranine sprayed could be accounted for. Wall losses, leakage, and effect of temperature on meter calibration were significant contributing causes, and were all subsequently corrected or allowed for. It was found, however, that the single greatest problem with the material balance was a time decay of the uranine solution fluorescence. Fluorescence decays of 30 to 50% were encountered over a period of 30 to 120 minutes. Such a decay was experienced only when tap water was used at a pH less than 10. When either (1) distilled water was used, (2) tap water was deaerated by boiling, or (3) tap water was raised to a pH of 10 or more before using, no decay was experienced. Because of the relatively large amount of water required for the aerosol chamber scrubber and wall-wash spray, it was not convenient to use distilled water there. For this reason, and because tap water by itself gave no significant background fluorescence, tap water was used for many dilutions as well. To avoid the decay problem, the uranine dye solution was alkalinized to such an extent that all subsequent dilutions with tap water could not drop below a pH of 10. This was done by adjusting the uranine feed solution to a pH of 12.5 by addition of NaOH. Once this was done, reasonable material balances were obtained. It was later suggested by H. J. Eding (verbal communication) that residual chlorine might be the agent responsible for the decay. When hypochlorite was added to distilled

water in concentration levels of a few parts per million, decay rates of the magnitude previously experienced did result. Although this is not conclusive evidence, it does suggest chlorine as the likely explanation.

Measurements were also checked with the feed uranine solution at pH values up to 13.5, to be certain that high pH did not result in decomposition of the uranine.

During the program, the density of the uranine powder particles used to make up the uranine solution was measured as 1.540 g/cc (two determinations yielded 1.536 and 1.544 g/cc) by displacement with xylene.

## VII EXPERIMENTAL RESULTS

The primary purpose of this investigation was to evaluate the performance of the mobility channel and probe assembly as a system for measuring aerosol charge distribution. Consequently, this and subsequent sections deal only with results aimed directly at this objective. Any results of preliminary evaluation and development not directly related, although necessary for attainment of the objectives (such as analytical techniques) are reported in previous sections.

Results of the primary study were all obtained with the final equipment arrangement depicted in Figs. 3 and 4d, and are summarized in Table II. This primary study consisted of a series of five types of runs. In the first series (Runs 1, 2, and 3), all high potential electrical power was off, and the objective was to establish material balances and wall deposition in the absence of electrostatic effects. The second series (Runs P1, P2, and P3) was aimed at establishing the purifier performance characteristics. The third (Runs A1, A2, and A3) and fourth (Runs B1, B2, and B3) series were aimed at actual operation of the mobility channel system for measuring aerosol characteristics. In the A-series, a constant channel velocity (3 cm/sec) and a constant potential difference across the metal electrodes ( $\pm 5000$  volts  $\approx$  10,000 volts difference) were used. In the B-series, both velocity and potential differences were doubled, but the purifier potential difference was the same as for the A-series. Thus, in the B-series, the particle electrical mobility conditions in the mobility channel were the same as in the A-series, but the purifier was not able to remove as low a mobility particle. The fifth series (S1, S2, S3, and S4) was made after Run A2 to assess deposition on the aerosol chamber walls only, since unexpectedly high deposition rates had been encountered in Runs A1 and A2.

#### A. Material Balances

Complete material balances were made in all runs. Each piece of equipment was washed down at the end of the run, and the washings were analyzed. It was not practical to measure either the aerosol escaping the aerosol chamber exhaust scrubber or the aerosol entering the vacuum pump. The latter was assumed to be negligible. This assumption seems justified on the grounds of the extremely low relative amount of aerosol collected on the last three of four filter papers (less than 2% of what is collected on the first filter paper). In some earlier measurements, each of four successive filter papers showed a similar percentage gradation in the amount of aerosol collected.

Material balances on the mobility channel system were made by adding all deposits to arrive at a "measured" quantity of dye entering the wooden channel. This could then be compared with the quantity that would be calculated, based on the air flow rate entering the wooden channel and the average aerosol chamber aerosol concentration corrected for aerosol-chamber wall deposit. In general, the agreement was within 5%, averaging about  $\pm 3\%$ . This adds further credence to the assumption that no significant aerosol escapes the filter.

A material balance on the aerosol generation system was made by assuming that the difference between the quantity of feed aerosol and the sum of all collections accounted for (including the mobility channel system) represented loss from the aerosol chamber exhaust-gas scrubber. On this basis, a scrubber efficiency of 95 to 98% was consistently indicated. This implies that losses to any source could not have been in excess of 5%, and were likely all accounted for by the small amount that escaped collection in the scrubber and passed to the atmosphere. The order of magnitude of aerosol escaping collection was also confirmed qualitatively by visual observation of the plume from the scrubber exhaust gases with a Tyndall beam.

Runs 1, 2, and 3 indicated that, in the absence of external electrostatic fields, less than 2% of the aerosol was collected on the combined purifier and mobility channel walls. This indicates that mechanical wall deposition was negligible.

In all the runs of Table II, the amount of aerosol deposited in the wood channel ranged from 5 to 10%, usually close to 10% at the low gas rates and 6% at the high gas rates. Allowing for the effect of the turning vanes, one would expect that all particles larger than 12-micron diameter would be removed by gravitational settling alone at the low gas rate. The corresponding particle diameter would be 17 microns at the high gas rate. Thus, the deposition in the wooden channel may represent a combination of wall deposition and gravitational settling of the largest particles. This would also imply that up to 10% of the original aerosol may be larger than 12 microns in diameter on a mass basis. This is a reasonable value if the mass median diameter of the aerosol were in the range of 2 to 5 microns, as was expected. It does mean, however, that the mobility channel will receive somewhat more large particles at the high rate than at the low rate.

The purifier collection efficiency,  $\eta_p$ , represents that portion of aerosol in the energized portion of the purifier that is deposited on the purifier plates. The mobility channel collection efficiency,  $\eta_{cm}$ , represents that portion of aerosol in the central electrode stream which is deposited on the mobility channel walls. These quantities were calculated from Equations C-11 and C-13 in Appendix C. The value for  $\eta_{cm}$  so calculated assumes that the aerosol escaping collection in the energized portion of the purifier passes on through the mobility channel without depositing. This assumption is probably not true. For those conditions where the purifier was more efficient (i.e., minimum collectible mobility was smallest), less purifier aerosol was passed on to the mobility channel when it might have deposited on the mobility channel electrodes. Hence the assumption used in calculating  $\eta_{cm}$  is more nearly realized when the

purifier efficiency is high. For minimum collectable mobilities of 0.2 and 0.4 (cm/sec)/(volt/ $\mu$ ), the purifier collection efficiency averaged 93 and 81 percent, respectively.

The mobility channel electrodes collected only some 24% of the entering aerosol in Runs A1, A2, A3, B1, B2, and B3. A large part of the material entering the mobility channel represents material that escaped collection in the energized portion of the purifier. The mobility channel collection efficiency,  $\eta_{cm}$ , however, ranged from 46 to 72%, averaging 56%. Since these runs were made at constant mobility conditions in the mobility channel, the true value of  $\eta_{cm}$  should be constant and should represent the mass fraction of the aerosol that has a mobility greater than the minimum collectible in the mobility channel [0.72 (cm/sec)/(volt/ $\mu$ ) in this case]. However, because of the assumption in calculating  $\eta_{cm}$ , the value of  $\eta_{cm}$  will be overestimated to an extent that becomes greater as the purifier efficiency drops. Any charged particles leaving the energized portion of the purifier will tend to deposit uniformly along the mobility channel wall to an extent dependent on their total quantity and mobility. This will have the same effect as having a constant additive error in the mass collected by the mobility channel. This is probably the reason that the value of  $\eta_{cm}$  is larger in Runs B1, B2, and B3 than in Runs A1, A2, and A3. This error could be avoided by having a more efficient purifier.

The quantity of dye collected on the mobility channel electrodes was determined in two ways: (1) by integration of a smooth curve drawn through the data obtained for the mass on each tape (appropriately corrected for tape height and width), and (2) by fluorometric analysis of the dye wiped from the entire polystyrene electrode surfaces after the tapes were removed. The results from these two methods are termed "calculated" and "measured" in Table II. The agreement between these two values was usually better than 5%, the calculated values tending toward the high side.

Before each mobility run, separate filter samples were also taken. This was done during a period when the system was at equilibrium conditions with the purifier energized, but when the mobility channel was not energized. The results from these determinations are labeled as "special test filter papers" in Table II, and also show agreement within 5% of the values subsequently obtained from the additive results of filter and electrode material when the mobility electrode was energized.

The deposit of dye on the aerosol chamber walls was usually about 10% of the aerosol sprayed, but occasionally went as high as 23%. From the horizontal aerosol-chamber cross-sectional area, one would expect that uranine particles larger than 15 microns diameter would settle out. Additional large particles could also be impacted against the walls, especially during the early stages of evaporation. The initial spray droplets are probably in the range of 2- to 20-micron diameter, where after evaporation they are probably in the range of 0.5 to 5 microns.

It should also be noted that at room temperature and for the specific aerosol chamber air and solution rates employed, all the water could not evaporate from the drops before the air became saturated with water vapor if adiabatic saturation conditions had prevailed. Because of the large exposed wall surface, the air inside the chamber could not cool more than a few degrees below room temperature. However, there existed a possibility that complete evaporation did not take place in the aerosol chamber, although there is adequate surface in the wooden flow channel to raise the air to room temperature and ensure complete evaporation there. Originally, it was intended to spray at a feed solution rate of 2 cc/minute, at which point there should have been no problem evaporating all of the water in the spray. However, because of problems with maintaining a steady pumping rate at 2 cc/minute, the rate was raised to 3 cc/minute. It is possible that the wall deposit in the aerosol chamber was a function of the degree of evaporation there. There is some indicated trend of magnitude of wall deposit with room temperature, although

this trend is not entirely consistent. Since radiation from exterior room walls (the temperatures of which are unknown) could be a sizable factor in chamber wall temperature; however, it is also possible that room temperature alone does not determine these evaporation effects.

#### B. Aerosol Characteristics

The detailed analyses of the tapes from the mobility channel electrodes are presented in Table III and plotted in Fig. 6a. Three basic quantities were established for each tape: (1) total charge deposited, by scanning with the probe electrode; (2) total mass of uranine deposited, by fluorometric analysis of the tape leachings; and (3) averaged electrical mobility of the deposit, calculated from the tape position and the channel operating conditions.

The mobility corresponding to each tape location is given in Table I. The values in this table are calculated from the results given in Appendix C, Fig. C-4. The results of Fig. C-4 are given for a guard plate that overlaps the plastic deposition electrode by 3/4 in., while the actual overlay was only 3/8 in. This difference should have no significant effect, however, provided all distances are measured from the end of the guard electrodes, as is the case for Fig. C-4. The specific normalized mobilities corresponding to each tape position given in Fig. C-4 are generally applicable. The specific values of mobility given in Table I are applicable only for Runs A1-A3 and B1-B3, for which conditions were chosen such that the actual mobilities were unchanged at each tape location. In calculating these mobilities, the field intensity  $\mathcal{E}_0$  was calculated from Equation D-7, ignoring any effect of charge accumulation on the electrodes. It should be noted that for the highest tape charge levels noted in Table III, the effect of back potential due to accumulated charge was just becoming significant, corresponding to 4% of the impressed field intensity.

In presenting the data for mass and charge distribution in Fig. 6a, the total mass and charge have been plotted against tape position expressed as a percent of the total electrode length. This was done for convenience,

since the position readout was set up in these terms on the instrument. The actual mobility corresponding to each position is, however, still given directly by Table I. It should be noted that the tape area was 5.8 square inches and substantially identical to the area of the probe electrode. It will be noted from the bottom of Table III that the total material entering the mobility channel was not quite the same for all the runs. For this reason the plots of mass deposits in the various runs cannot be compared directly. The mass fraction plot, however, overcomes this problem. A similar problem exists with the simple charge distribution plots. In that case the subsequent plot of charge-to-mass ratio essentially overcomes this problem.

For simplicity, the points for a given run in Fig. 6 have been connected by straight lines rather than by a smooth curve, to better show the agreement (or disagreement) previously discussed. For purposes of material balance integrations, arithmetic plots were used with smooth curves drawn through the data points.

In early runs an abnormally low probe reading was obtained at the center electrode position, or at any point where there were spacers between the plastic collection and metal electrodes, even though the electrodes had initially been discharged. Such a phenomenon could result from one of two causes: (1) increased local capacitance due to the presence of spacers, which could be enhanced by any increase in conductivity of spacer surface due to glue or other surface contamination; and (2) triboelectric charges accumulated at these points as the result of vibrational rubbing. Because the effect was always to lower probe reading regardless of whether the electrode was originally charged positively or negatively, it is believed that the first of these explanations applied.

The spacers were originally fastened to the metal electrodes with metal screws. Replacement of these with nylon screws did not prevent the low probe reading. However, when the central spacers on one electrode were removed, reasonably normal probe readings were obtained at that point. The spacers on the other electrode originally were left in place

to provide a check, both on this phenomenon and the possible effect on electrode clearance of removing the spacer. Unfortunately they were not removed later. For this reason, while all charge measurements at the 50% position have been recorded in Table III, an additional value of charge was calculated by interpolation from the 40% and 60% values, and is also given in Table III. This interpolated value was used as the best representative point, and is designated by "dog ears" to compare it with the corresponding uncorrected points, which are also plotted.

In all runs, each of the pair of mobility channel electrodes was used with a given sign of potential, except in Run B1, where the sign of the potential was reversed. Note in Fig. 6 that in all the runs except B1, the charge distribution data at the 50% location, which appear to diverge from the rest of the data, are those for the positive particles (i.e., deposited on the negatively charged electrode). For Run B1, it is the point for the particles deposited on the positively charged electrode. In all cases, the divergent data correspond to the electrode that contained the spacers at the center.

The charge-to-mass ratio for each tape is obtained by a direct division of measured charge by measured mass. The average effective diameter and corresponding average specific particle surface gradient were calculated from the charge-to-mass ratio, and the corresponding mobility listed in Table I by means of Equations C-7, C-8, and C-10. All these values are shown plotted in Fig. 6b as a function of tape position.

Figure 7 presents the mobility distribution of the aerosol as determined in the various runs, on both a frequency basis and a cumulative basis. The data plotted in Figure 7 are summarized in Table VI. The data points on a frequency basis are obtained directly from the mass distribution data of Table III, using the incremental mobility values given in Table I. The cumulative curve is based on an integration under an arithmetic plot of the mass distribution data vs electrode length. In both cases, it was assumed that the deposit was uniformly distributed vertically so that the deposit corresponding to the full channel height

could be calculated by simply multiplying the tape deposit by the ratio of full height (10 in.) to tape height (7.75 in.). It was also assumed that the total effective amount of aerosol entering the mobility channel was 1/13 of that entering the purifier. This is tantamount to assuming that any aerosol escaping the energized position of the purifier is not deposited on the mobility electrode.

Figure 7a shows a solid line drawn as a smooth representation of the data over the entire mobility distribution. The solid line in Fig. 7b is this same line on a frequency basis. The dashed line in Fig. 7a is drawn as an extreme representation of the data with a point of inflection at the zero mobility level. The dashed line in Fig. 7b is this same dashed line converted to a frequency basis.

In the early runs with a horizontal mobility channel, the variation of dye deposit density on the electrodes and tapes was obvious to the eye and reflected the various convection or leakage currents in the channel. With the mobility channel in the vertical position (as used for all runs reported in Tables II and III), no visual variations in the deposit along the length of a specific tape was noted. Only three narrow, dye-deficient streaks were noted on those tapes located on the front half of the electrode. These streaks corresponded to the level of spacers used between the purifier electrodes (two sets of guard plate spacers were in line with two of the purifier spacers). A variation in deposit density along the length of the channel was noted, which visually corresponded to the variation shown in Fig. 6.

## VIII DISCUSSION OF RESULTS

Runs in the A-series were intended as check runs, as were the B-series runs. Therefore, the spread in values within each series should be a measure of overall reproducibility. In examining the data plotted in Fig. 6, it will be noted that the spread in the data is usually greater at the inlet or high mobility end of the channel, becoming less at the discharge end. Part of this may reflect the fact that mobility becomes more sensitive to position at the inlet end. Table V has been prepared to permit some quantitative comparison. This table gives average mean spread of the data from the mean. The values given are based on a visual inspection of the comparable data and are not the result of any rigorous statistical analysis. It has given smaller weight to the values at the inlet end of the channel and has completely ignored two sets of peak (or minimum) values reported for Runs B1 and B2. These will be discussed separately later.

In general, it would seem that the apparent reproducibility is some  $\pm 20\%$ . There is little difference in the relative mass of positive and negative particles at a given mobility, but the negative particles have a higher apparent charge and hence must be somewhat finer. Although there are some values that deviate considerably more from the mean, the above gives a reasonable estimate of the overall indicated precision.

Series B data show a greater spread than Series A data. In general, the material deposited in Series-B runs represents a 50% greater mass fraction than for Series A, has a 20% lower charge-to-mass ratio, and is consequently 10% larger.

Superficially, there is no reason to expect a difference between Series A and Series B data. Although Series B runs were made at twice the air flow rate of Series A runs, the mobility channel electrode potentials were also twice as great, so that particles of the same electrical mobility should be collected at the same points in the channel. The

basic differences in the two series are: (1) because of the higher gas rate, less aerosol can settle out in the wooden channel and hence the aerosol reaching the mobility channel may be somewhat coarser; (2) because of the higher gas rate and no corresponding increase in potential in the purifier, the latter will allow more aerosol to reach the mobility channel. The average particle size in B-series runs was slightly larger than for A-series runs, and B-series runs did have a greater mass fraction deposited on the mobility channel electrodes.

The purifier will drive those particles with the same charge sign as the high potential purifier electrode toward the outer channel wall. Correspondingly, particles of the opposite sign will tend to be drawn away from the outer channel wall. Therefore, in the subsequent mobility channel, one would expect that these low mobility particles escaping the purifier of the same sign as the purifier electrode (negative in all current runs) would deposit on the mobility channel at a greater rate than those of the opposite sign (at least in the upstream end of the mobility channel). Thus, one might expect that the increase in mass deposit of negative particles in the B-series and the mass deposit in the A-series would be greater for negative particles than for positive particles. Actually, this is the case for the very first tape but is reversed in subsequent tapes. The latter effect could mean that there are more low mobility positive particles escaping the purifier than negative particles, which could serve to more than compensate for the higher expected deposition rates of negative particles.

The general range in the average effective particle diameter is 0.7 to 1.0 micron, showing little trend with mobility level. An indicated overall average diameter is approximately 0.8 micron. In another study (Robinson, McLeod, and Lapple, 1959), a similar nozzle gave a mass median diameter of 5.4 microns for the final aerosol particle when operated at 35 psig air pressure. In that case, the nozzle was 1/4 in. in diameter; liquid feed rates were 100 to 200 cc/minute; and the uranine concentration was 20%. On the basis of these data, if a 2% solution had been sprayed, the mass median diameter of the final particle should be 2.5 microns. Because the nozzle was smaller and the relative liquid rates lower in

the present study, the mass median diameter should be even smaller. Thus, it is reasonable to expect a mass median diameter of 2 microns in the present study. Visual observation of tapes under the microscope indicated that the deposited particles were in the range of 1 to 5 microns with an estimated mass median diameter of 2 to 3 microns. The particles were viscous liquids and could be smeared with a needle. Allowing for the fact that the particles on the tape are probably flattened, these observations would confirm that 2 microns is a reasonable estimate for the mass median diameter.

However, the aerosol would also be expected to have a distribution corresponding to a standard geometric deviation of 2 to 3, probably closer to 3. The effective average diameter measured by the mobility channel is essentially the volume-to-diameter mean,  $\bar{D}_{31}$ , (as defined in Appendix A) in this case. As shown in Appendix B, for a standard geometric deviation of 2 the mass median diameter would be 1.62 times the volume-to-diameter mean. For a standard geometric deviation of 3, this ratio would be 3.34. Thus the volume-to-diameter mean corresponding to a mass median diameter of 2 microns would probably be 0.6 to 1.2 microns, which encompasses the range of the experimental data. While this is too crude an estimate to prove the validity of the experimental results, it does indicate that the experimental values are reasonable.

The fact that the average effective diameter is nominally the same at each mobility level would imply that the size distribution at each mobility level is approximately the same. This is a unique and unexpected result. Since data on both charge and size distribution of aerosols are almost nonexistent in the literature, it is not possible to say how common this unique result is. It could be related specifically to the mechanism by which the aerosol particles became charged. In the present study the aerosol was generated by a pneumatic atomization process. Other methods of aerosol generation, or even other methods of atomization, might yield different types of charge and size distributions. It is conceivable that the form of the relative distributions might be used as a means for identifying the source of an aerosol.

In leaving the central liquid feed tube, the liquid could acquire an electrical charge relative to the grounded central tube. Such a charge would be expected to be homopolar. However, any charge acquired in this manner would be expected to be negligible in magnitude. It is likely that any charge acquired by the drops is the result of the atomization process itself. As discussed on Page XII-67 of Technical Report No. 1 (Lapple, 1965), such a mechanism might be expected to create drops with a charge level, expressed as average specific particle surface gradient, corresponding to a nominal range of 0.001 to 0.65 volt/ $\mu$ , and the net charge of the aerosol would be zero. Because of evaporation (see Appendix C), the charge level of the final uranine drop would increase by a factor of 18 for the conditions of the present study, assuming that no charge is lost during evaporation. Thus, the charge level of the uranine particles might be expected to be of the order of 0.02 to 1 volt/ $\mu$ . This does correspond to the range of values actually found for the average specific particle surface gradient,  $\bar{E}_{psae}$ .

In Run B1, an unusual peak was shown in the charge at the 70% position, where in Run B2 such a peak occurred at the 30% position. No corresponding unusual effect on mass fraction deposited was noted at these positions. This might be ascribed to experimental error or freaks were it not for the fact that in both cases the peak showed up for both the negative and the positive particles at the same position. Since measurements for the positive and negative particles are essentially independent of each other, it has not been possible to conceive of any error in procedure or in instrumentation that could reflect itself in a similar way in both measurements, let alone do this in two runs. One must assume, therefore, that these peak charge values are real.

If these peaks were uranine, they must reflect extremely fine particles of uranine to have such a high charge-to-mass ratio that a corresponding peak is not observed in the mass fraction data. In fact, the size must be smaller than the 0.3- or 0.5-micron calculated for the average effective diameter from the data in each run at these positions. It is inconceivable that particles of such size should suddenly be produced. The only plausible explanation is that the peak charges

represent a deposit of charged particles that are not uranine. Such particles might be oil carried over from the compressed air line, becoming atomized and charged by the compressed air jet in a fashion similar to that causing the charge on the uranine particles and yielding both positively and negatively charged particles in approximately equal amounts. Although the compressed air line is equipped with a filter, oil deposits have been found downstream of the filter, probably penetrating the filter at times when a heavy oil or water surge comes through the line. Such particles need not be as fine as the 0.3 microns calculated for the average effective size, since the latter reflects the fact that the mass of these highly charged particles was not included in the mass measurement.

The main disconcerting aspect of this explanation is that the charge peaks are so sharp. In fact, they were even sharper than Fig. 6 would indicate. Actual observation of the electrode position indicator during the scanning showed that the entire charge rise range extended over a distance equivalent to only 5 to 8% of the electrode length. This would mean that these extraneous (oil?) particles must have had an extremely uniform mobility. It is difficult to understand the mechanism for generating particles of such uniform mobility.

Run B1 was the only run in which the mobility channel electrode polarity was reversed from what it was in the otherwise check runs (B2 and B3). The comparison of the various properties of negatively and positively charged particles for Run B1 deposited on the downstream half of the electrodes are as follows: (1) no significant difference in mass fraction deposited; (2) positive particles have a higher charge than the negative ones; (3) the charge-to-mass ratio is greater for positive particles; and (4) the negative particles have a larger average size. In general these are the reverse of the corresponding trends shown for Runs B2 and B3. For the upstream half of the electrodes the relative trends are variable. These differences, although not major, might indicate nonsymmetry in the system, either in flow or geometry, since it is difficult to admit that the aerosol charge could have changed so consistently for this one run in which the electrode potential was reversed. The lack

of symmetry is equally hard to understand in view of general tolerances in equipment construction and the check in calibration capacitance obtained for each electrode (as described in Appendix E).

The spray nozzle head was originally electrically insulated from the rest of the system as shown in Fig. 5a. This was done so that the nozzle could be electrically charged to induce a charge on the spray droplets. It was found, however, that the droplets developed adequate charge levels during breakup so that the external electrostatic field was not needed. There is the possibility, however, that the spray head could have become charged either by selective deposition of drops of a given charge from the spray chamber or by deposited liquid being torn off of the spray head. Such a charge would in effect present the equivalent of an external electrical field and could modify the charging of the atomized uranine. Because of the source of this field, this could produce an erratic effect on uranine particle charge.

Previous paragraphs have discussed the spread in the data and some of the anomalous results obtained. In a broad sense, the data from all runs show nominal agreement and indicate that the positive and negative aerosol particles are present in approximately equal quantity and have equivalent characteristics (size and charge). However, the spread in and the discrepancies in the data were greater than allowable by the expected precision of measurement. The following are possible alternative explanations:

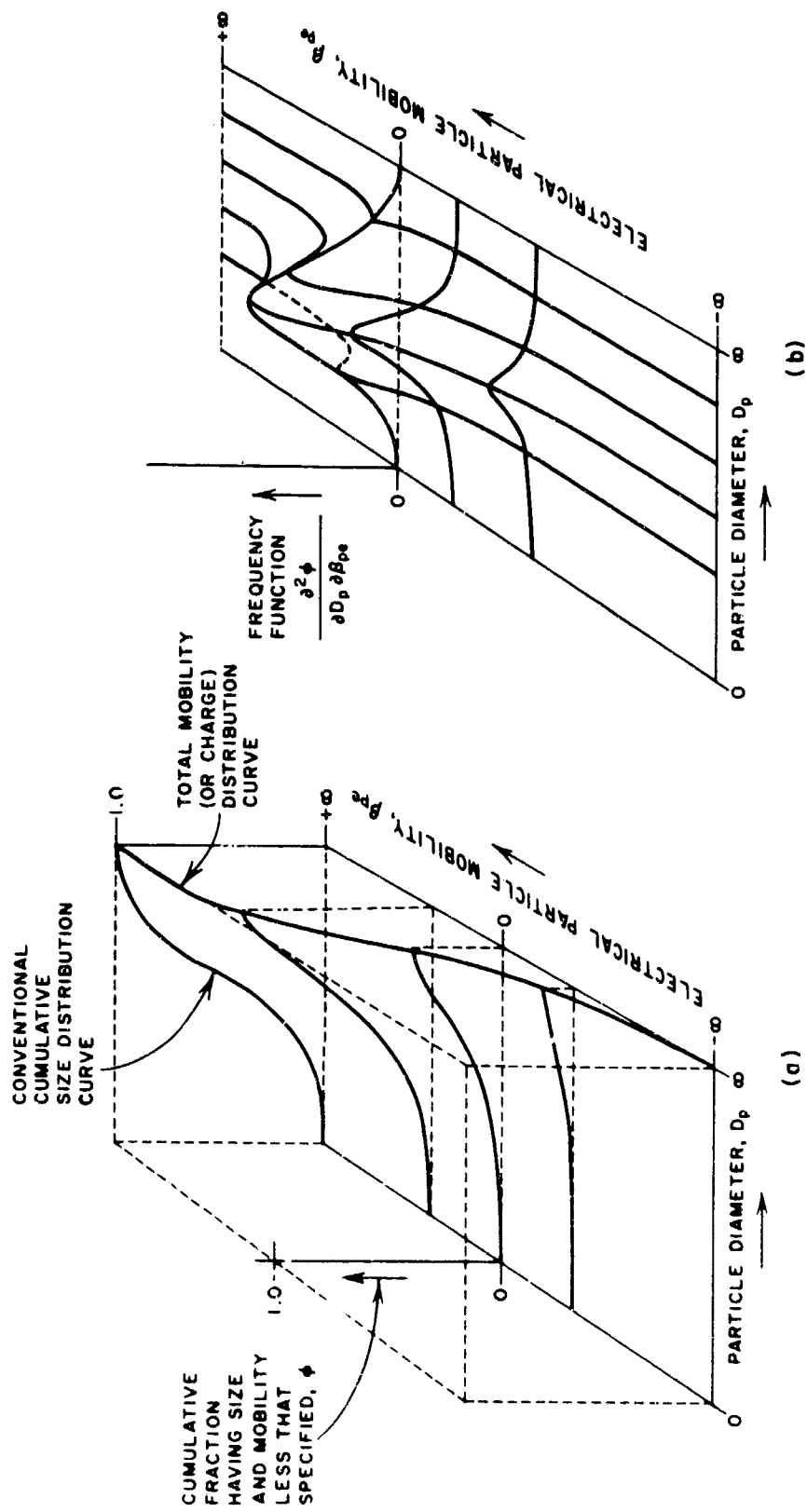
1. General experimental error. In the light of the general precision and consistency of trends usually indicated by the tapes as a whole, it is difficult to explain the variation on this basis. If general experimental errors were involved, it would be expected to find more erratic rather than systematic variations.
2. Interfering influences due to purifier inefficiency. While, as explained before, the purifier can affect the absolute results, it too was carefully controlled. The only obvious manner in which it could have had a deleterious effect on reproducibility was through momentary electrical arc-overs that were not detected. Normally an arc-over could be detected by the behavior of the power supply meter, and no such problems were known to occur during the runs involved.

3. Change in aerosol characteristics. It is difficult to admit that any significant variation could arise from the mechanical aspects of the atomization process. Because of the high spray rates and possible limitations on water evaporation rates, it is possible that aerosol variations could arise from that source. Such variations, however, could be expected to affect mainly the coarser droplets. Since these droplets probably have the highest mobility and are subject to removal in the aerosol chamber channel it is possible that such variations in aerosol properties did occur. These variations could also show up as apparent systematic shifts in the magnitude and character of negative and positive particles. In addition, the failure to ground the atomizing nozzle head could have caused spurious particle charge effects.
4. Other uncontrolled influences. The chief uncontrolled factor that might effect the results lies in any convective currents that may be set up by leaks or by thermal gradients. It is questionable whether these were significant factors in these final runs because of the uniform appearance of the deposit on the tapes. Any velocity unbalance should show up as a streak or as a density variation in the aerosol deposits on the tapes.

Figure 7 is basically a generalized version of the mass fraction data of Fig. 6 in which the mass distribution for all charge levels (including neutral particles) is shown as a function of charge level. The spread in the data points is seemingly less than in Fig. 6, because the data are desensitized in this plot, each previous item being only a piece of the total. The absolute validity of Fig. 7 is subject to the assumption that all particles escaping the purifier do not deposit on the mobility channel electrodes. Consequently, Fig. 7 is in error in the direction of indicating a somewhat greater fraction of charged particles of all mobility levels than is actually the case. There is, however, no way in which a correction can be applied at present. This error will be greater for the data from Series-B runs than from Series-A runs. In general, there is good agreement between the data of the two series of runs for the distribution data for the negatively charged particles. Series-B data, however, show a greater fraction of high mobility positive particles than Series-A data.

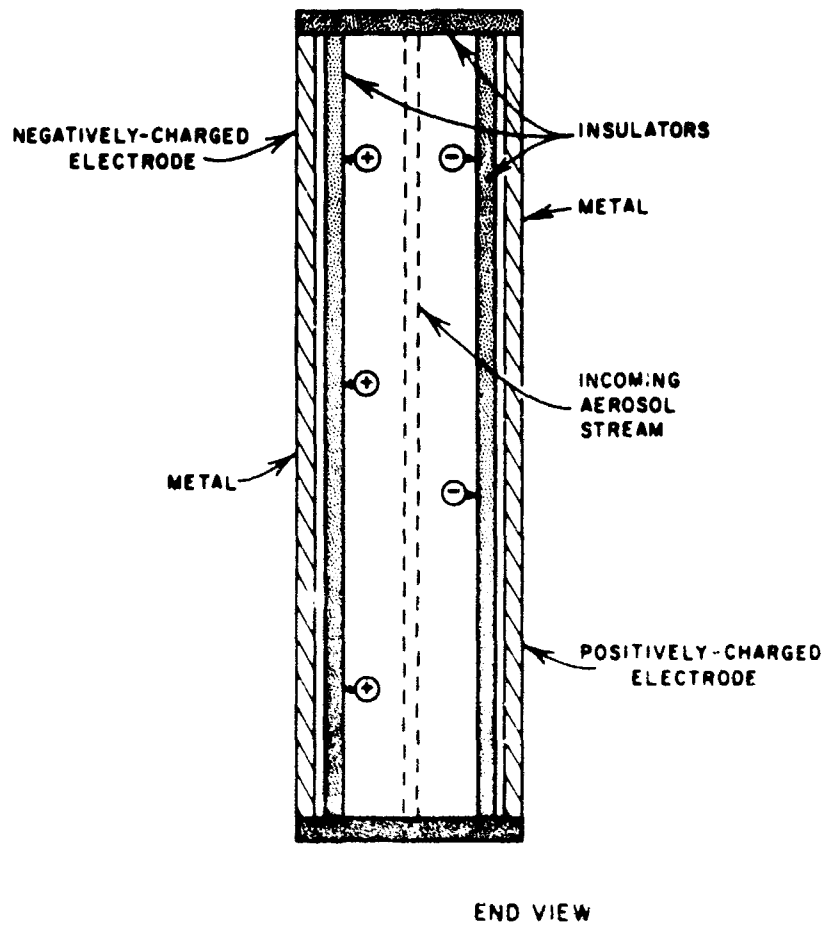
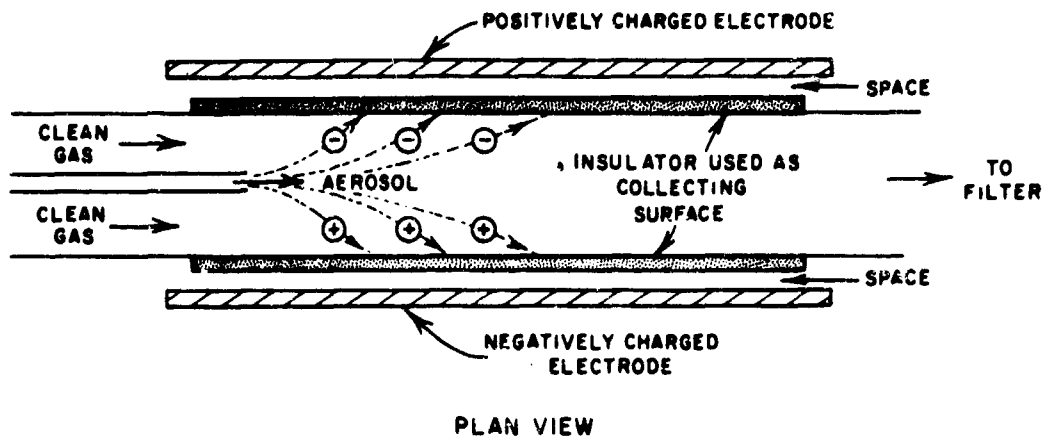
The solid curves in Fig. 7 give a smooth representation of the data over the entire mobility range with a maximum frequency at zero mobility (uncharged particle). The dashed curve gives a better fit of data for low mobility particles and has been deliberately drawn so that the frequency goes to zero at zero mobility. The fact that the dashed line fits the data better may, at least in part, reflect the error introduced by inefficiency of the purifier. While the solid curve would appear to offer a more reasonable type of distribution curve, present data are not adequate to indicate which, if either, of these forms is basically correct.

The present system has been operated at a maximum flow rate of 1.24 cfm. As indicated in Appendix C, it should be possible to operate the channel at capacities up to 6 cfm. The higher capacities would mitigate any undesirable influences of thermal convective currents. However, it is not known what other problems might be encountered at the higher velocities. Although explainable on other grounds, it does happen that Series B runs were made at a higher capacity than Series A runs and did show a greater scatter in the data. At a flow rate of 6 cfm, the channel should be capable of accommodating aerosol particles up to 30 microns in diameter (which would have a settling velocity of some 10% of the channel velocity). Such large particles could not be handled at lower gas rates, since gravitational settling would be a significant factor in the particle trajectory. It would be possible to devise a channel for the larger particles that would make use of such gravitational effects to obtain both a charge and a size distribution. The gravitational effect, however, is too small to make such a concept feasible for particles under 10 microns diameter.



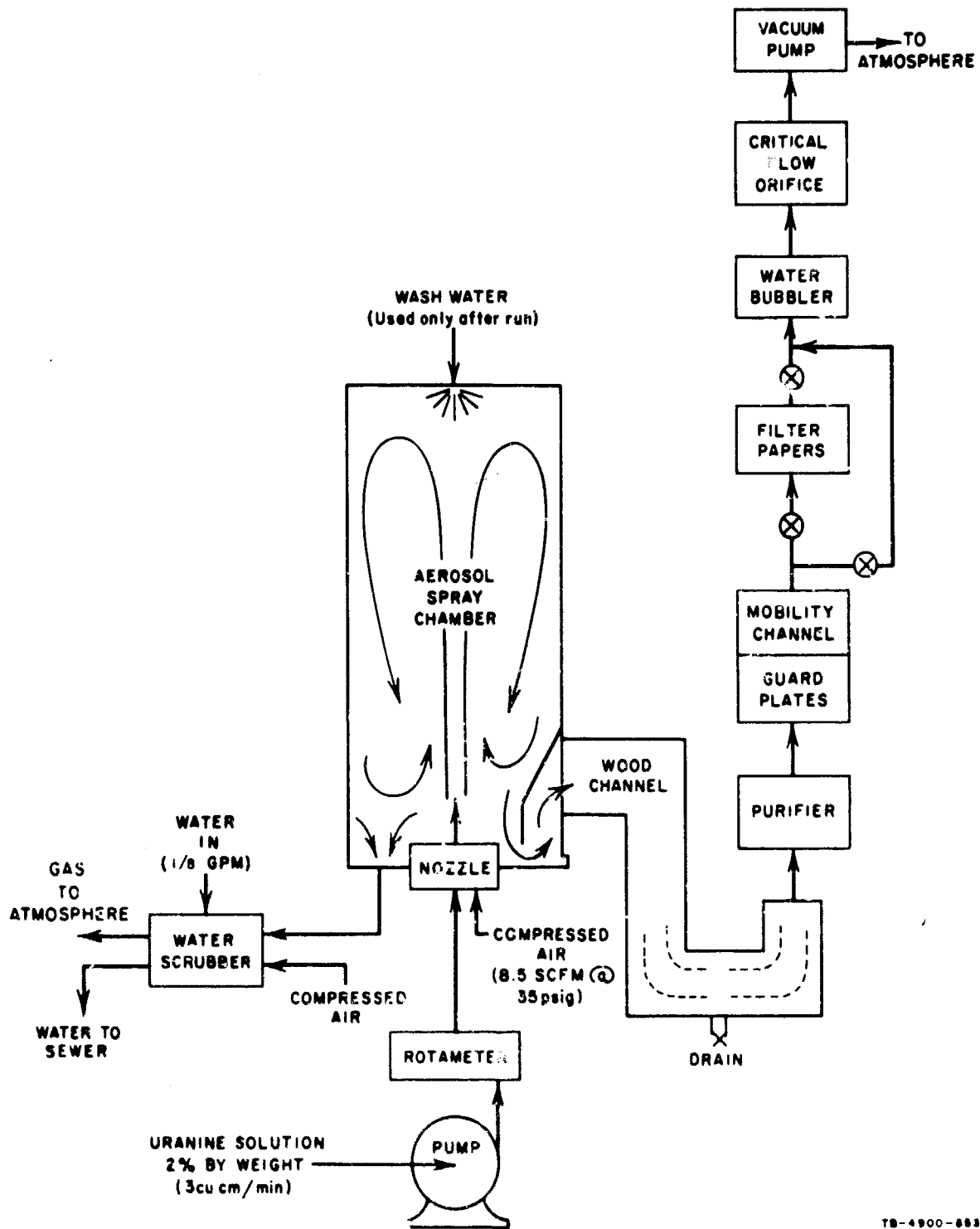
TS-4900-630

FIG. 1 FORM OF A COMPLETE CURVE FOR EXPRESSING BOTH SIZE AND ELECTRICAL MOBILITY (OR CHARGE) DISTRIBUTION OF AEROSOLS OR POWDERS  
 (a) Cumulative distribution (b) Frequency distribution



YA-4800-652

FIG. 2 PRINCIPLE OF OPERATION OF MOBILITY CHANNEL



TR-4900-883

FIG. 3 SCHEMATIC ARRANGEMENT OF EXPERIMENTAL EQUIPMENT  
(as used in final phase of study)

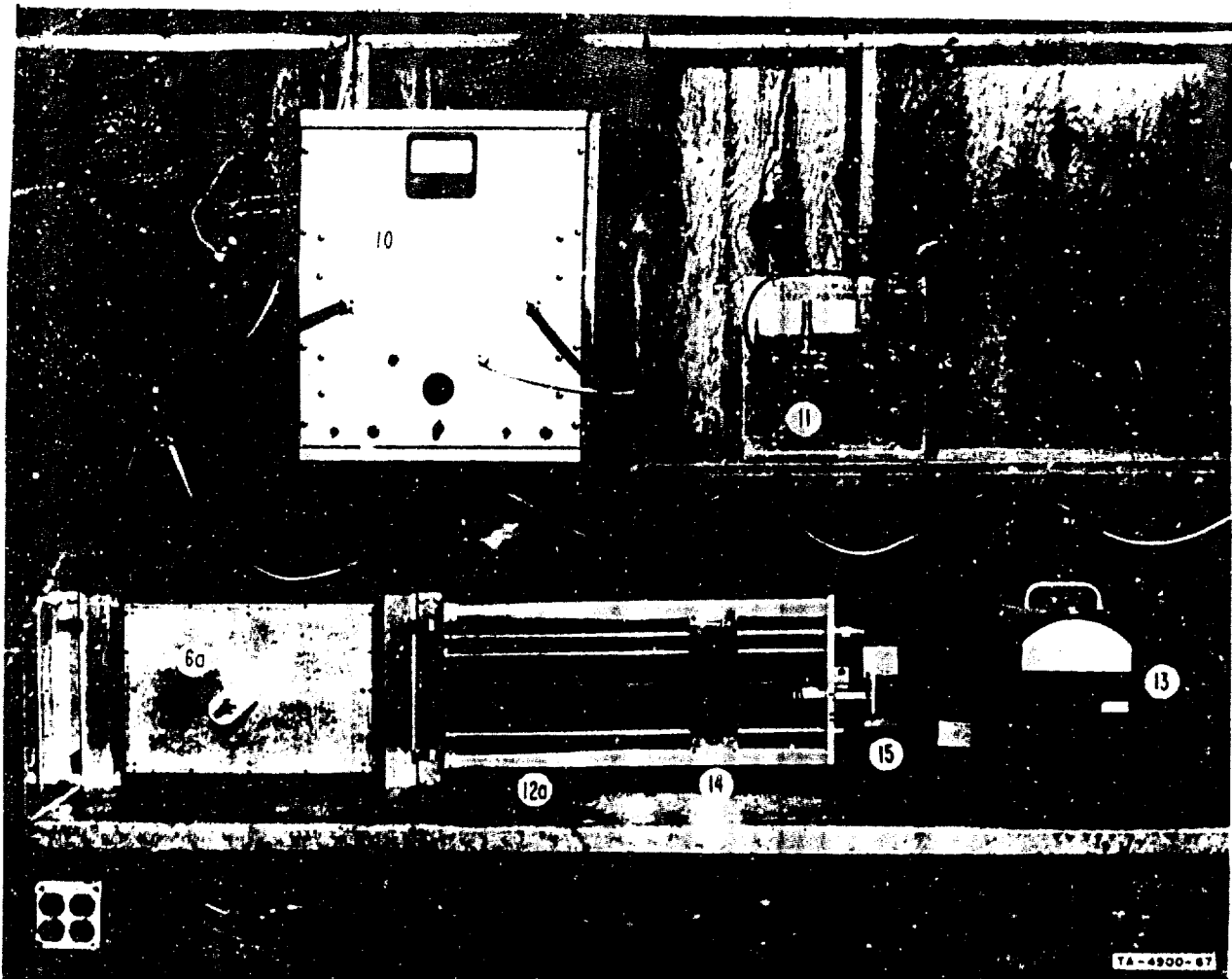
#### FIG. 4 PHOTOGRAPHS OF EQUIPMENT

- a. Exploded view of aerosol generation and charge measurement apparatus (as used in original phase of study)
- b. Close-up view of mobility channel and charge analyzer
- c. Assembled view of experimental apparatus used in early phase of study
- d. Assembled view of experimental apparatus used in final phase of study
- e. Upstream side of purifier (connected to mobility channel)
- f. Close-up view of mobility channel
- g. Inside face of mobility channel collection electrode with tapes in place
- h. View of probe assembly partially inserted into mobility channel (probe electrode exposed) and electrometer
- i. View of probe assembly
- j. Details of base of aerosol chamber
- k. Liquid supply system for aerosol generation



- |   |                                    |
|---|------------------------------------|
| ① AEROSOL CHAMBER   | ⑦ MOBILITY CHANNEL ELECTRODE COVER |
| ⑩a AEROSOL CHAMBER SAMPLING PORT (CONTAINS FLOW STRAIGHTENER)                               | ⑧ BAG FILTER                       |
| ② AEROSOL ATOMIZING NOZZLE  | ⑨ EXHAUST PLENUM CHAMBERS          |
| ③ AEROSOL MATERIAL METERING PUMP  | ⑩ HIGH VOLTAGE POWER SUPPLY        |
| ④ AEROSOL CHAMBER EXHAUST SCRUBBER  | ⑪ HIGH VOLTAGE MICROAMMETERS       |
| ⑤ PURIFIER  | ⑫ CHARGE ANALYZER WITH CASE        |
| ⑥ MOBILITY CHANNEL (WITH FRONT ELECTRODE REMOVED AND SPECIAL CALIBRATING ELECTRODE IN BACK) | ⑬ ELECTROMETER                     |

FIG. 4 (a) EXPLODED VIEW OF AEROSOL GENERATION AND CHARGE MEASUREMENT APPARATUS (as used in original phase of study)



- ⑥a MOBILITY CHANNEL (WITH FRONT ELECTRODE IN PLACE)
  - ⑩ HIGH VOLTAGE POWER SUPPLY
  - ⑪ HIGH VOLTAGE MICROAMMETERS
  - ⑫a CHARGE ANALYZER IN PROCESS OF BEING INSERTED IN MOBILITY CHANNEL
- ⑬ ELECTROMETER
  - ⑭ SCANNING PROBE AND CARRIAGE
  - ⑮ CARRIAGE DRIVE MOTOR AND CONTROL

FIG. 4 Continued  
 (b) Close-up view of mobility channel and charge analyzer

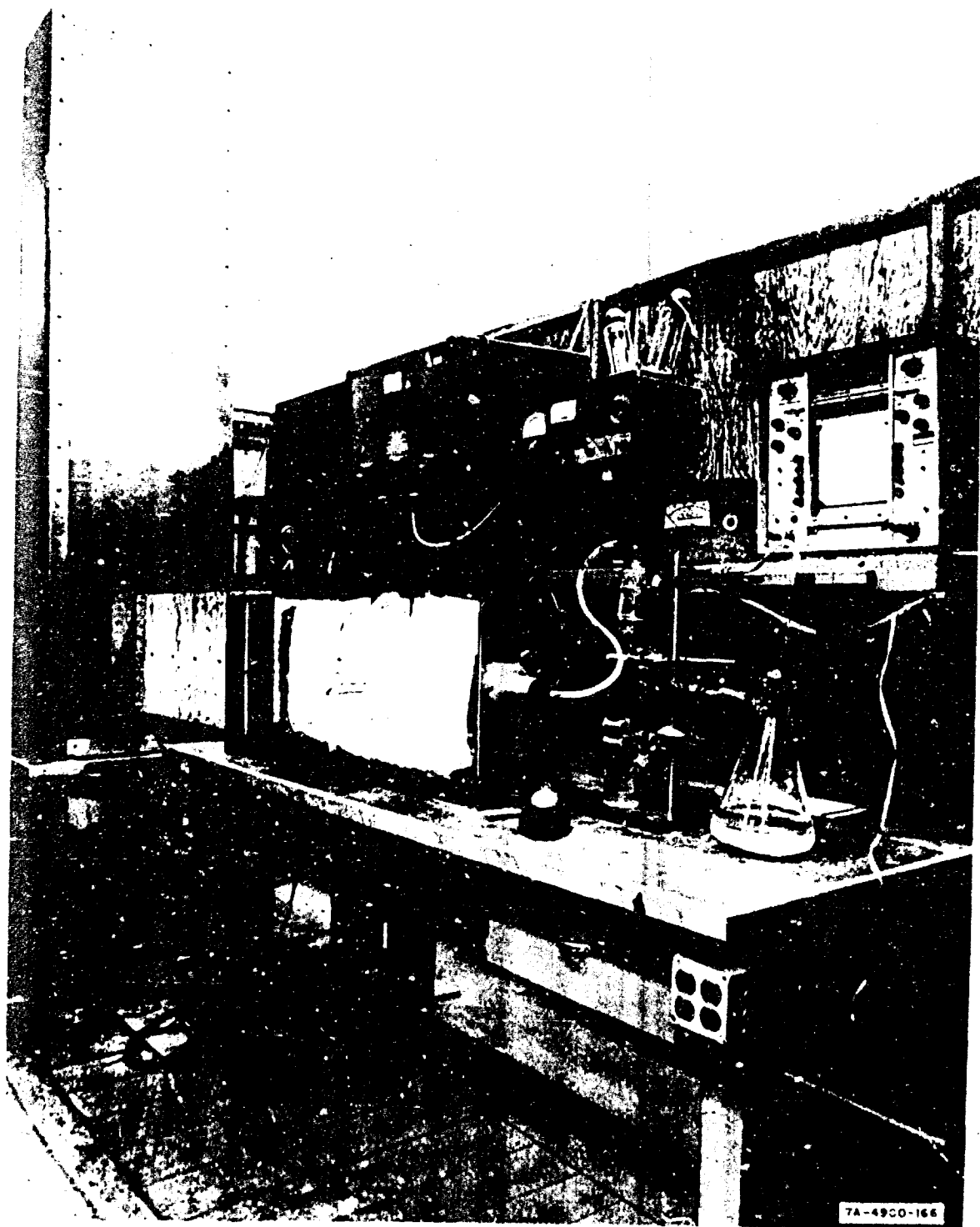


FIG. 4 Continued  
(c) Assembled view of experimental apparatus used in early phase of study



FIG. 4 Continued  
(d) Assembled view of experimental apparatus used in final phase of study

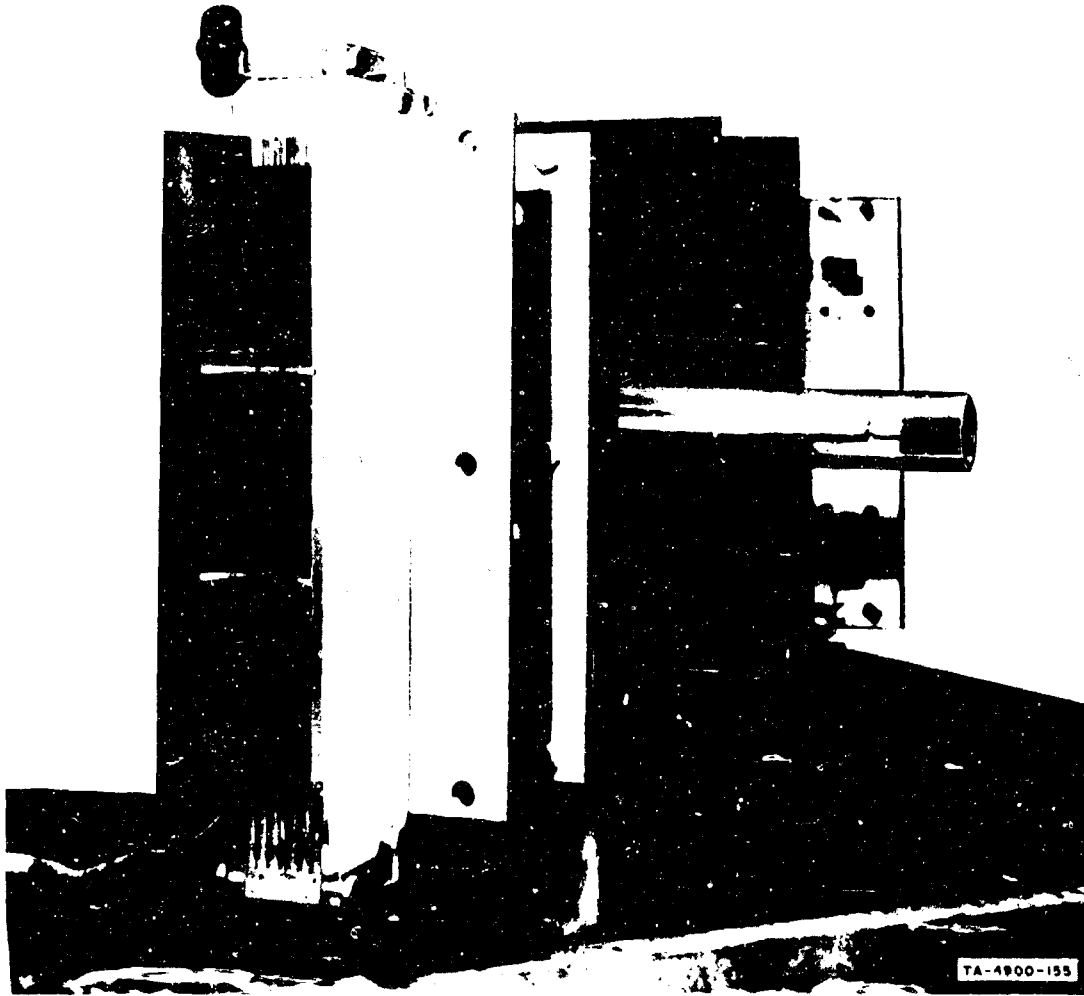


FIG. 4 Continued  
(e) Upstream side of purifier (connected to mobility channel)

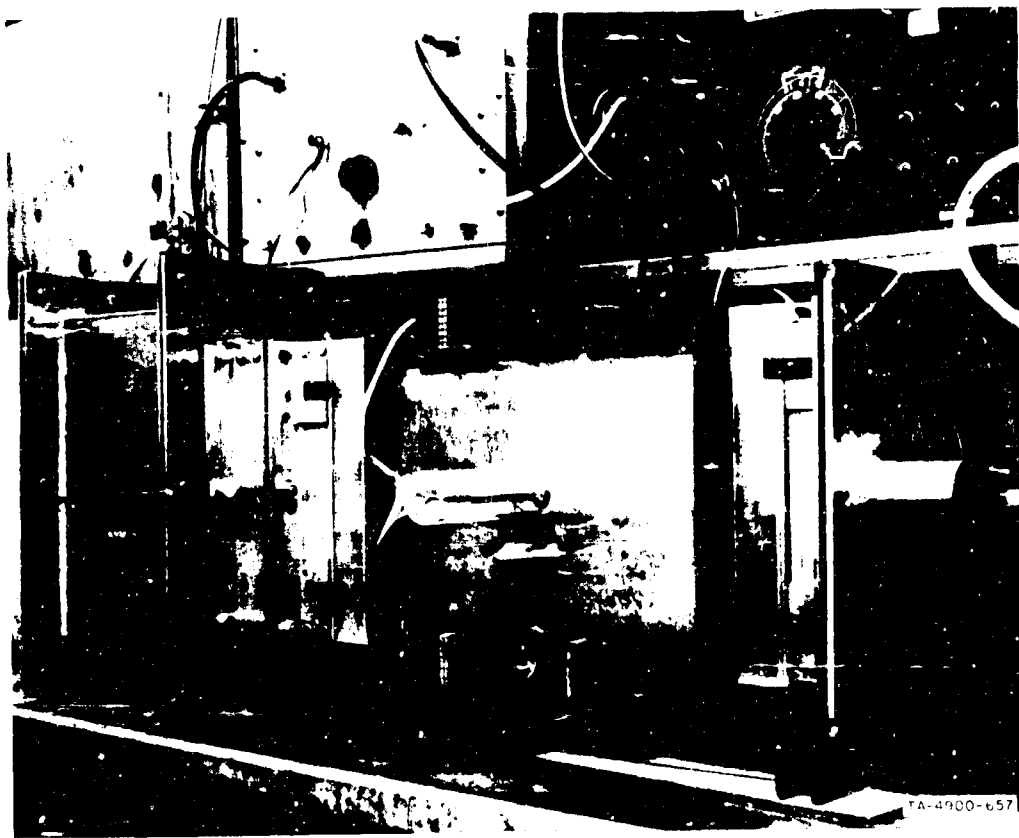
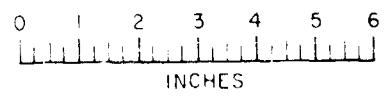


FIG. 4 Continued  
(f) Close-up view of mobility channel

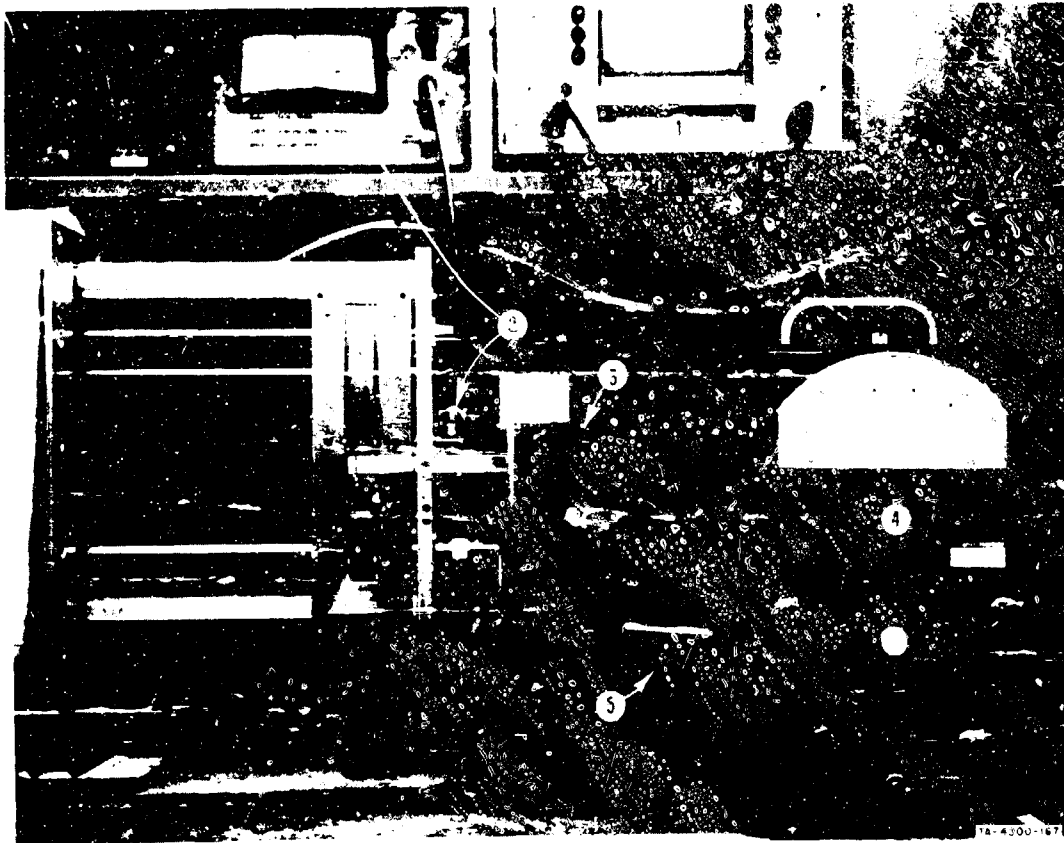


←  
AIR FLOW



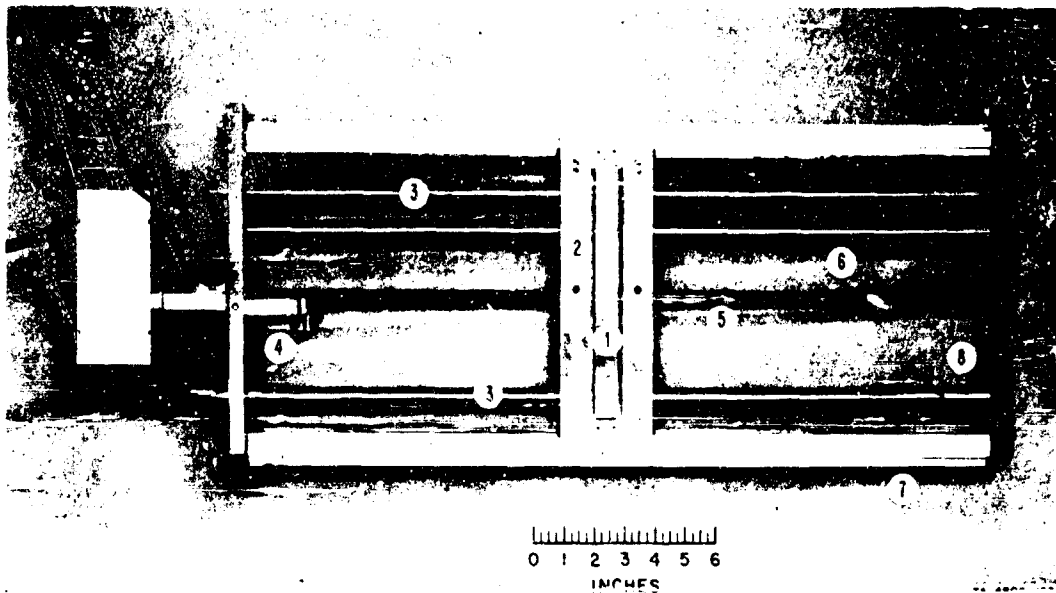
TA-4900-164R

FIG. 4 Continued  
(g) Inside face of mobility channel collection electrode with tapes in place



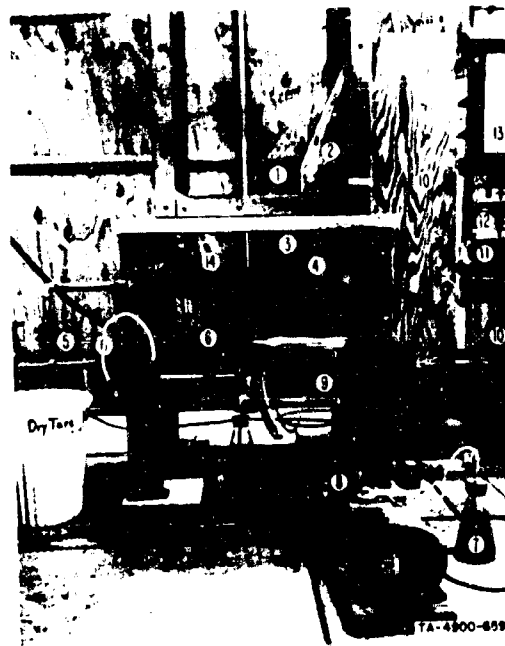
- |                      |                          |
|----------------------|--------------------------|
| ① RECORDER           | ④ ELECTROMETER           |
| ② POSITION INDICATOR | ⑤ CAPACITANCE SWITCH BOX |
| ③ CARRIAGE MOTOR     |                          |

FIG. 4 Continued  
(h) View of probe assembly partially inserted into mobility channel  
(probe electrode exposed) and electrometer



- |                         |                              |
|-------------------------|------------------------------|
| ① PROBE                 | ⑤ PROBE CARRIAGE DRIVE SCREW |
| ② PROBE SHIELD          | ⑥ LIMIT SWITCH CABLES        |
| ③ SLIDE WIRE SHIELDS    | ⑦ GUIDE RAIL                 |
| ④ PROBE GROUNDING CLIPS | ⑧ LIMIT SWITCH               |

FIG. 4 Continued  
 (i) View of probe assembly



- ① SPRAY NOZZLE
- ② HOOD OVER OUTLET TO WOOD CHANNEL
- ③ AEROSOL CHAMBER OUTLET TO SCRUBBER
- ④ COMPRESSED AIR JET TO SCRUBBER
- ⑤ SCRUBBER OUTLET
- ⑥ COMPRESSED AIR SUPPLY LINE TO SPRAY NOZZLE
- ⑦ URANINE SOLUTION SUPPLY

- ⑧ SUPPLY SOLUTION PUMP
- ⑨ SUPPLY SOLUTION ROTAMETER
- ⑩ VERTICAL WOOD CHANNEL
- ⑪ PURIFIER
- ⑫ GUARD PLATE SECTION
- ⑬ MOBILITY CHANNEL
- ⑭ AUXILIARY AIR INLET

FIG. 4 Concluded  
 (j) Details of base of aerosol chamber  
 (k) Liquid supply system for aerosol generation

FIG. 5 EQUIPMENT DETAILS

- a. Aerosol spray nozzle
- b. Aerosol spray and exhaust
- c. Purifier
- d. Mobility channel
- e. Mobility channel electrodes
- f. Probe assembly



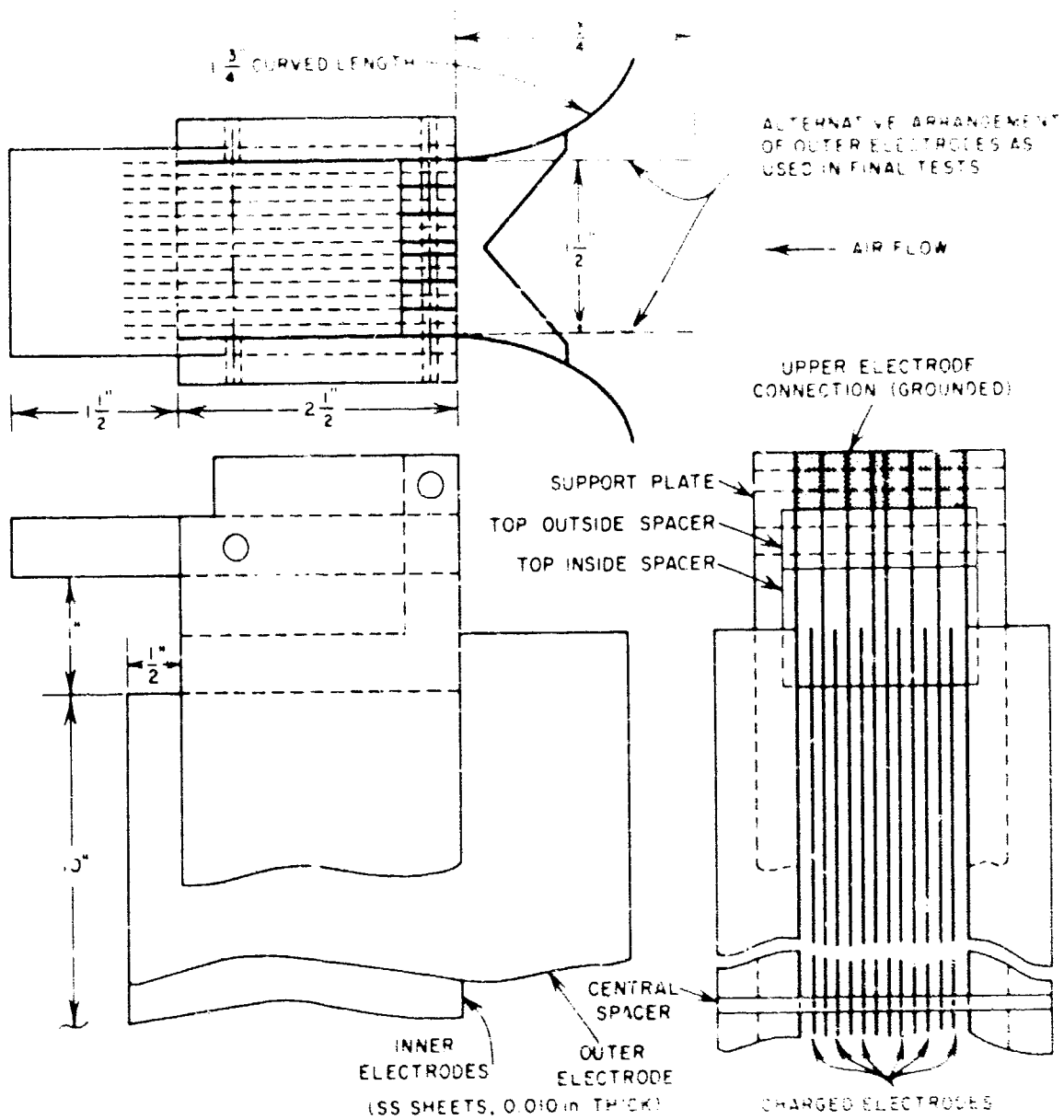


FIG. 5 Continued  
Elect. Purifier

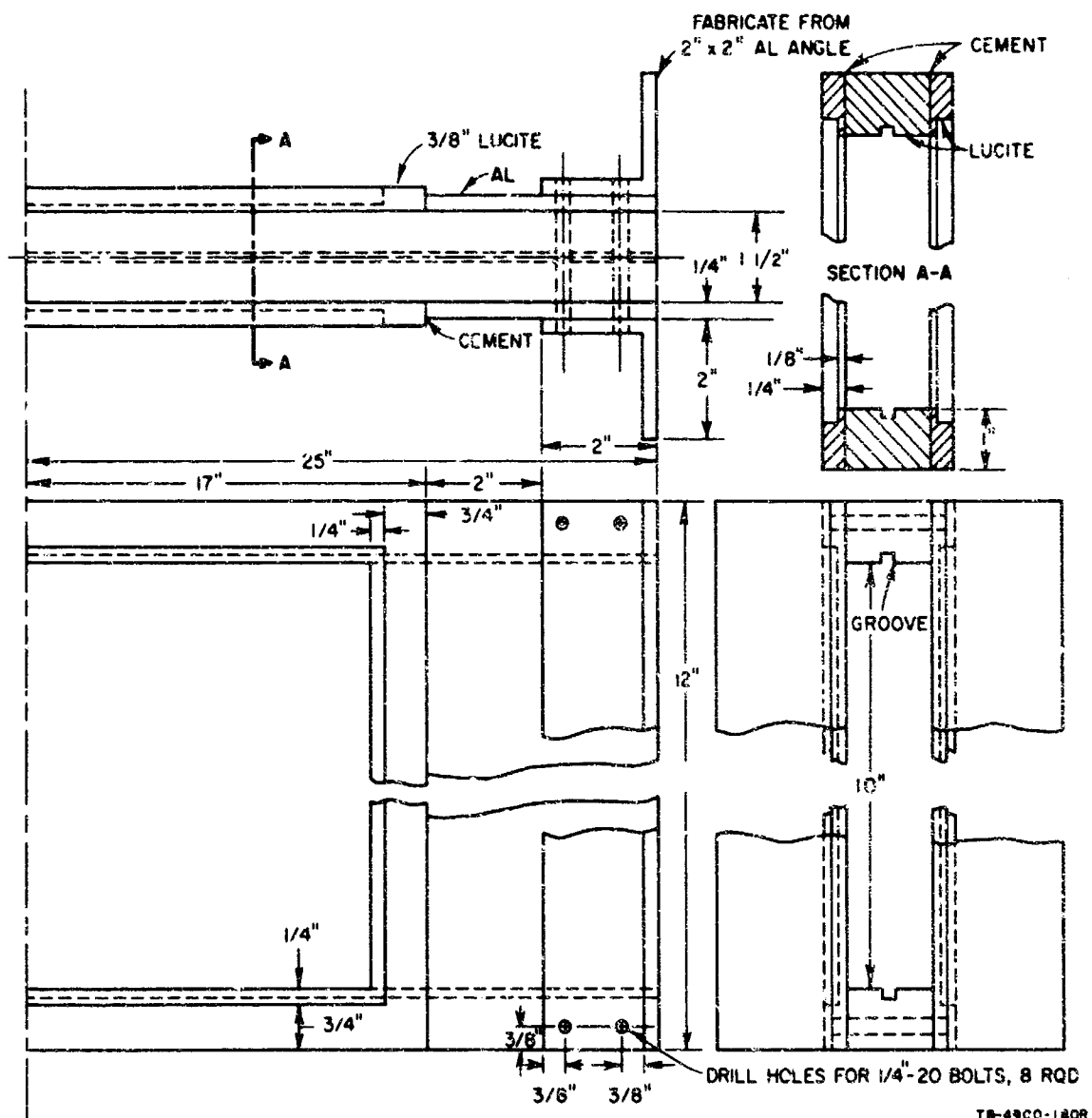
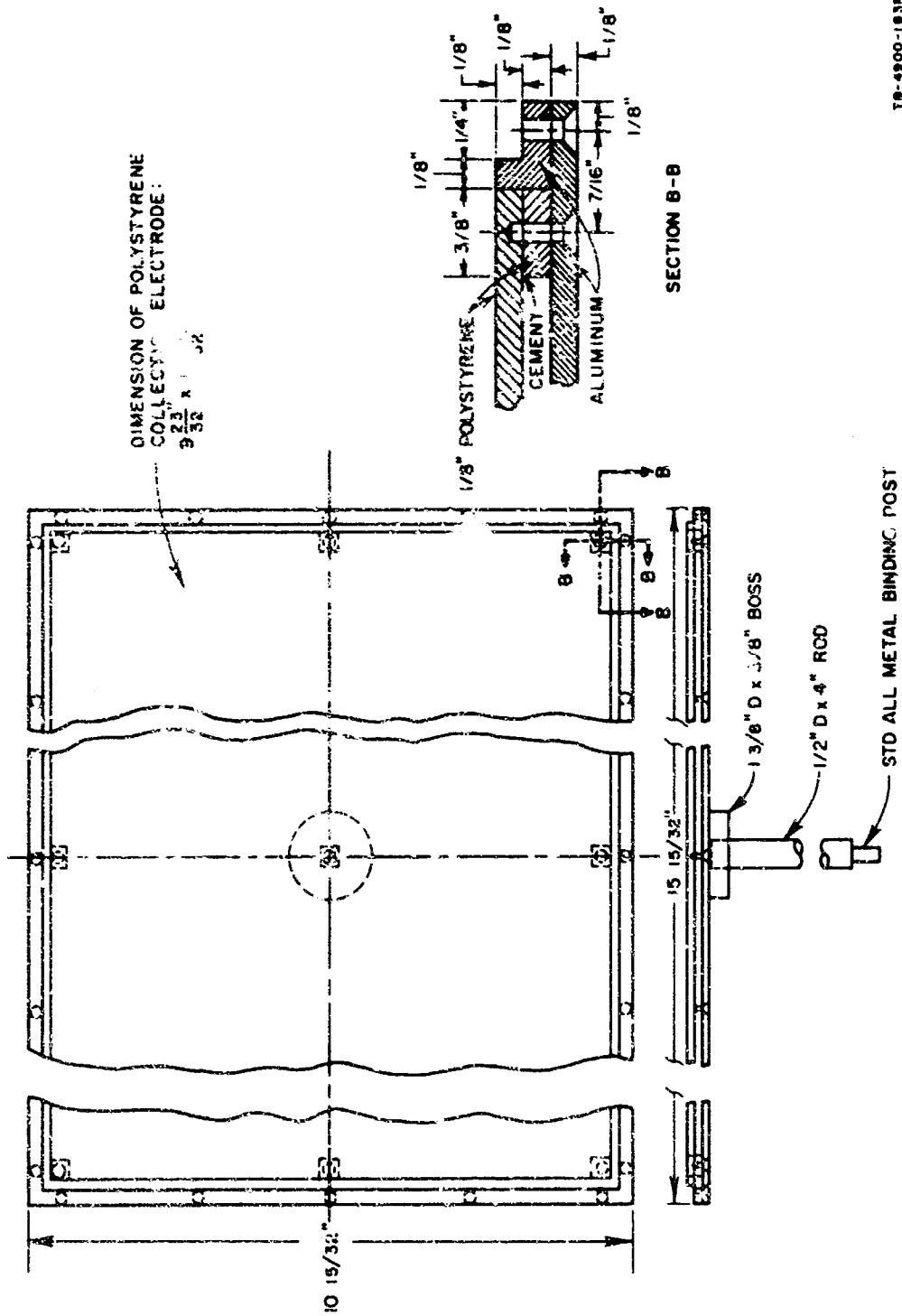
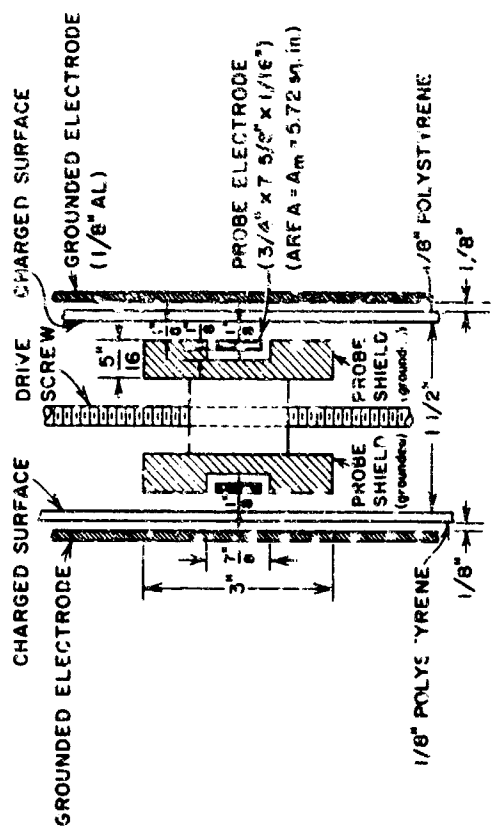
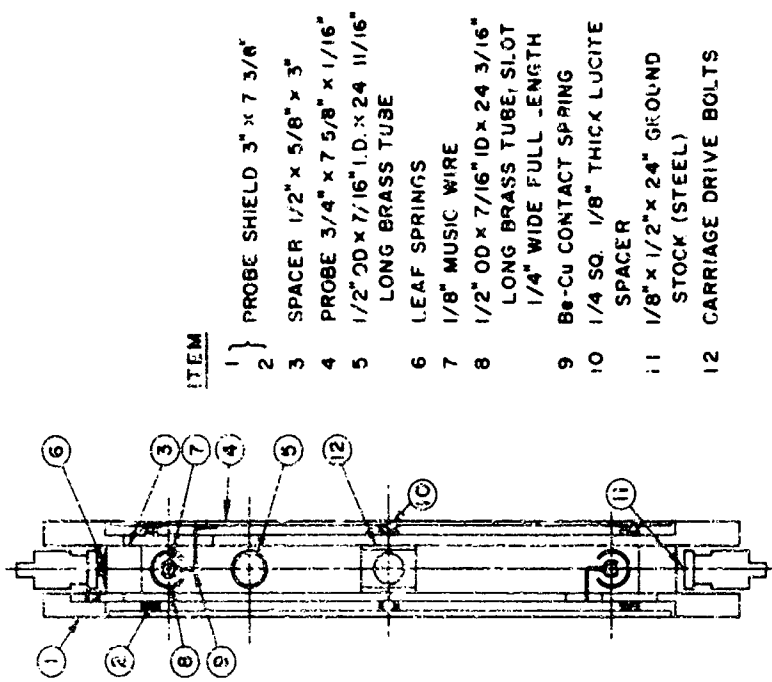


FIG. 5 Continued  
 (d) Mobility channel



TR-4900-183R

FIG. 5 Continued  
 (e) Mobility channel electrodes



CROSS-SECTIONAL TOP VIEW OF PROBE ELEMENT  
IN MOBILITY CHANNEL. (not to scale)

TA-4900-33-H

TA-4900-184

FIG. 5 Concluded  
(f) Probe assembly

77

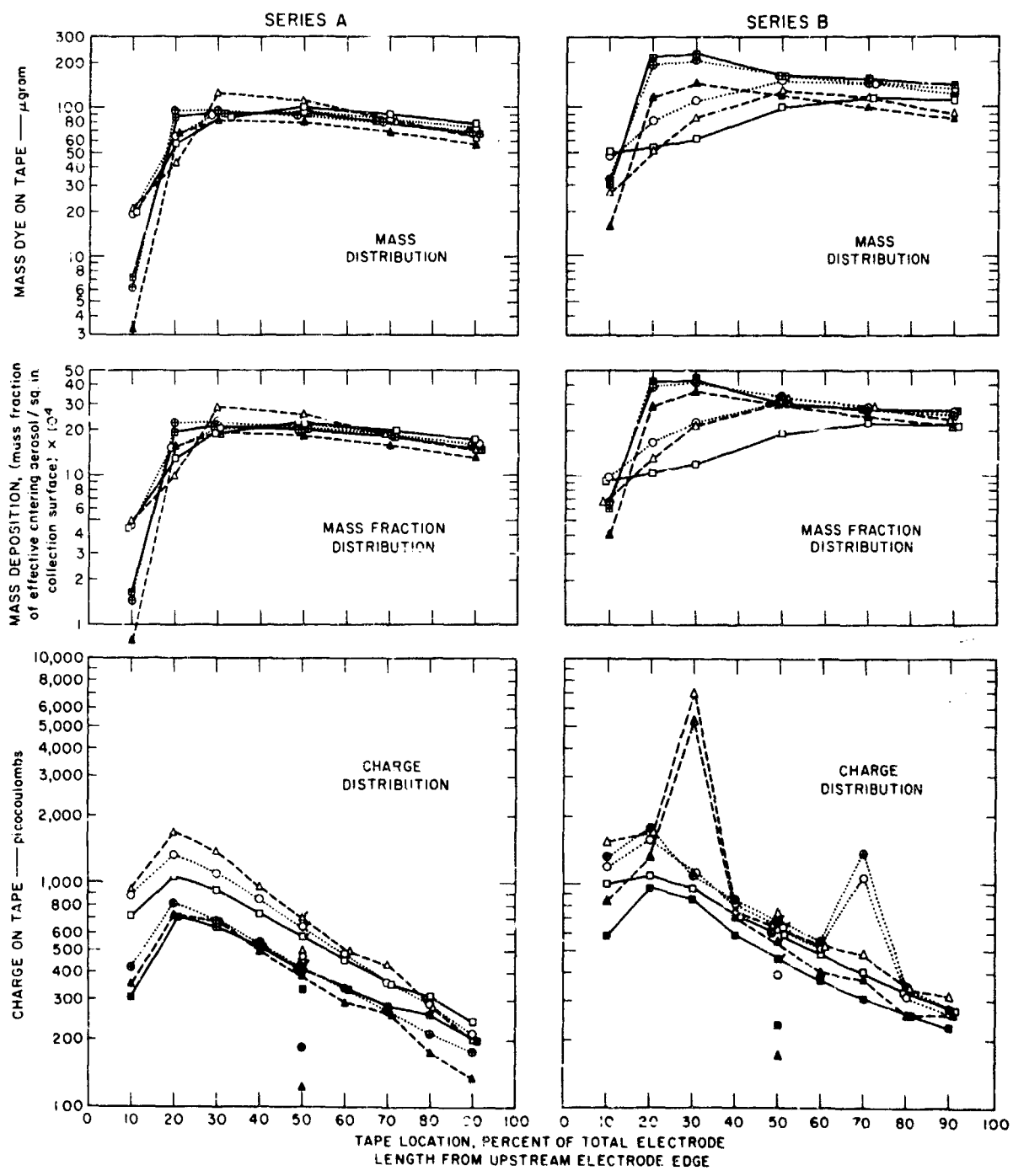
FIG. 6 ANALYSIS OF TAPE DEPOSITS

- a. Measured Values
- b. Calculated Values

Legend:

Run Number		Curve Designation	Symbol for Measured Values	
Series A	Series B		Negative Particles	Positive Particles
A1	B1	.....	○	⊕
A2	B2	-----	△	▲
A3	B3	————	□	⊞

- Note: (1) Dog-ear (e.g. ◊) on symbol indicates that the value was an interpolated value rather than a directly measured value.  
 (2) End of guard plate corresponds to a position of 2.5% of the total electrode length from the upstream electrode edge.



TR-4802-870

FIG. 6 ANALYSIS OF TAPE DEPOSITS  
(a) Measured values

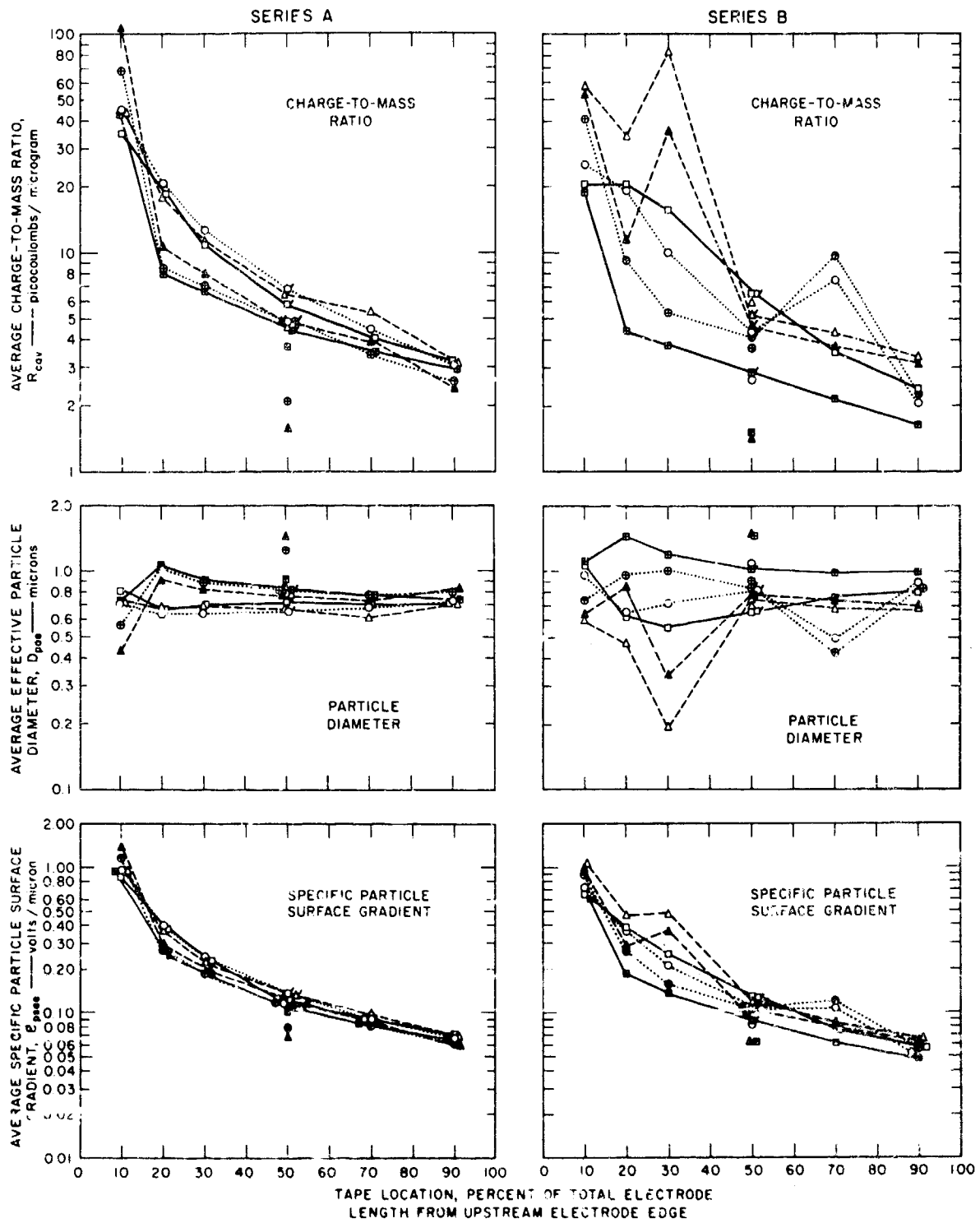
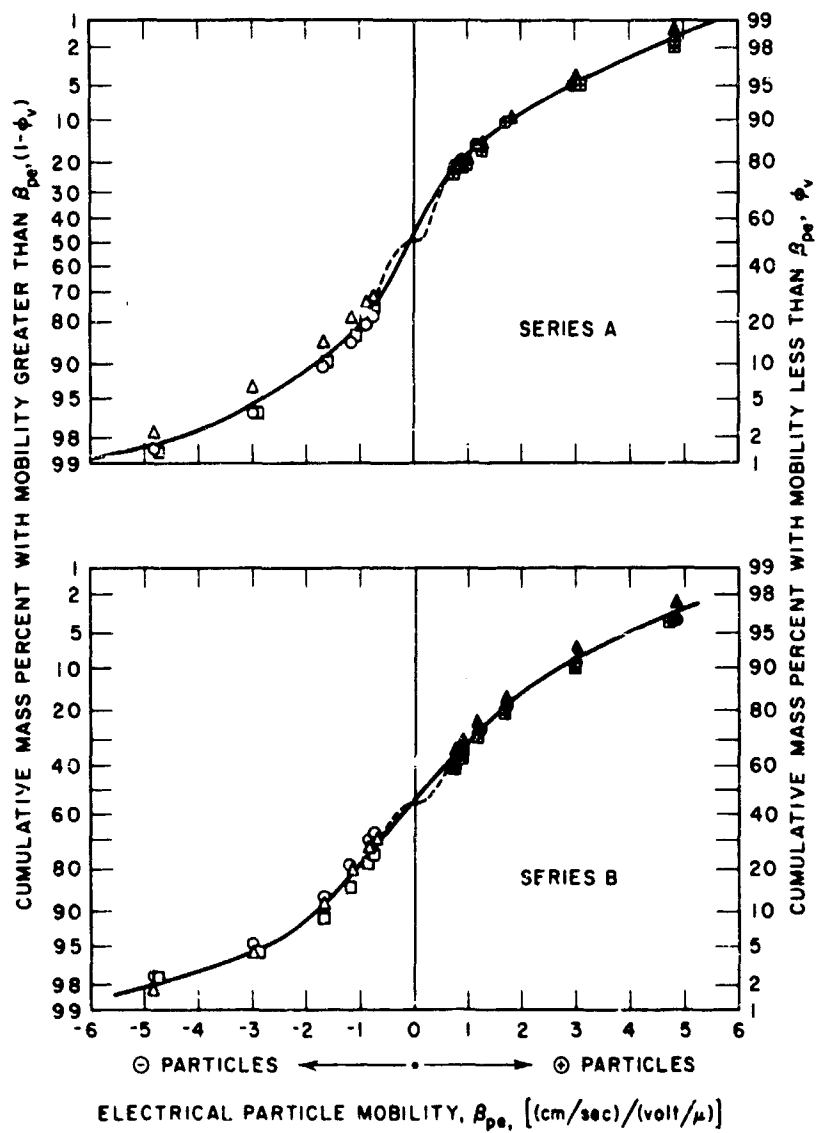


FIG. 6 Continued  
(b) Calculated values

FIG. 7 MOBILITY DISTRIBUTION OF AEROSOL  
a. Cumulative Basis  
b. Frequency Basis

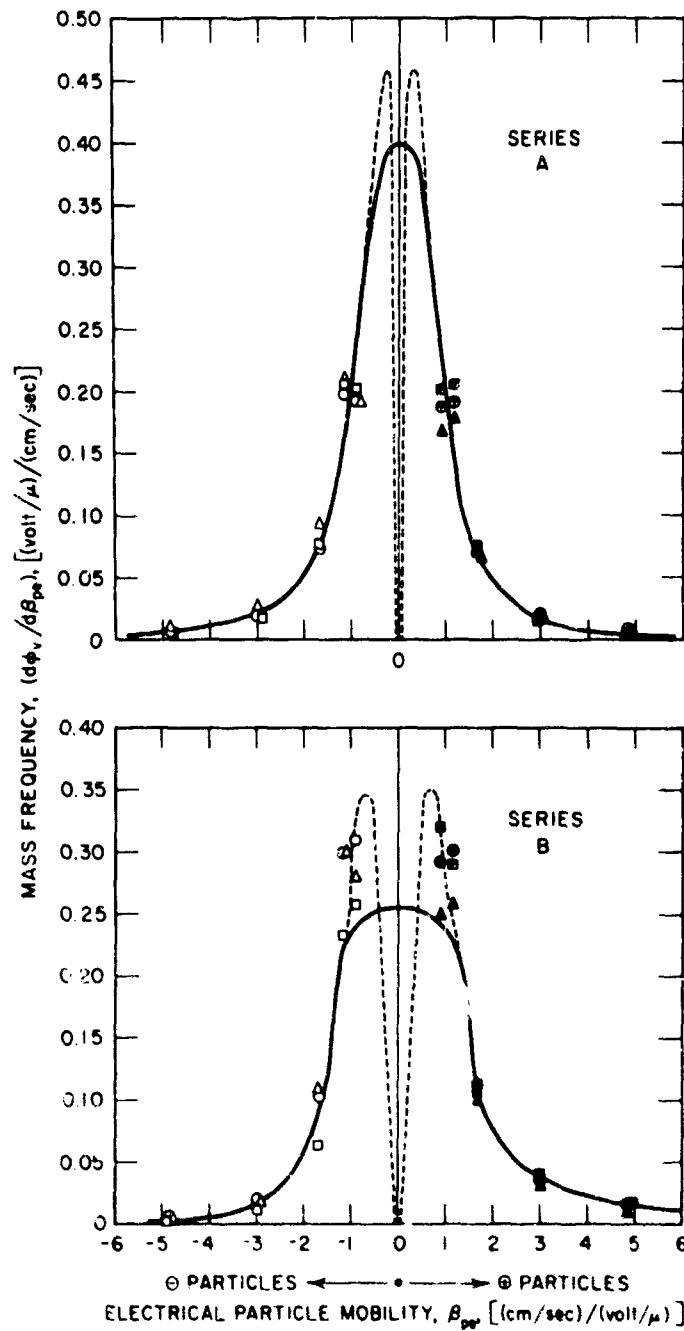
Legend:

Run Number		Symbol	
Series A	Series B	Negative Particles	Positive Particles
A1	B1	○	⊙
A2	B2	△	▲
A3	B3	□	⊞



TC-4900-672

FIG. 7 MOBILITY DISTRIBUTION OF AEROSOL  
(a) Cumulative basis



TC-4900-677

FIG. 7 Continued  
(b) Frequency basis

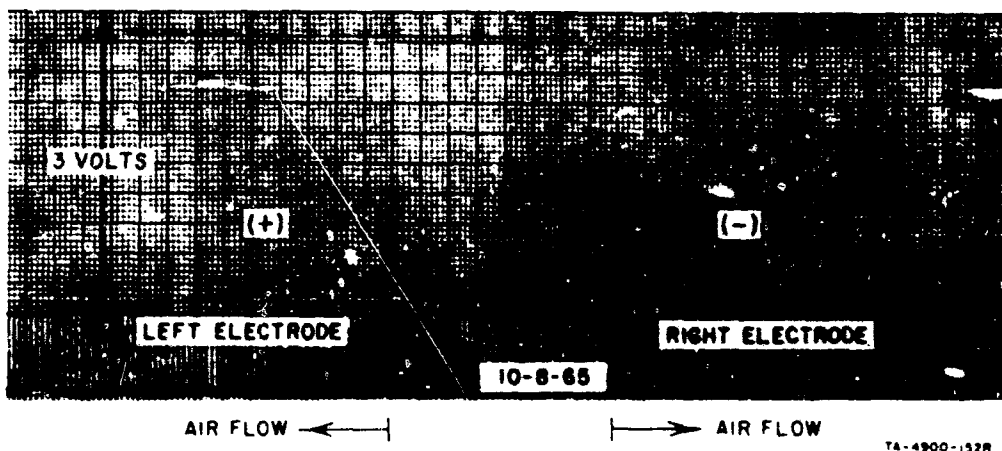


FIG. 8 ILLUSTRATIVE PROBE SCAN RECORD

Table I

## SUMMARY OF MOBILITIES USED IN ANALYSIS OF TAPE DEPOSITS

TAPE NUMBER	TAPE POSITION			MOBILITY DATA		
	Distance From Tape Centerline to Inlet End of Electrode, % of Total Electrode Length	Distance from Tape Centerline to End of Guard Channel*		Mobility For Deposit at Tape Centerline		Change in Mobility Across Tape $\frac{\Delta\beta_{pe}}{\left[\frac{(\text{cm/sec})}{(\text{volt}/\mu)}\right]}$
		in.	L/B	Normalized <sup>†</sup> $\frac{\beta_{pe} \epsilon_o}{u}$ [dimensionless]	Actual <sup>§</sup> $\beta_{pe}$ [cm/sec] [volt/ $\mu$ ]	
1	10	1.10	0.733	0.91	12.9	14.1
2	20	2.57	1.71	0.340	4.83	1.60
3	30	4.04	2.69	0.210	2.98	0.58
4	50	7.00	4.67	0.118	1.67	0.181
5	70	9.94	6.62	0.082	1.16	0.089
6	90	12.90	8.60	0.063	0.90	0.053
-	100	14.38	9.59	0.056	0.72	--

\* front edge of plastic electrode was 3/8-in. upstream of end of guard channel.

† taken as average of normalized mobilities for Case IIIa and Case IIIb (see Fig. C-4)

§ for conditions in Runs A1-A3 and B1-B3 shown in Tables II and III and corrected for dielectric constant of polystyrene electrode (assumed = 2.55). Tape extends  $\pm 3/8$  in. to each side of centerline.

Table II  
SUMMARY OF EXPERIMENTAL DATA

RUN NUMBER	1	2	3	P1	P2	P3
Type of Run	High Potential Power Off			Purifier Power on Only		
Date of run (1966) (Runs listed in chronological order)	6/9	6/14	6/16	6/21	6/22	6/24
<b>Operating conditions</b>						
Ambient temperature, °C	22.3	25.8	21.7	21.3	21.8	20.3
Gas flow rate, cfm						
Entering spray chamber*	8.50 <sup>(3)</sup>	8.50 <sup>(3)</sup>	8.50 <sup>(3)</sup>	8.50 <sup>(3)</sup>	8.50 <sup>(3)</sup>	8.50 <sup>(3)</sup>
Entering wood channel*	0.620	0.620	0.620	0.620	0.572	0.572
<b>Purifier conditions</b>						
Central (unenergized) channel condition	Open	Open	Open	Open	Closed	Closed
Gas velocity in purifier, cm/sec	3.290	3.290	3.290	3.290	3.290	3.290
Gas velocity in mobility channel, cm/sec	3.025	3.025	3.025	3.025	2.792	2.792
<b>Electrical potentials, volts</b>						
Across purifier plates*	0	0	0	-750	-750	-1,500
Across mobility channel*	0	0	0	0	0	0
<b>Filter</b>						
Total time in operation, min	30.0	29.0	28.0	29.0	29.0	29.0
Dye on first filter paper, * mg/min	3.82	3.94	3.66	1.130	0.736	0.34
Dye on next three filter papers, * mg/min	0.00154	0.0713	0.0012	0.0017	0.0013	0.00
% of dye on filter	0.040	1.81	0.033	0.150	0.177	0.46
<b>Mobility channel</b>						
Length of time electrode plates energized, * min	0	0	0	0	0	0
<b>Dye collected on electrodes<sup>(7)</sup></b>						
On (+) electrode, measured, * mg/min	--	--	--	--	--	--
On (+) electrode, calculated, mg/min <sup>(4)</sup>	--	--	--	--	--	--
On (+) electrode, % of dye entering mobility channel	--	--	--	--	--	--
On (-) electrode, measured, * mg/min	--	--	--	--	--	--
On (-) electrode, calculated, mg/min <sup>(4)</sup>	--	--	--	--	--	--
On (-) electrode, % of dye entering mobility channel	--	--	--	--	--	--
Total dye on electrodes, measured, * mg/min	--	--	--	--	--	--
Total dye on electrodes, calculated, mg/min <sup>(4)</sup>	--	--	--	--	--	--
Total dye on electrodes, % of dye entering mobility channel	--	--	--	--	--	--
<b>Dye on non-energized walls<sup>(6)</sup></b>						
mg/min*	(1)					
% of dye entering mobility channel	--	0.0369	0.0180	0.0089	0.0098	0.00
Mobility channel collection efficiency, $\eta_{cm}$	--	0.91	0.49	0.78	1.31	1.54
Total dye entering mobility channel, mg/min	--	4.05	3.68	1.14	0.747	0.34
Dye on special test filter paper, * mg/min	--	--	--	--	--	--
Minimum collectable mobility, (cm/sec)/(volt/ $\mu$ )	--	--	--	--	--	--

Table II  
EXPERIMENTAL DATA

P2	P3	A1	A2	S1	S2	S3	S4	A3	B1	B2	B3
Power on Only		Total System		Spray Chamber Deposition				Total System			
5/22	6/24	7/1	7/8	7/15	8/11	8/12	8/17	8/23	9/7	9/15	9/29
21.8	20.3	21.2	19.6	24.1	24.0	20.9	24.8	23.3	23.4	19.6	24.9
8.50 <sup>(3)</sup>	8.50 <sup>(3)</sup>	8.50 <sup>(3)</sup>	8.50 <sup>(3)</sup>	8.50	8.50	8.50	8.50	8.50	8.50	8.50	8.50
0.572	0.572	0.620	0.620	0	0	0	0	0.620	1.24	1.24	1.24
Closed	Closed	Open	Open	--	--	--	--	Open	Open	Open	Open
3.290	3.290	3.290	3.290	--	--	--	--	3.290	6.59	6.59	6.59
2.792	2.792	3.025	3.025	--	--	--	--	3.025	6.06	6.06	6.06
-750	-1,500	-1,500	-1,500	--	--	--	--	-1,500	-1,500	-1,500	-1,500
0	0	±5,000	±5,000	--	--	--	--	±5,000	±10,000	±10,000	±10,000
29.0	29.0	30.0	30.0	--	--	--	--	30.0	15.0	15.0	15.0
0.736	0.349	0.355	0.283	--	--	--	--	0.368	1.192	0.275	1.820
0.0913	0.0016	0.0076	0.0038	--	--	--	--	0.0019	0.0079	0.0107	0.0049
0.177	0.462	0.739	1.35	--	--	--	--	0.517	0.661	1.223	0.270
0	0	30.0	30.0	--	--	--	--	30.0	15.0	15.0	15.0
--	--	--	--	--	--	--	--	0.0597	0.185	0.1421	0.1480
--	--	0.0609	0.0692	--	--	--	--	0.0635	0.197	0.1502	0.1489
--	--	12.2	16.4	--	--	--	--	11.8 <sup>(5)</sup>	10.9 <sup>(5)</sup>	11.6 <sup>(5)</sup>	6.49 <sup>(5)</sup>
--	--	--	--	--	--	--	--	0.0574	0.220	0.1539	0.2415
--	--	0.0622	0.0520	--	--	--	--	0.0620	0.239	0.1660	0.2525
--	--	12.4	12.3	--	--	--	--	11.4 <sup>(5)</sup>	13.0 <sup>(5)</sup>	12.6 <sup>(5)</sup>	10.60 <sup>(5)</sup>
--	--	--	--	--	--	--	--	0.117	0.405	0.296	0.389
--	--	0.123	0.121	--	--	--	--	0.126	0.436	0.316	0.401
--	--	24.6	28.7	--	--	--	--	23.2 <sup>(5)</sup>	23.9 <sup>(5)</sup>	24.2 <sup>(5)</sup>	17.1 <sup>(5)</sup>
0.0098	0.0055	0.019	0.014	--	--	--	--	0.014	0.073	0.042	0.0639
1.31	1.54	3.80	3.25	--	--	--	--	2.79	4.31	3.40	2.80
--	--	0.505	0.539	--	--	--	--	0.460	0.720	0.650	0.507
0.747	0.356	0.500	0.422	--	--	--	--	0.501 <sup>(5)</sup>	1.678 <sup>(5)</sup>	1.224 <sup>(5)</sup>	2.778 <sup>(5)</sup>
--	--	0.482	0.407	--	--	--	--	0.524	1.640	1.127	2.060
--	--	0.72	0.72	--	--	--	--	0.72	0.72	0.72	0.72

2

Table III  
DETAILS OF TAPE DEPOSITS FOR RUNS A1-A3 AND

QUANTITY	TAPE LOCATION <sup>(1)</sup>			Series A (Low Air Rate)			
	Distance <sup>(1)</sup>		Corresponding <sup>(3)</sup> Mobility $\beta_{pe}$ [ (cm/sec) / (volt/ $\mu$ ) ]	Run A1		Run A2	
	Inches	% Of Total Electrode Length		Positive Particles	Negative Particles	Positive Particles	Negative Particles
Total Mass on Tape, <sup>(2)</sup> micrograms (measured)	1.48 2.95 4.42 7.38 10.32 13.28	10 20 30 50 70 90	12.9 4.83 2.98 1.67 1.16 0.90	6.2 94.0 95.4 87.5 78.4 67.8	19.6 64.1 86.9 92.1 80.5 68.9	3.34 66.8 82.1 78.4 67.3 56.2	21.2 42.6 121.9 108.6 80.0 63.6
Fractional Mass Deposition <sup>(7)</sup> (mass fraction/in <sup>2</sup> ) $\times 10^4$ (calculated)	1.48 2.95 4.42 7.38 10.32 13.28	10 20 30 50 70 90	12.9 4.83 2.98 1.67 1.16 0.90	1.46 22.13 22.43 20.60 18.46 15.96	4.61 15.10 20.45 21.65 18.94 16.21	0.78 15.60 19.20 18.30 15.70 13.13	4.95 9.95 28.45 25.38 18.69 14.87
Total Charge on Tape, picocoulombs (measured)	1.48 2.95 4.42 5.90 7.38 7.38 8.85 10.32 11.80 13.28	10 20 30 40 50 50 <sup>(5)</sup> 60 70 80 90	12.9 4.83 2.98 2.14 1.67 1.67 1.38 1.16 1.00 0.90	421 802 668 533 182 415 330 243 208 173	880 1316 1088 843 444 628 472 355 281 209	355 714 655 491 122 380 289 261 171 134	936 1662 1367 954 492 698 488 424 277 199
Charge-to-Mass Ratio, picocoulombs/microgram (calculated)	1.48 2.95 4.42 7.38 7.38 10.32 13.28	10 20 30 50 50 <sup>(5)</sup> 70 90	12.9 4.83 2.98 1.67 1.67 1.16 0.90	67.8 8.53 7.00 2.07 4.74 3.39 2.55	44.8 20.5 12.52 4.82 6.81 4.41 3.03	106.3 10.69 7.97 1.564 4.84 3.87 2.37	44.1 17.9 11.2 4.53 6.42 5.30 3.12
Average Particle Diameter, microns (calculated)	1.48 2.95 4.42 7.38 7.38 10.32 13.28	10 20 30 50 50 <sup>(5)</sup> 70 90	12.9 4.83 2.98 1.67 1.67 1.16 0.90	0.557 1.019 0.872 1.230 0.786 0.774 0.787	0.703 0.628 0.632 0.779 0.643 0.669 0.716	0.428 0.901 0.813 1.429 0.777 0.718 0.818	0.705 0.678 0.673 0.806 0.665 0.603 0.703
Average Specific Particle Surface Gradient, volts/micron (calculated)	1.48 2.95 4.42 7.38 7.38 10.32 13.28	10 20 30 50 50 <sup>(5)</sup> 70 90	12.9 4.83 2.98 1.67 1.67 1.16 0.90	1.096 0.252 0.177 0.0741 0.1830 0.0762 0.0583	0.915 0.374 0.230 0.1091 0.1271 0.0856 0.0630	1.323 0.280 0.1881 0.0649 0.1093 0.0809 0.0565	0.908 0.353 0.219 0.106 0.123 0.092 0.053
Total Equivalent Mass of Dye Entering <sup>(4)</sup> Mobility Channel, micrograms				7310		7360	

- (1) Position of the center of the tape, measured from the upstream edge of the polystyrene mobility plate.
- (2) Each tape was 7.75 inches long and 0.75 inch wide; the downstream edge of the guard plate is 3/8 inch downstream of the upstream edge of the tape.
- (3) The corresponding mobility at a point in the mobility channel is a function only of the ratio of gas velocity to plate voltage. This ratio was 0.0015.
- (4) This quantity is one-thirteenth of the amount of dye entering the purifier during the run.
- (5) The second value given for total charge at the 50% position is an interpolated value obtained from a smooth curve through the rest of the points. The interpolated value of total charge is 7.38 micrograms.
- (6) In this run the sign of the potential on the electrodes was the reverse of what it was for Runs B2 and B3 and Runs A1-A3.
- (7) Calculated by dividing total mass on tape by area of tape (5.8 sq. in.) and by total equivalent mass entering mobility channel. <sup>(4)</sup>

FOR RUNS A1-A3 AND B1-B3

VALUE OF QUANTITY									
Series A (Low Air Rate)				Series B (High Air Rate)					
Run A2		Run A3		Run B1 <sup>(6)</sup>		Run B2		Run B3	
Positive Particles	Negative Particles	Positive Particles	Negative Particles	Positive Particles	Negative Particles	Positive Particles	Negative Particles	Positive Particles	Negative Particles
3.34	21.2	7.25	20.14	32.6	47.5	16.0	26.7	30.9	49.6
66.8	42.6	86.4	57.2	190.5	81.7	114.8	50.7	216.3	53.0
82.1	121.9	93.7	84.8	204.0	110.0	145.2	85.3	223.5	61.2
78.4	108.6	90.1	99.1	164.1	149.0	118.7	124.8	160.0	97.1
67.3	80.0	78.9	87.4	142.1	140.8	98.6	113.3	143.4	114.5
56.2	63.6	65.7	75.7	121.4	128.3	83.8	94.6	139.2	111.7
0.78	4.95	1.54	4.54	6.64	9.66	4.03	6.74	6.01	9.63
15.66	9.95	19.50	12.91	38.80	16.64	29.00	12.80	42.10	10.30
19.20	28.45	21.15	19.14	41.50	22.40	36.60	21.53	43.50	11.90
18.30	25.38	20.35	22.38	33.40	30.32	29.96	31.50	31.05	18.88
15.70	18.69	17.80	19.73	28.96	28.64	24.90	29.60	27.85	22.22
13.13	14.87	14.83	17.10	24.73	26.14	21.15	23.85	27.00	21.65
355	936	309	708	1320	1192	847	1537	586	1009
714	1662	701	1055	1769	1561	1320	1714	951	1089
655	1367	629	916	1082	1109	5228	7049	847	961
491	954	513	727	845	817	713	766	589	718
122	492	331	466	599	391	171	740	233	632
380	698	407	573	682	637	552	643	458	632
289	488	331	452	553	513	405	520	371	484
261	424	277	353	1378	1056	373	485	308	404
171	277	256	309	350	315	257	343	257	333
134	199	196	238	276	265	263	316	228	266
106.3	44.1	42.7	35.2	40.5	25.1	52.9	57.5	18.96	20.3
10.69	17.9	8.11	18.4	9.28	19.12	11.50	33.7	4.40	20.5
7.97	11.2	6.71	10.8	5.30	10.09	36.0	82.5	3.78	15.70
1.564	4.53	3.68	4.70	3.65	2.62	1.442	5.92	1.457	6.50
4.84	6.42	4.52	5.79	4.16	4.28	4.64	5.16	2.86	6.50
3.87	5.30	3.50	4.04	9.69	7.49	3.78	4.28	2.15	3.72
2.37	3.12	2.97	3.14	2.27	2.07	3.12	3.34	1.639	2.38
0.428	0.709	0.722	0.804	0.744	0.967	0.641	0.611	1.124	1.083
0.901	0.678	1.046	0.667	0.973	0.654	0.866	0.472	1.450	0.628
0.813	0.673	0.893	0.687	1.015	0.713	0.339	0.197	1.215	0.556
1.429	0.806	0.903	0.790	0.908	1.084	1.491	0.695	1.483	0.660
0.777	0.665	0.807	0.704	0.845	0.832	0.795	0.750	1.035	0.660
0.718	0.603	0.759	0.702	0.425	0.494	0.728	0.680	0.992	0.758
0.818	0.703	0.723	0.702	0.839	0.882	0.703	0.678	1.002	0.817
1.323	0.908	0.895	0.821	0.875	0.704	0.984	1.021	0.619	0.639
0.280	0.353	0.246	0.357	0.262	0.363	0.289	0.463	0.1851	0.374
0.1881	0.219	0.1740	0.215	0.1561	0.209	0.356	0.473	0.1336	0.253
0.0649	0.1060	0.0965	0.1078	0.0961	0.0827	0.0924	0.1195	0.0627	0.1245
0.1002	0.1239	0.1059	0.1183	0.1020	0.1034	0.1073	0.1122	0.0860	0.1245
0.0809	0.0928	0.0773	0.0824	0.1196	0.1076	0.0800	0.0845	0.0619	0.0775
0.0565	0.0638	0.0624	0.0639	0.0553	0.0531	0.0638	0.0657	0.0477	0.0565
7360		7620		8450		6820		8850	

upstream edge of the polystyrene mobility plate.

voltage. This ratio was purposely kept constant for each of the six runs.

the rest of the points. The second value of each subsequent quantity at the 50% position is based on this

channel. (4)

2

Table II (Concluded)

RUN NUMBER	1	2	3	P1	P2	P3
Type of Run	High Potential Power Off			Purifier Power on Only		
<b>Purifier</b>						
Total time in operation, min	--	30.0	29.0	30.0	30.0	30.0
Dye collected on plates	(1)					
mg/min*	--	0.0292	0.0174	2.41	2.65	2.84
% of dye entering purifier	--	0.72	0.47	68.0	80.3	89.0
Purifier collection efficiency, $\eta_p$	--	--	--	0.736	0.845	0.96
Minimum collectable mobility, (cm/sec)/(volt/ $\mu$ )	--	--	--	0.409	0.409	0.20
<b>Wood channel</b>						
Dye collected on walls						
mg/min*	0.200 <sup>(1)</sup>	0.418	0.311	0.364	0.358	0.35
% of dye entering wood channel <sup>(2)</sup>	4.98	9.31	7.76	9.29	9.80	9.92
<b>Aerosol spray chamber</b>						
Total time in operation, min	55.0	60.0	60.0	65.0	65.0	65.0
Dye sprayed,* mg/min	61.0	65.6	60.2	59.6	60.4	58.4
mg/cu ft <sup>(3)</sup>	7.18	7.72	7.09	7.01	7.11	6.87
Dye on walls						
mg/min*	7.58	5.71	5.67	7.07	8.41	8.68
% of dye sprayed	12.4	8.72	9.43	11.86	13.9	14.8
Dye entering wood channel, mg/min						
As measured*	4.02	4.49	4.01	3.92	3.76	3.55
As calculated from gas flow rates	3.90	4.64	4.22	3.79	3.75	3.58
% deviation, calculated from measured	-3.0	+3.3	+5.2	-3.3	-0.3	+0.9
<b>Scrubber</b>						
Total time of sampling, min	30.5	10.0	10.0	12.0	15.0	15.0
Dye entering, mg/min	49.4 <sup>(2)</sup>	55.4 <sup>(2)</sup>	50.5 <sup>(2)</sup>	48.6 <sup>(2)</sup>	48.3 <sup>(2)</sup>	46.2 <sup>(2)</sup>
Dye collected,* mg/min	46.8	54.5	50.4	47.2	46.9	46.2
Collection efficiency, %	94.8	98.5	99.8	97.2	97.2	100

\* Items that were measured directly.

- (1) Dye on walls of wood channel, purifier, and mobility channel combined. Deposition for all channels shown under wood channel.
- (2) Based on measured value of dye entering wood channel.
- (3) An additional air flow of up to 0.3 cfm into the aerosol spray chamber may have been present due to a leak around the compressed-air atomizer.
- (4) Dye on electrode plates calculated by graphical integration of dye on the individual tapes.
- (5) Determined from "measured" values.
- (6) Where mobility channel was not energized, includes deposition on electrode plates. Otherwise it includes only deposits in the guard plate.
- (7) Negatively charged particles are collected on (+) electrode, positively charged particles on (-) electrode.

Table II (Concluded)

P2	P3	A1	A2	S1	S2	S3	S4	A3	B1	B2	B3
Power on Only		Total System		Spray Chamber Deposition				Total System			
30.0	30.0	52.0	61.0	--	--	--	--	48.0	32.0	38.0	35.0
2.65	2.84	2.67	2.50	--	--	--	--	2.80	5.63	4.69	5.39
80.3	89.0	84.2	85.7	--	--	--	--	84.9	76.9	79.4	70.5
0.845	0.964	0.913	0.928	--	--	--	--	0.920	0.834	0.860	0.762
0.409	0.204	0.204	0.204	--	--	--	--	0.204	0.409	0.409	0.409
0.358	0.352	0.332	0.329	--	--	--	--	0.335	0.416	0.437	0.555
9.80	9.92	9.49	10.1	--	--	--	--	9.21	5.38	6.38	6.74
65.0	65.0	83.0	92.0	--	--	--	--	87.0	71.0	70.0	90.0
60.4	58.4	59.6	57.4	63.4	63.2	59.2	64.4	62.4	62.4	57.4	64.4
7.11	6.87	7.01	6.76	7.46	7.44	6.97	7.58	7.34	7.34	6.75	7.58
8.41	8.68	10.03	11.56	6.35	6.44	6.46	5.95	10.03	6.28	13.20	7.45
13.9	14.8	16.9	20.2	10.0	10.2	10.9	9.25	16.1	10.05	23.0	11.6
3.76	3.55	3.50	3.25	--	--	--	--	3.64	7.74	6.35	6.23
3.75	3.58	3.62	3.35	--	--	--	--	3.82	8.18	6.44	8.32
-0.3	+0.9	+3.4	+3.1	--	--	--	--	+4.9	+5.7	+1.4	+1.1
15.0	15.0	15.0	15.0	15.0	15.0	15.0	15.0	15.0	13.0	13.0	13.0
48.3 <sup>(2)</sup>	46.2 <sup>(2)</sup>	46.1 <sup>(2)</sup>	42.6 <sup>(2)</sup>	57.0	56.8	52.7	50.8	48.7 <sup>(2)</sup>	48.4 <sup>(2)</sup>	37.8 <sup>(2)</sup>	48.7 <sup>(2)</sup>
46.9	46.2	45.3	40.8	53.8	55.0	49.6	48.4	44.9	46.0	36.3	46.4
97.2	100	98.2	95.7	94.6	96.8	94.1	95.4	92.2	95.0	96.9	95.3

channel.

compressed-air atomizer nozzle threads. This leakage was neglected in all calculations.

in the guard plate duct and in the mobility channel upstream and downstream of the electrodes.

2

Table IV  
SPECIFICATIONS FOR MAJOR UNITS OF COMMERCIAL EQUIPMENT USED

EQUIPMENT NAME	MANUFACTURER	NO. USED	SPECIFICATIONS
Feed Pump	Sigmamotor, Inc. Berkeley, Calif.	1	Finger-type peristaltic pump; T-8 series with No. 786 Zero-Max transmission drive; 1/8 hp
Vacuum Pump	Welch Mfg. Co. Chicago, Ill.	1	Two-stage vacuum-pump with vented exhaust; "D.o-Seal" Model No. 1397B; free air capacity 425 liters/min; 1 hp
Ionizing Bar	Nuclear Products Co. El Monte, Calif.	2	6-in. long, each 2000 microcuries of Po <sup>210</sup>
Probe Carriage Motor	Bodine Electric Co. Chicago, Ill.	1	8.5 watt synchronous gear motor; 1.3 in.-oz torque; 300 rpm output; Model No. KYC-23R6
Probe Position Indicator	Bourns, Inc. Riverside, Calif.	1	10-turn potentiometer; 1000 ohms $\pm$ 3% $\pm$ 0.2% linearity; Model No. 35505-1-102
Purifier Power Supply	Calibration Standards Corp. Alhambra, Calif.	1	0-3100 volt regulated power supply; Model No. 127
Mobility Channel Power Supply	Spellman High Voltage Co. Bronx, N.Y.	2	0-60,000 volt power supply; reversible polarity; 1 ma output current; Model No. LA5-60PN
Electrometer	General Radio Co. Los Altos, Calif.	1	High-impedance electrometer and DC amplifier; voltage ranges 0-30 millivolts to 0.10 volts; input impedance $10^{14}$ ohms; Model No. 1230-A
Fluorometer	G. K. Turner Associates Palo Alto, Calif.	1	Split-beam servo-driven fluorometer with automatic readout; ultimate sensitivity for uranine $\sim 10^{-6}$ ppm; Model No. 111

Table V  
EVALUATION OF TAPE DEPOSIT DATA

TYPE PROPERTY	SERIES A DATA		SERIES B DATA*		COMPARISON BETWEEN SERIES A AND SERIES B DATA*
	Average Spread From Mean	Remarks	Average Spread From Mean	Remarks	
Mass Fraction	±10%	⊖ particles slightly higher than ⊕	±20%	⊕ particles somewhat higher; greatest spread at high mobility end	Series B values 50% higher than Series A
Charge	±10%	⊖ particles 50% greater than ⊕	±20%	⊖ particles mostly 10% higher than ⊕	Series B values 25% higher than Series A
Average Charge-to-Mass Ratio	±20%	⊖ particles 30% higher than ⊕	±30%	Trend between ⊖ and ⊕ particles mixed	Series B values 20% lower than Series A
Average Particle Diameter	±5%	⊖ particles 15% smaller than ⊕	±20%	Trend between ⊖ and ⊕ particles mixed	Series B values 10% larger than Series A
Average Specific Particle Surface Gradient	±5%	⊖ particles 10% higher than ⊕	±10%	Trend between ⊖ and ⊕ particles mixed	Little differences on average between Series A and Series B values

\* Not including two sets of peak values for Runs B1 and B2

Table VI

## SUMMARY OF AEROSOL MOBILITY DISTRIBUTION DATA

RUN NUMBER	TAPE NUMBER	ELECTRICAL PARTICLE MOBILITY [(cm/sec)/(volt/ $\mu$ )]		POSITIVE PARTICLES		NEGATIVE PARTICLES	
		Value at Tape Centerline $\beta_{pe}$	Difference Across Tape $\Delta\beta_{pe}$	Mass Frequency $\Delta\phi_v/\Delta\beta_{pe}$ [cm/sec] <sup>-1</sup> [volt/ $\mu$ ]	Cumulative Mass Fraction With Mobility Less Than $\beta_{pe}$ $\phi_v$	Mass Frequency $\Delta\phi_v/\Delta\beta_{pe}$ [cm/sec] <sup>-1</sup> [volt/ $\mu$ ]	Cumulative Mass Fraction With Mobility Less Than $\beta_{pe}$ $\phi_v$
A1	1	12.9	14.1	0.00015	0.9998	0.00041	0.0011
	2	4.83	1.60	0.00917	0.9824	0.00625	0.0147
	3	2.98	0.58	0.0199	0.9529	0.0181	0.0374
	4	1.67	0.181	0.0698	0.896	0.0734	0.0944
	5	1.16	0.089	0.132	0.847	0.197	0.1444
	6	0.90	0.053	0.168	0.802	0.191	0.1904
	P*	0.72	--	--	0.783	--	0.2118
A2	1	12.9	14.1	0.000076	0.9999	0.00049	0.0010
	2	4.83	1.60	0.00708	0.9874	0.00979	0.0224
	3	2.98	0.58	0.0186	0.9585	0.0276	0.0619
	4	1.67	0.181	0.0679	0.9032	0.0941	0.1445
	5	1.16	0.089	0.179	0.856	0.212	0.2111
	6	0.90	0.053	0.169	0.807	0.192	0.2622
	P*	0.72	--	--	0.778	--	0.2821
A3	1	12.9	14.1	0.00015	0.9999	0.00041	0.0017
	2	4.83	1.60	0.00809	0.9811	0.00536	0.0145
	3	2.98	0.58	0.0187	0.9517	0.0170	0.0376
	4	1.67	0.181	0.0691	0.893	0.0759	0.0982
	5	1.16	0.089	0.186	0.839	0.206	0.1588
	6	0.90	0.053	0.175	0.794	0.202	0.2108
	P*	0.72	--	--	0.774	--	0.2352
B1	1	12.9	14.1	0.00060	0.9989	0.00087	0.0064
	2	4.83	1.60	0.0161	0.9629	0.00692	0.0253
	3	2.98	0.58	0.0369	0.9067	0.0199	0.0536
	4	1.67	0.181	0.113	0.803	0.103	0.1304
	5	1.16	0.089	0.301	0.718	0.299	0.2141
	6	0.90	0.053	0.292	0.644	0.309	0.2942
	P*	0.72	--	--	0.610	--	0.3299
B2	1	12.9	14.1	0.00036	0.9998	0.00060	0.0033
	2	4.83	1.60	0.0121	0.9749	0.00475	0.0181
	3	2.98	0.58	0.0326	0.9309	0.0191	0.0430
	4	1.67	0.181	0.101	0.832	0.107	0.1176
	5	1.16	0.089	0.259	0.757	0.298	0.2040
	6	0.90	0.053	0.250	0.691	0.281	0.2811
	P*	0.72	--	--	0.663	--	0.3109
B3	1	12.9	14.1	0.00054	0.9991	0.00086	0.0101
	2	4.83	1.60	0.0174	0.9605	0.00427	0.0246
	3	2.98	0.58	0.0385	0.899	0.0105	0.0421
	4	1.67	0.181	0.106	0.793	0.0641	0.0882
	5	1.16	0.089	0.290	0.708	0.233	0.1522
	6	0.90	0.053	0.320	0.630	0.257	0.2200
	P*	0.72	--	--	0.590	--	0.2511

\* Position at downstream edge of mobility channel electrode.

#### REFERENCES

- Gillespie, T., and G. O. Langstroth, "An Instrument for Determining the Electric-Charge Distribution in Aerosols," *Can. J. Chem.* 30, 1056-68 (1952).
- Lapple, C. E., "Aerosol Dissemination Processes - A Critical Review," Vol. I, Chap. XII, "Electrostatic Phenomena," Special Technical Report No. 2, Contract DA-18-035-AMC-122(A), Stanford Research Institute, October 31, 1965.
- Robinson, E., J. A. MacLeod, and C. E. Lapple, "A Meteorological Tracer Technique Using Uranine Dye," *J. Meteorol.* 16, 1, 63-67 February 1959.
- Sergiyeva, A. P., "The Electrical Charges of Cloud Particles," *Akad. Nauk. SSSR, Izvestiya, Seriya Geofizicheskaya* No. 3, 247-57 (1958).

**NOMENCLATURE**  
(Glossary)

Any consistent system of units can be used in any equations, unless other specific units are specified. The MKSA system is given below by way of example.

- A = area or surface, sq. m
- $A_f$  = area available for flow, sq. m
- $A_m$  = area of face of measuring probe, sq. m
- B = width of mobility channel available for flow, m
- $B_e$  = spacing between electrode surfaces, m
- $B_1$  = clearance between metal and collecting electrode, m
- $B_2$  = thickness of collecting electrode, m
- $B_3$  = distance between surface of collection electrode and face surface of measuring probe electrode, m
- $B_4$  = distance between under-surface of measuring probe electrode and grounded shield, m
- $C_c$  = calibration capacitance of probe electrode =  $2\epsilon_0/E_m$ , farads
- $C_m$  = combined capacitance of meter, slide wire and cable connected to probe, farads.
- $C_p$  = combined capacitance =  $C_m + (\epsilon \delta A_m/B_4)$ , farads
- $C_s$  = capacitance per unit area of deposition surface, farads/sq. m
- $C_x$  = known external capacitance, farads
- $C_{cx}$  = capacitance of probe electrode in presence of additional external capacitance,  $C_x$ , farads
- d = "derivative of"
- D = diameter of circular duct, m
- $D_h$  = hydraulic diameter =  $4A_f/L_{pw}$ , m

- $D_m$  = median particle diameter, m  
 $D_{mn}$  = median particle diameter on number basis, m  
 $D_{mv}$  = median particle diameter on volume (or mass) basis, m  
 $D_p$  = particle diameter, m  
 $D_{po}$  = initial solution drop diameter, m  
 $D_{pf}$  = final drop diameter after evaporation of solvent, m  
 $D_{pae}$  = average effective particle diameter, m  
 $\bar{D}_{qp}$  = mean particle diameter (defined by Equation B-1), m  
 $Q_n$  = normal electric displacement, coulombs/sq.m  
 $Q_{ni}$  = normal electric displacement in medium i, coulombs/sq.m  
 $Q_{nj}$  = normal electric displacement in medium j, coulombs/sq.m  
 $e$  = natural logarithmic base, 2.718 . . . .  
 $E$  = potential or potential difference, volts  
 $E_e$  = potential difference between adjacent electrodes, volts  
 $E_m$  = electrometer reading on probe electrode, volts  
 $E'_m$  = electrometer reading on alternate probe electrode, volts  
 $E_{mx}$  = electrometer reading on probe electrode with additional external capacitance  $C_x$ , volts  
 $\mathcal{E}$  = potential gradient or field intensity, volts/m  
 $\mathcal{E}_o$  = potential gradient or field intensity in mobility channel, volts/m  
 $\mathcal{E}_{ps}$  = specific particle surface gradient for particle of size  

$$D_p = \frac{2}{p} \frac{\epsilon \delta}{c} D_p^2 = \frac{\rho D_p R}{p c} \frac{\epsilon \delta}{c}, \text{ volts/m}$$
 $\mathcal{E}_{psae}$  = specific particle surface gradient of particle of size  

$$D_{pae} = \frac{\rho D_{pae} R_{cav}}{p_{pae} c_{av}} \frac{\epsilon \delta}{c}, \text{ volt/m}$$
 $\mathcal{E}_{psf}$  = specific surface gradient of particle of size  $D_{pf}$ ,  
 volt/m  
 $\mathcal{E}_{pso}$  = specific surface gradient of particle of size  $D_{po}$ , volt/m

- $\mathcal{E}_1$  = field intensity between metal and collecting electrodes, volts/m  
 $\mathcal{E}_2$  = field intensity in collecting electrode, volts/m  
 $\mathcal{E}_{ea}$  = apparent field strength across metal electrodes =  $E_e/B_e$ , volts/m  
 $\mathcal{E}_{qa}$  = apparent field strength due to accumulated charge  
 =  $Q_y/6 \epsilon$ , volts/m  
 $H$  = height of mobility channel, m  
 $k$  = dimensionless constant  
 $k_C$  = Stokes-Cunningham correction factor on particle of size  $D_p$ , dimensionless  
 $k_{Cae}$  = Stokes-Cunningham correction factor on particle size of  $D_{pae}$ , dimensionless  
 $k_{Ce}$  = correction factor on electric field strength to allow for dielectric constant of collecting electrode, dimensionless  
 $k_{Cq}$  = correction factor on apparent field due to accumulated charge to allow for charge image effects, dimensionless  
 $\ln$  = "natural logarithm of"  
 $L$  = distance in mobility channel downstream from guard plate, m  
 $L_1$  = distance in mobility channel downstream from inlet edge of collection electrode, m  
 $L_{pw}$  = length of wetted perimeter, m  
 $m$  = mass, kg  
 $m_{fo}$  = total mass of aerosol entering filter, kg  
 $m_{mo}$  = total mass of aerosol entering mobility channel, kg  
 $m_{pc}$  = total mass of aerosol collected in purifier, kg  
 $m_{po}$  = total mass of aerosol entering purifier, kg  
 $n_{fp}$  = total number of flow channels in purifier, dimensionless  
 $n_{p\delta}$  = number of particles having a mobility of  $\beta_{pe}$ , dimensionless

- $N_{Re}$  = Reynolds number, dimensionless =  $D_h \rho \bar{u} / \mu$   
 $p$  = exponent (Equation B-1)  
 $q$  = exponent (Equation B-1)  
 $q_f$  = volumetric gas flow rate, cu m/sec  
 $Q_e$  = charge induced on face of measuring probe electrode, coulombs  
 $Q_b$  = charge induced on face of grounded electrode, coulombs  
 $Q_c$  = charge induced on face of shield electrode, coulombs  
 $Q_d$  = total charge on collection electrode in projected area under measuring probe electrode, coulombs  
 $Q_p$  = charge on particle, coulombs  
 $Q_s$  = concentration of charge on a surface or at an interface, coulombs/sq. m  
 $Q_{sig}$  = concentration of charge at an interface between media i and j, coulombs/sq. m  
 $R_c$  = charge-to-mass ratio on particle of size  $D_p$ , coulombs/kg  
 $R_{cav}$  = average charge-to-mass ratio, coulombs/kg  
 $t$  = time, sec  
 $t_{ps}$  = specific stopping time of particle of size  $D_p$   
 $= k_{Cp} \rho_p D_p^2 / 18 \mu$ , sec  
 $t_{psae}$  = specific stopping time of particle of size  $D_{pae}$   
 $= k_{Cae} \rho_p D_{pae}^2 / 18 \mu$ , sec  
 $u$  = fluid velocity, m/sec  
 $\bar{u}$  = average fluid velocity =  $q_f / A_f = q_f / BH$ , m/sec  
 $u_{pe}$  = migration velocity of particle under influence of and in direction of electrostatic field, m/sec

- $x$  = distance, m  
 $w_f$  = mass gas flow rate, kg/sec  
 $\rho$  = fluid density, kg/cu m  
 $\rho_p$  = true particle density, kg/cu m  
 $\rho_{pf}$  = density of drop of size  $D_{pf}$  after evaporation of solvent, kg/cu m  
 $\rho_{po}$  = density of drop of solution of size  $D_{po}$ , kg/cu m  
 $\mu$  = fluid viscosity, (kg)/(m)(sec)  
 $\sigma$  = geometric standard deviation (for log-probability size distribution), dimensionless  
 $\delta$  = dielectric constant of fluid (gas), dimensionless  
 $\delta_2$  = dielectric constant of collection electrode, dimensionless  
 $\delta_m$  = composite dielectric constant for the electrode surface which determines the sensitivity of calibration capacitance to electrode surface capacitance =  $C_s B_3 / \epsilon \delta$ , dimensionless  
 $\epsilon$  = permittivity of free space,  $8.854 \times 10^{-12}$  (coulombs)<sup>2</sup>/(m)<sup>2</sup>(newton)  
 $\varphi_p$  = cumulative fraction of particles having a size less than  $D_p$  and a mobility less than  $\beta_{pe}$ , dimensionless  
 $\varphi_v$  = cumulative volume (or mass) fraction of particles having a size less than  $D_p$  and a mobility less than  $\beta_{pe}$ , dimensionless  
 $\varphi_{po}$  = mass fraction of solute in drop of size  $D_{po}$ , dimensionless  
 $\varphi_n$  = cumulative number fraction of particles having a size and mobility less than  $D_p$  or  $\beta_{pe}$ , respectively, dimensionless  
 $\beta_{pe}$  = electrical mobility of particle, (m/sec)/(volt/m)  
 $\gamma$  = exponent (Table B-I)  
 $\eta$  = fractional efficiency, dimensionless  
 $\eta_p$  = mass fraction of particles entering energized channel of purifier that are deposited in purifier, dimensionless  
 $\eta_{cm}$  = mass fraction of aerosol in central stream collected on mobility channel electrodes, dimensionless

## Appendix A

### SIGNIFICANCE OF AVERAGE DIAMETER MEASURED BY MOBILITY CHANNEL

Basically, the charge analyzer measures three independent quantities at any specific location: (1) electrostatic mobility,  $\beta_{pe}$ , determined by the operating conditions and the location in the channel; (2) total charge of material deposited at that location; and (3) total mass of material deposited at that location. From these, it is possible to calculate the average charge-to-mass ratio,  $R_{cav}$ , of the material deposited at that location. It is also possible to calculate an average particle diameter,  $D_{pae}$ , defined as the diameter particle that has both the same charge-to-mass ratio and the same mobility as the material deposited.

For a given particle

$$\beta_{pe} = u_{pe} / \mathcal{E}_o = k_C \mathcal{Q}_p / 3\pi\mu D_p \quad (A-1)$$

and

$$R_c = \mathcal{Q}_p / (\pi\rho_p D_p^3 / 6) \quad (A-2)$$

Therefore

$$\beta_{pe} = k_C \rho_p D_p^2 R_c / 18\mu \quad (A-3)$$

Based on Equation A-3, the "average" diameter,  $D_{pae}$ , is defined by

$$D_{pae}^2 = 18\mu\beta_{pe} / k_{Cae} \rho_p R_{cav} \quad (A-4)$$

where  $k_{Cae}$  is the Stokes-Cunningham factor corresponding to  $D_{pae}$ .

But, also by definition,

$$R_{cav} = \frac{\sum_0^{n_{p\beta}} 2 \rho_p dn_{p\beta}}{\sum_0^{n_{p\beta}} (\pi \rho_p D_p^3 / 6) dn_{p\beta}} \quad (A-5)$$

where  $n_{p\beta}$  is the total number of particles at any location (i.e., total number of particles having a mobility  $\beta_{pe}$ ).

By substituting for  $2 \rho_p$  from Equation A-1 and remembering that all particles deposited at a specific location in the channel have the same mobility,  $\beta_{pe}$ , Equation A-5 becomes

$$R_{cav} = \left[ \frac{18 \mu \beta_{pe}}{\rho_p} \right] \frac{\sum_0^{n_{p\beta}} (D_p / k_C) dn_{p\beta}}{\sum_0^{n_{p\beta}} D_p^3 dn_{p\beta}} \quad (A-6)$$

Hence, by combining Equations A-4 and A-6,

$$D_{pae} = \left[ \frac{\sum_0^{n_{p\beta}} D_p^3 dn_{p\beta}}{\sum_0^{n_{p\beta}} D_p (k_{Cae} / k_C) dn_{p\beta}} \right]^{1/2} \quad (A-7)$$

For large particles (much larger than the mean free path of gas molecules; e.g., greater than 1 micron diameter at atmospheric conditions),  $k_C$  approaches unity and

$$D_{pae} = \left[ \frac{\sum_0^{n_{p\beta}} D_p^3 dn_{p\beta}}{\sum_0^{n_{p\beta}} D_p dn_{p\beta}} \right]^{1/2} \quad (A-8)$$

Thus, by reference to the definition of mean diameters given in Appendix b,  $D_{pae}$  becomes identical to  $\bar{D}_{31}$  for the case of large particles. In other words, when dealing with large aerosol particles, the mobility channel essentially measures the volume-to-diameter mean.

For very small particles (much smaller than the mean free path of the gas molecules; e.g., smaller than  $0.01\mu$  at atmospheric conditions), the drag on the particles is essentially all molecular and  $k_c$  becomes inversely proportional to particle diameter. In this case, Equation A-7 reduces to

$$D_{pae} = \frac{\sum_0^{n_{p\beta}} \frac{D^3}{p} dn_{p\beta}}{\sum_0^{n_{p\beta}} \frac{D^2}{p} dn_{p\beta}} \quad (A-9)$$

Thus for very small particles,  $D_{pae}$  becomes identical to  $\bar{D}_{32}$ , which is the Sauter or surface-to-volume mean diameter.

The average diameter,  $D_{pae}$ , may also be related to the volume mean diameter, but the conversion depends on the nature of the distribution as discussed in Appendix B.

If the particles follow a log-probability distribution, the relationship between  $D_{pae}$  and volume median is given by

For very large particles

$$D_{mv} = D_{pae} e^{\ln^2 \sigma} \quad (A-10)$$

For very small particles

$$D_{mv} = D_{pae} e^{(1/2)\ln^2 \sigma} \quad (A-11)$$

## Appendix B

### DEFINITION OF AND INTERRELATIONSHIP BETWEEN MEAN DIAMETERS

In general, mean diameter can be defined by

$$\bar{D}_{qp} = \left[ \frac{\int_0^1 D^q d\varphi_n}{\int_0^1 D^p d\varphi_n} \right]^{1/(q-p)} \quad (\text{B-1})$$

If particles obey a log-probability distribution, Equation B-1 becomes

$$\bar{D}_{qp} = D_{mn} e^{[(q+p)/2] \ln^2 \sigma} = D_{mv} e^{[(q+p-6)/2] \ln^2 \sigma} \quad (\text{B-2})$$

The Sauter mean diameter is defined as the particle diameter that has the same specific surface as the collection of particles as a whole. From this definition it follows that the Sauter diameter corresponds to a mean for which  $q = 3$  and  $p = 2$ ; i.e., the Sauter diameter is  $\bar{D}_{32}$ .

The Sauter diameter will always be smaller than the volume or mass median diameter. If the particles follow a log-probability relationship, the ratio between the volume (or mass) median diameter and the Sauter diameter is found from Equation B-2 to be

$$(D_{mv}/\bar{D}_{32}) = e^{(1/2) \ln^2 \sigma} \quad (\text{B-3})$$

Table B-I lists values of  $e^{\gamma \ln^2 \sigma}$  as a function of  $\gamma$  and  $\sigma$ . This table is useful for converting one kind of mean diameter to another. The ratio  $D_{mv}/\bar{D}_{32}$  is then given for various standard geometric deviations,  $\sigma$ , by the column of numbers under  $\gamma = 1/2$ . Thus, if a distribution corresponds to a value of  $\sigma$  of 2, the value of  $D_{mv}$  will be 1.2715 times

(or 27% larger than) the Sauter diameter. If  $\sigma$  is 1.3, the mass median diameter will be only 3.5% larger than the Sauter diameter.

While the values in the second column of Table B-I (corresponding to  $\gamma = 1/2$ ) give the ratio of the mass median to the Sauter diameter, it can also be shown that the last column (for  $\gamma = 3$ ) gives the ratio of mass median to number median diameter.

Table B-II lists various types of mean diameters together with the names commonly applied to them.

Table B-I

VALUE OF  $e^{\gamma \ln^2 \sigma}$  AS A FUNCTION OF  $\sigma$  AND  $\gamma$ 

$\sigma$	FOR VALUE OF $\gamma$ OF						
	0	$\frac{1}{2}$	1	$\frac{3}{2}$	2	$\frac{5}{2}$	3
1	1.0000	1.0000	1.0000	1.0000	1.0000	1.0000	1.0000
1.3	1.0000	1.0350	1.0713	1.1088	1.1476	1.1878	1.2294
1.5	1.0000	1.0857	1.1787	1.2797	1.3893	1.5083	1.6376
2	1.0000	1.2715	1.6168	2.0558	2.6141	3.3239	4.2264
2.5	1.0000	1.5217	2.3154	3.5233	5.3611	8.1578	12.413
3	1.0000	1.8285	3.3433	6.1130	11.177	20.438	37.369
3.5	1.0000	2.1918	4.8038	10.529	23.077	50.579	110.86
4	1.0000	2.6141	6.8333	17.863	46.694	122.06	319.08
4.5	1.0000	3.0991	9.6047	29.766	92.250	285.89	886.03
5	1.0000	3.6515	13.334	48.688	177.79	649.19	2370.5
5.5	1.0000	4.2763	18.287	78.198	334.40	1430.0	6115.0
6	1.0000	4.9789	24.789	123.42	614.50	3059.5	15233.0

Table B-II

TYPES AND DEFINITIONS OF VARIOUS MEAN DIAMETERS

NAME OF MEAN DIAMETER	q	p	$\left(\frac{q+p}{2}\right)$	$-\left(\frac{q+p-6}{2}\right)$
Geometric mean	0	0	0	3
Linear mean (number mean)	1	0	0.5	2.5
Surface mean (surface-to-number mean)	2	0	1	2
Volume mean (volume-to-number mean)	3	0	1.5	1.5
Surface-to-diameter	2	1	1.5	1.5
Volume-to-diameter	3	1	2	1
Sauter (volume-to-surface mean)	3	2	2.5	0.5
De Brouckere (mass mean)	4	3	3.5	-0.5

## Appendix C

### BASIC PERFORMANCE RELATIONSHIPS

#### Electrical Particle Mobility

The mobility channel essentially classifies particles by their mobility. Consequently, the first requirement is to relate particle mobility with the position where the particle deposits on the electrode as a function of apparatus geometry and operating conditions. This is done for idealized conditions. Then the significance of deviations from idealized conditions are discussed together with the methods for applying proper corrections where indicated.

#### Idealized Conditions

First, we will consider conditions where an infinitely thin stream of aerosol moving with the same uniform velocity,  $\bar{u}$ , as a surrounding sheath of clean air is suddenly exposed to a uniform electrical field,  $\mathcal{E}_0$ , in the absence of any gravitational field. Under these conditions, a particle of electrical mobility  $\beta_{pe}$  will acquire a velocity perpendicular to the stream flow given by

$$u_{pe} = \beta_{pe} \mathcal{E}_0 \quad (C-1)$$

The distance downstream,  $L$ , that this particle will move before contacting the channel wall is given by

$$L = \bar{u}B/2\beta_{pe} \mathcal{E}_0 \quad (C-2)$$

This assumes that (1) the particle retains the forward velocity component of the gas, (2) the period of acceleration in attaining its cross velocity of  $u_{pe}$  is negligible, and (3) the particle is suddenly exposed to a field  $\mathcal{E}_0$  at and downstream of the guard plate.

From Equation C-2, the mobility of a particle that deposits at a position L downstream from the guard plate under the specified operating conditions ( $\bar{u}$  and  $\mathcal{E}_o$ ) is given by

$$\beta_{pe} = \bar{u}B/2\mathcal{E}_oL \quad (C-3)$$

or, in a normalized form,

$$\left(\frac{\beta_{pe}\mathcal{E}_o}{\bar{u}}\right) = \frac{1}{2(L/B)} \quad (C-4)$$

#### Calculation of Field Strength

If the collection electrodes had a dielectric constant of unity and no particles had accumulated, the field strength,  $\mathcal{E}_o$ , would be given by  $E_e/B_e$ . However, the actual field strength will be higher because the dielectric constant is greater than unity and lower because of effects due to accumulated charged particles. Normally the mobility channel would not be operated at particle accumulation levels where this latter effect becomes significant. In either event, the effective field strength can be calculated from Equation D-7 in Appendix D. This allows for both the dielectric constant of the collecting electrode and any accumulated charge.

Equation D-7 may be regarded as the definition of  $\mathcal{E}_o$ . The fringing fields at the end of the channel actually involve a variation in field intensity and are separately accounted for as discussed below.

#### Effect of Velocity Distribution

Equation C-4 was developed for the case of a stream having a uniform velocity profile. The velocity profile will not be uniform in actual practice.

With a uniform field intensity, the lateral gas velocity distribution (i.e., velocity profile in a direction normal to the plane of the thin aerosol stream) has no separate effect on the point where a particle deposits, providing the velocity profile is symmetric on each side of the aerosol plane. In such a case, Equations C-2 to C-4 will still apply

with  $\bar{U}$  defined as the average velocity given by dividing the volumetric flow rate by the cross-sectional flow area of the channel. A longitudinal velocity profile (i.e., at right angles to the flow direction but parallel to the plane of the aerosol stream), however, would have a direct influence on the point of aerosol deposition. It is minimize this effect that the mobility channel was made narrow and wide since the effect of longitudinal velocity profile is not easily allowed for.

In the case of a varying field strength (as with fringing fields), the lateral velocity distribution will also influence the results to an extent dependent on the field variation. Consequently, this aspect is dealt with in combination with field-variation effects below.

#### Effect of Fringing Fields

Fringing fields may be present at the ends of the electrodes. The relative effect of such fields would be most serious at the inlet end of the channel where the particles of greatest mobility are being deposited. To assess the magnitude of the effects of such fringing fields, calculations were performed for specific arbitrary electrode geometries and flow patterns. Because of mathematical complexities, a graphical method of field and trajectory plotting was used.

The fields were obtained experimentally by a method of analog field simulation with a conductive paper of uniform resistivity (Teledeltos paper). The particle trajectories were then developed graphically by calculating and plotting successive incremental displacements. The three arrangements shown in Fig. C-2 were considered. For one of these arrangements (Arrangement III) two fluid flow patterns were assumed.

The results of the evaluations are compared in Fig. C-3 with predictions for the idealized case of Equation C-4. Figure C-3 gives a plot of normalized mobility against normalized position on the plastic collecting electrode. Physically, the normalized mobility (defined by the ordinate) represents the ratio of the migration velocity of the particles toward the mobility channel walls to the average velocity of the fluid in the channel. The abscissa gives the position at which a particle of the indicated mobility will land on the electrode, expressed as channel

widths from the inlet end of the plastic electrode. For this purpose the ideal case has also been calculated assuming that the field starts at the inlet end of the plastic electrode (i.e.,  $L$  in Equation C-4 was taken as  $L_1$ ).

The specific data obtained in the evaluation for Arrangement III are summarized in Table C-I and separately plotted in Fig. C-4. In this table and figure, position has been expressed in terms of distance from the edge of the guard plate. For the ideal case it was assumed that the field starts at the edge of the guard plate (i.e.,  $L$  in Equation C-4 was taken as  $L$ ).

In both Figs. C-3 and C-4, term  $\epsilon_o$  is defined as  $E_e/B_e$ . The term  $B_e$  is different from  $B$  because of the thickness of the plastic collecting surfaces on the electrodes and the air gap between these surfaces. In making the evaluations on which both Figs. C-3 and C-4 are based, it was assumed that the dielectric constant of the plastic collecting electrode is the same as for air (unity) because no simple way of graphically allowing for the difference in dielectric constants has been devised.

In calculating the curves of Figs. C-3 and C-4, it was assumed that the aerosol stream started at the center of the channel and had no significant width. A few checks were made to compare the spreading of the deposit that would be predicted for an otherwise idealized case to that which would result for Case III a. For the idealized conditions, the range in  $L$  for a given mobility would be the same percentages as the range in the initial aerosol stream width expressed as a percent of the total channel width. For a 0.115-in. aerosol stream width and a 1.50-in channel width, this percentage is  $\pm 8\%$ . Although the absolute levels of mobility were different between the ideal case and Case III a, particularly at the inlet end of the channel, the percentage spread in the deposit position was about the same over the entire length of the mobility channel.

#### Application

No guard plates were used in the early runs with the mobility channel; one electrode was grounded and one was charged. Thus, deviations from

ideality for deposits on one electrode were greater than for Case I (which assumed oppositely charged electrodes and a grounded outer upstream plate) and were reversed for deposits on the other electrode. This nonsymmetry of deposit was actually observed in the early runs and was one of the reasons for performing the above analysis.

The final mobility channel employed guard plates as for Arrangement III. Because of gasket requirements, the distance between the downstream edge of the guard plates and the upstream edge of the plastic collection electrode was 3/8 in. instead of 3/4 in. as for Arrangement III. The results calculated for Arrangement III, however, should still apply for all practical purposes, provided the edge of the guard plates is used as a reference position (as was done in Fig. C-4).

The above equations for particle mobility are intrinsically applicable for estimating purifier performance. However, in the mobility channel a particle must traverse only half the channel width before it deposits on the channel wall. In the purifier some particles must traverse essentially no distance while others must traverse the entire channel width. Thus the lowest-mobility particle completely collectable in the purifier is given by the following counterpart of Equation C-3.

$$(\beta_{pe})_{\min} = \bar{u}B / \xi_o L \quad (C-5)$$

where  $\bar{u}$  and  $\xi_o$  are the velocity and field strength in the purifier and B and L are the width and overall length of the individual purifier channels. This equation holds regardless of the transverse velocity profile but assumes a uniform longitudinal velocity profile.

#### Average Particle Diameter

A given location on the electrode corresponds to a particle having a given mobility,  $\beta_{pe}$ . The average charge-to-mass ratio of all the particles collected at the location is measured as  $R_{cav}$ . By definition

$$D_{pae} = \sqrt{(18\mu/p_p k_{Cae})(\beta_{pe}/R_{cav})} \quad (C-6)$$

This follows from the definition of electrical particle mobility. The quantity  $D_{pae}$  is a specific type of average effective particle diameter. It is that sized particle which has a mobility,  $\beta_{pe}$ , and a charge-to-mass ratio,  $R_{cav}$ , equal to that of the collected particles as a whole. The significance of this type of average diameter is fully discussed in Appendix A.

Because of the Stokes-Cunningham factor, direct calculation of  $D_{pae}$  would involve a trial-and-error solution unless one has available a plot of  $D_p \sqrt{k_C}$  vs.  $D_p$ . To calculate  $D_{pae}$  the quantity  $D_{pae} \sqrt{k_{Cae}}$  is then first calculated from a rearrangement of Equation C-6.

$$D_{pae} \sqrt{k_{Cae}} = \sqrt{(18\mu/\rho_p)(\beta_{pe}/R_{cav})} \quad (C-7)$$

At atmospheric temperatures and pressure it can be shown that, for the size range above  $0.3\mu$ , the following approximation is good to better than 5%.

$$D_{pae} = D_{pae} \sqrt{k_{Cae}} - 0.020 \quad (C-8)$$

where both  $D_{pae}$  and  $D_{pae} \sqrt{k_{Cae}}$  are in microns. For atmospheric conditions this may be used as an alternate to the use of a plot of  $D_p \sqrt{k_C}$  vs.  $D_p$ .

#### Average Specific Stopping Time

From the definition of specific stopping time

$$t_{psae} = \beta_{pe} / R_{cav} \quad (C-9)$$

and represents the specific stopping time of a particle of size  $D_{pae}$ .

#### Average Specific Particle Surface Gradient

From the definition of specific particle surface gradient

$$\mathcal{E}_{psae} = (1/\epsilon\delta) \sqrt{(\mu\rho_p/2k_{Cae}) \beta_{pe} R_{cav}} \quad (C-10)$$

and represents the specific surface gradient of a particle of size  $D_{pae}$ .

### Purifier and Mobility Channel Performance

The overall performance of both the purifier and the mobility channel as collectors of charged particles can be calculated from the material balance data.

#### Purifier Performance

Assume (1) that the flow is equally distributed between all the purifier flow channels, (2) that all channels are equal in size, (3) that only the central one is not energized, and (4) that mechanical deposition on the channel walls is negligible. The amount of aerosol leaving with the gas stream in the central channel is  $m_{po}/n_{fp}$ , while the total amount leaving the other channels is  $m_{po}[(n_{fp} - 1)/n_{fp}](1 - \eta_p)$ . The sum of these two quantities constitutes the quantity of aerosol entering the mobility channel,  $m_{mo}$ . Setting up this equality and solving for  $\eta_p$ .

$$\begin{aligned}\eta_p &= \left[ \frac{m_{po} - m_{mo}}{m_{po}} \right] \left( \frac{n_{fp}}{n_{fp} - 1} \right) \\ &= \left( \frac{m_{pc}}{m_{po}} \right) \left( \frac{n_{fp}}{n_{fp} - 1} \right) \quad (C-11)\end{aligned}$$

This gives the fraction of the total aerosol collected in the energized portion of the purifier.

#### Mobility Channel Performance

Assume (1) that material leaving the energized channels of the purifier is uncharged and passes through the mobility channel and (2) that there is no mechanical deposition on the mobility channel walls. By definition, the amount of material in the central aerosol stream collected in the mobility channel is  $\eta_{cm}(m_{po}/n_{fp})$ . The amount of material (initially in this central stream) leaving the mobility channel is, therefore,  $(1 - \eta_{cm})(m_{po}/n_{fp})$ . The material entering the filters is the sum of this, plus the material escaping the energized portion of the purifier, or

$$(1 - \eta_{cm})(m_{po}/n_{fp}) + (1 - \eta_p)(m_{po})[(n_{fp} - 1)/n_{fp}] = m_{fo} \quad (C-12)$$

Substituting for  $\eta_p$  from Equation C-11 and solving for  $\eta_{cm}$

$$\eta_{cm} = [n_{fp}(m_{mo} - m_{fo})/m_{po}] \quad (C-13)$$

Subject to the assumptions above  $(1 - \eta_{cm})$  gives the fraction of the aerosol that has an electrical mobility less than the minimum collectible in the mobility channel.

#### Limiting Channel Capacity

One essential requirement for the reliable operation of the mobility channel is that the flow be streamline in nature and not subject to turbulent or eddy mixing. In addition the velocity profile must be, at least, known. As previously mentioned, it is desirable that the longitudinal velocity profile be uniform to avoid major mathematical complexities.

To minimize the effect of mixing or circulation due to either thermal currents or minor leakages, it is desirable to operate at as high a gas velocity as possible. However, the upper limit on gas velocity is determined by the point at which the flow becomes turbulent. This point can be specified in terms of the Reynolds number.

$$N_{Re} = D_h \bar{U} \rho / \mu \quad (C-14)$$

For a narrow channel, the hydraulic diameter is essentially equal to twice the channel width (i.e., twice its smallest dimension) or

$$\begin{aligned} N_{Re} &= 2B\bar{U}\rho/\mu \\ &= 2q_f \rho / \mu H = (2\rho/\mu)(q_f/H) \\ &= 2w_f/\mu H \end{aligned} \quad (C-15)$$

For a circular channel, the hydraulic diameter is equal to the actual diameter and

$$\begin{aligned} N_{Re} &= D\bar{U}\rho/\mu \\ &= (4/\pi)(\rho/\mu)(q_f/D) = (4/\pi)w_f/\mu D \end{aligned} \quad (C-16)$$

The following are values of  $q_f/H$  and  $q_f/D$  corresponding to various values of  $N_{Re}$  as calculated from Equations C-15 and C-16 when dealing with atmospheric air (air at 25°C;  $\rho = 0.0740$  lb/cu. ft;  $\mu = 0.0184$  cp):

Reynolds Number (dimensionless)	Corresponding Capacity	
	Narrow Channel $q_f/H$ (cfm/in.)	Circular Duct $q_f/D$ (cfm/in.)
100	0.0418	0.066
500	0.209	0.328
1,000	0.418	0.656
1,500	0.627	0.985
2,000	0.836	1.312

To ensure streamline flow,  $N_{Re}$  must be below 1,500. Therefore, the maximum possible capacity for a narrow channel is 0.63 cfm/in. of height independent of channel width. The narrower the channel, however, the higher the allowable velocity and hence the less the susceptibility to the interfering influences of convective currents. For a channel 1.5 in. wide, the maximum allowable velocity (i.e., such that  $N_{Re} < 1500$ ) at atmospheric conditions would be 1.0 ft/sec or 30 cm/sec.

#### Size and Charge of Solution Drops After Evaporation

It is readily shown that when a drop has completely evaporated, the final drop diameter is given by

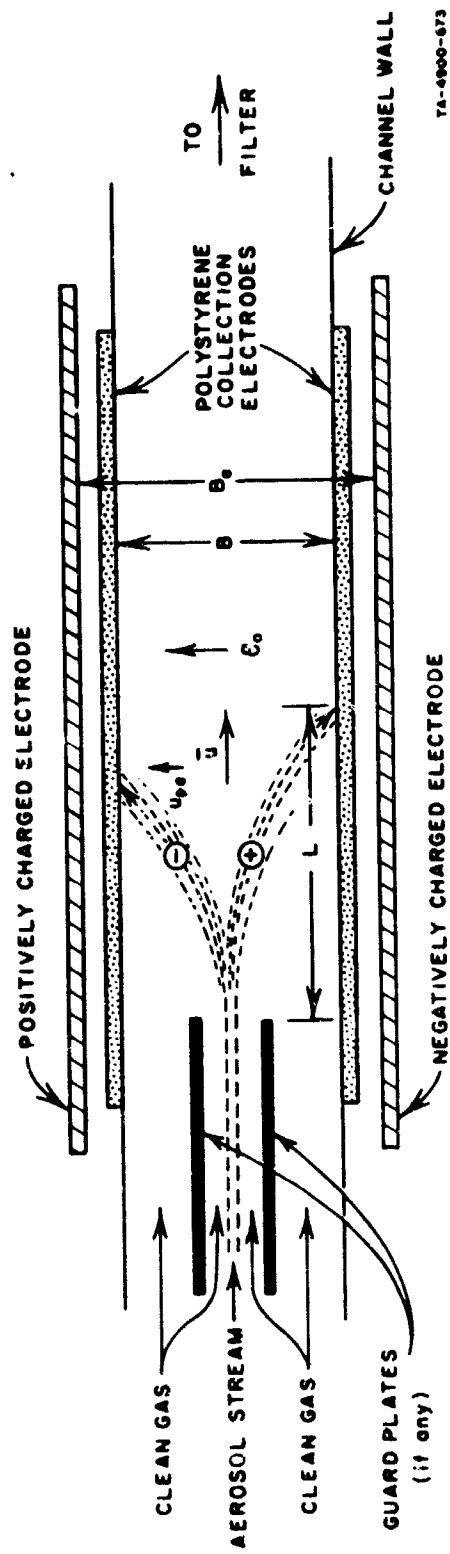
$$(D_{pf}/D_{po}) = (\varphi_{po} \rho_{po} / \rho_{pf})^{1/3} \quad (C-17)$$

If the drop is initially charged and no charge is lost during evaporation, it is also readily shown that the charge level after complete evaporation is given by

$$(\varepsilon_{psf}/\varepsilon_{pso}) = (D_{po}/D_{pf})^2 = (\rho_{pf}/\rho_{po} \varphi_{po})^{2/3} \quad (C-18)$$

This assumes, of course, that the final drop is still spherical.

Thus, if  $\varphi_{po} = 0.02$ ,  $\rho_{po} = 1.0$  g/cc, and  $\rho_{pf} = 1.5$  g/cc, it follows from Equations C-17 and C-18 that  $D_{pf}/D_{po} = 0.237$  and  $\mathcal{E}_{psf}/\mathcal{E}_{pso} = 17.8$ . Thus the final drop will be approximately one fourth as large as the initial drop but bear a specific surface charge gradient 18 times as great.



74-6900-673

FIG. C-1 DIAGRAM ILLUSTRATING MOBILITY CHANNEL OPERATION

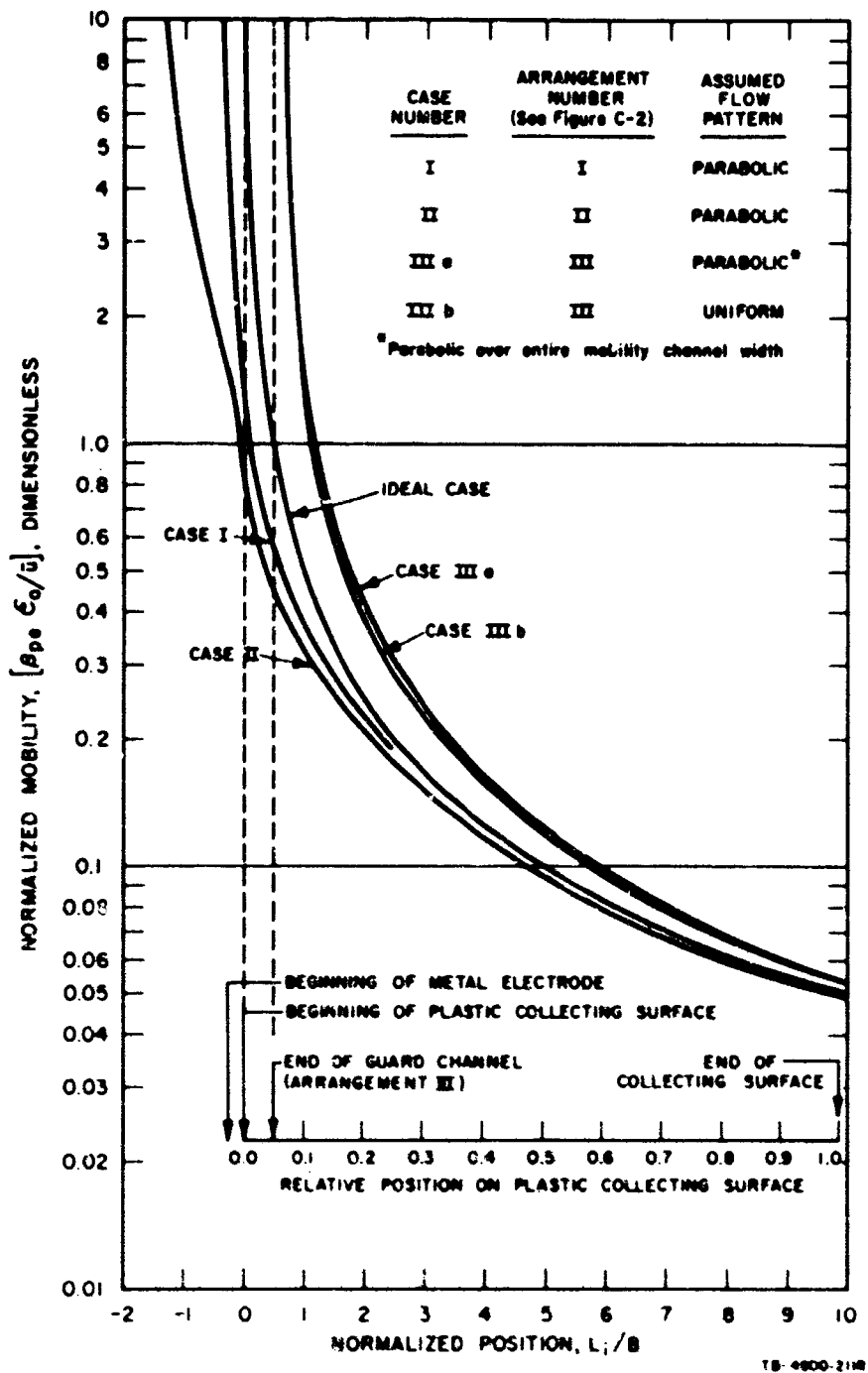
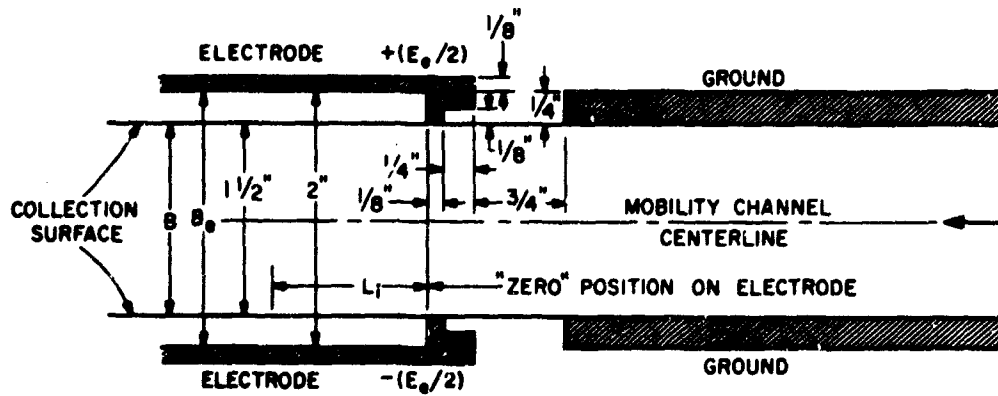
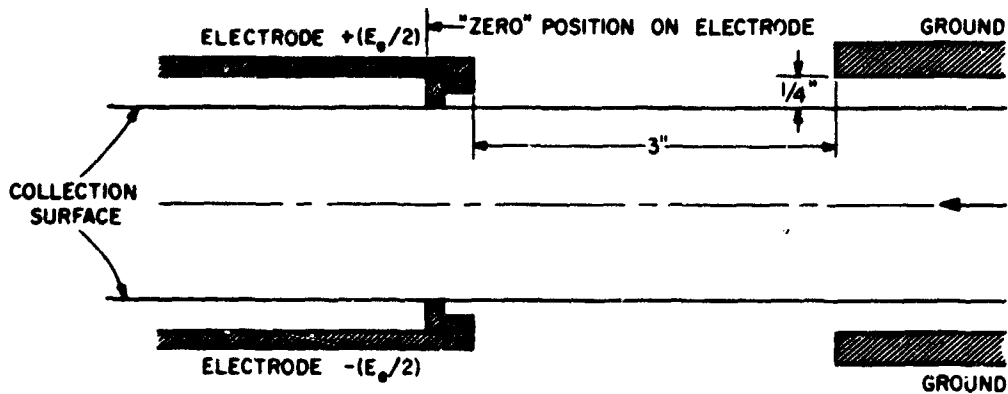


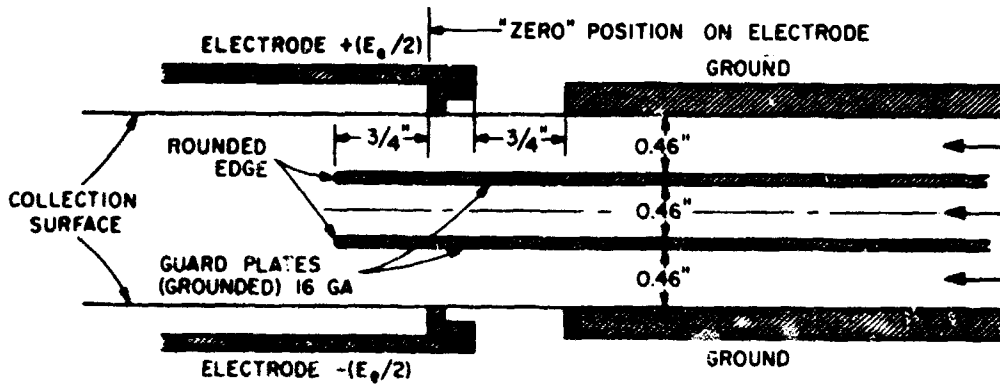
FIG. C-2 DETAILS OF APPARATUS ARRANGEMENTS EVALUATED FOR FIELD DISTRIBUTION



ARRANGEMENT I



ARRANGEMENT II



ARRANGEMENT III

Cross-hatching indicates conductor  
 Dimensions not shown are identical to Arrangement I

TR-4900-2109

FIG. C-3 RELATIONSHIP BETWEEN MOBILITY AND POSITION ON ELECTRODE

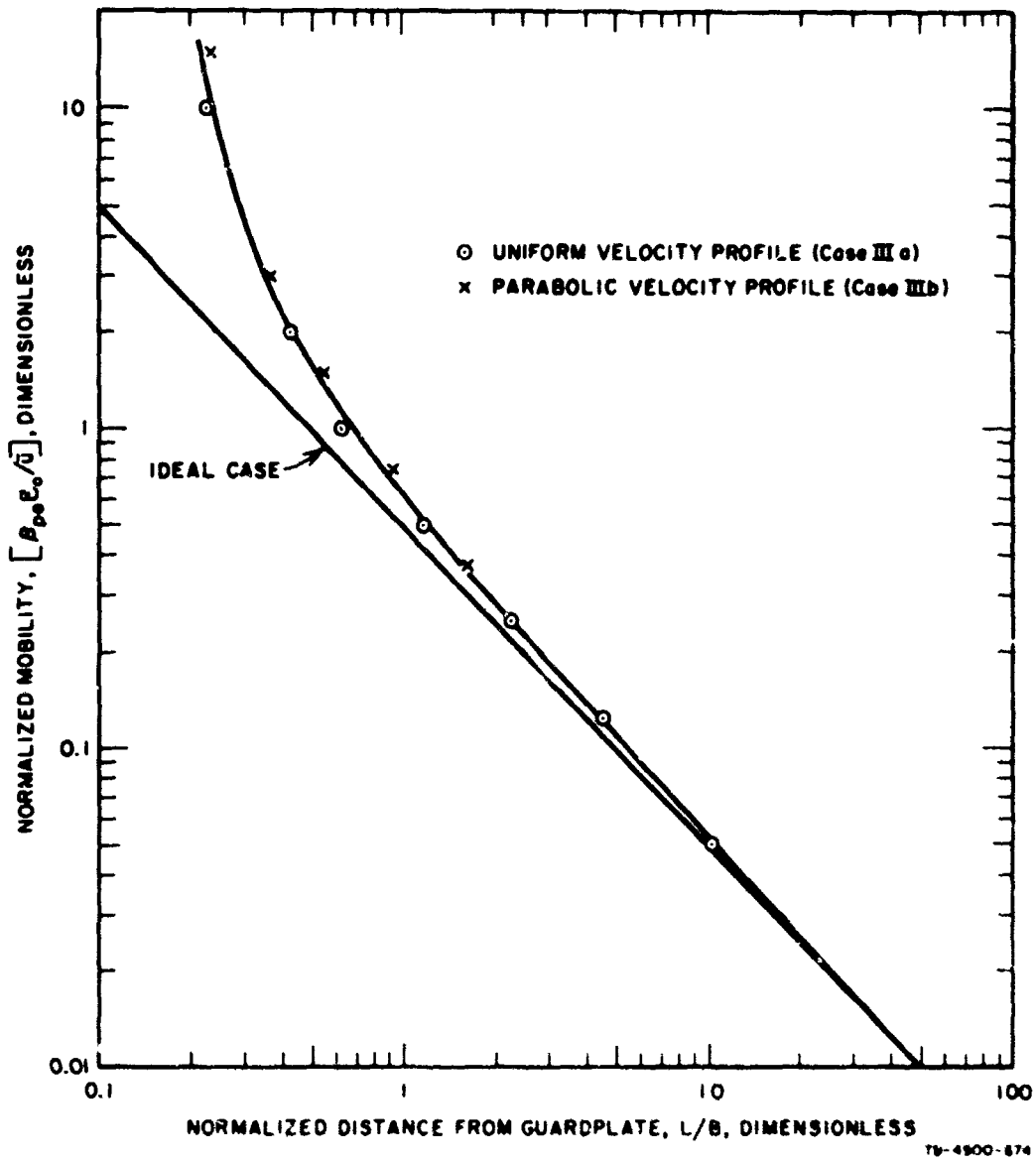


FIG. C-4 RELATIONSHIP BETWEEN MOBILITY AND POSITION ON ELECTRODE FOR ARRANGEMENT III

Table C-1  
 CALCULATED TRAJECTORIES OF PARTICLES  
 FOR CASES IIIa AND IIIb  
 FROM GRAPHICAL EVALUATIONS

TYPE FLOW PROFILE	NORMALIZED MOBILITY $\left(\frac{\beta \epsilon_0}{\rho_e \bar{u}}\right)$ (Dimensionless)	POINT OF DEPOSITION ON PLASTIC ELECTRODE* (L/B)
Uniform (Case IIIa)	10	0.225
	2	0.425
	1	0.625
	0.5	1.165
	0.25	2.25
	0.125	4.25
Parabolic (Case IIIb)	15	0.23
	3	0.365
	1.5	0.525
	0.75	0.925
	0.375	1.61

\* L is distance downstream from end of guard plate;  
 B is clearance between inside plastic electrode faces;  
 $\epsilon_0$  is apparent field gradient in mobility channel =  $E_0/B_0$ ;  
 $\bar{u}$  is average flow velocity in mobility channel =  $q_f/BH$ .

## Appendix D

### FIELD INTENSITY FOR IDEAL MOBILITY CHANNEL

#### Introduction

For this purpose, the concern is with a uniform channel as illustrated in Fig. D-1. The following assumptions are involved in this idealized channel: (1) uniformly distributed, equal and opposite charges on inside surfaces of plastic electrode, (2) infinitely long channel height and length relative to width,  $B_0$  (to eliminate any fringe field effects), (3) symmetric electrode arrangements as shown in Fig. D-1; and (4) infinite resistance of plastic electrodes (i.e., no charge can leak off).

The following discussion derives the relationship needed to calculate the field intensity inside this channel for the prescribed geometry, imposed potential difference, and accumulated charge.

#### Fundamental Relationships

By definition

$$E_0 = \int \mathcal{E} dx \quad . \quad (D-1)$$

Since the normal components of electric displacement across a boundary differ by the surface charge density at the boundary

$$\mathcal{E}_{ni} - \mathcal{E}_{nj} = \rho_{sij} \quad . \quad (D-2)$$

#### Derivation

From Equation D-1

$$2B_1 \mathcal{E}_1 + 2B_2 \mathcal{E}_2 + B \mathcal{E}_0 = E_0 \quad . \quad (D-3)$$

From Equation D-2

$$\delta \underline{\epsilon} \underline{\epsilon}_1 - \delta \underline{\epsilon} \underline{\epsilon}_2 = 0 \quad (D-4)$$

$$\delta \underline{\epsilon} \underline{\epsilon}_2 - \delta \underline{\epsilon} \underline{\epsilon}_o = \underline{Q}_s \quad (D-5)$$

Solving Equations D-3, 4, and 5 simultaneously for  $\underline{\epsilon}_o$

$$\underline{\epsilon}_o = \left\{ \frac{\underline{E}_e}{[B + 2B_1 + 2B_2(\delta/\delta_2)]} \right\} - \left( \frac{\underline{Q}_s}{\delta \underline{\epsilon}} \right) \left[ \frac{2B_1 + 2B_2(\delta/\delta_2)}{B + 2B_1 + 2B_2(\delta/\delta_2)} \right] \quad (D-6)$$

### Conclusions

Equation D-3 can be rearranged to

$$\begin{aligned} \underline{\epsilon}_o &= \left( \frac{\underline{E}_e}{B_e} \right) \left[ \frac{B_e}{B + 2B_1 + 2B_2(\delta/\delta_2)} \right] - \left( \frac{\underline{Q}_s}{\delta \underline{\epsilon}} \right) \left[ \frac{2B_1 + 2B_2(\delta/\delta_2)}{B + 2B_1 + 2B_2(\delta/\delta_2)} \right] \\ &= \underline{\epsilon}_{ea}^k \underline{\epsilon}_e - \underline{\epsilon}_{qa}^k \underline{\epsilon}_q \quad (D-7) \end{aligned}$$

where  $\underline{\epsilon}_{ea}$  = apparent field strength =  $\underline{E}_e/B_e$

$\underline{\epsilon}_{qa}$  = apparent field strength due to accumulated charge

$$= \underline{Q}_s /$$

$\underline{\epsilon}_e$  = correction factor on electrical field strength to allow for dielectric constant of plastic electrodes

$$= B_e / [B + 2B_1 + 2B_2(\delta/\delta_2)]$$

$\underline{\epsilon}_q$  = correction factor on apparent field due to accumulated charge to allow for charge image effects.

$$= [2B_1 + 2B_2(\delta/\delta_2)] / [B + 2B_1 + 2B_2(\delta/\delta_2)]$$

For the actual experimental arrangements used

$$B = 1.5 \text{ in}$$

$$B_e = 2.0 \text{ in}$$

$$B_1 = 1/8 \text{ in}$$

$$B_2 = 1/8 \text{ in}$$

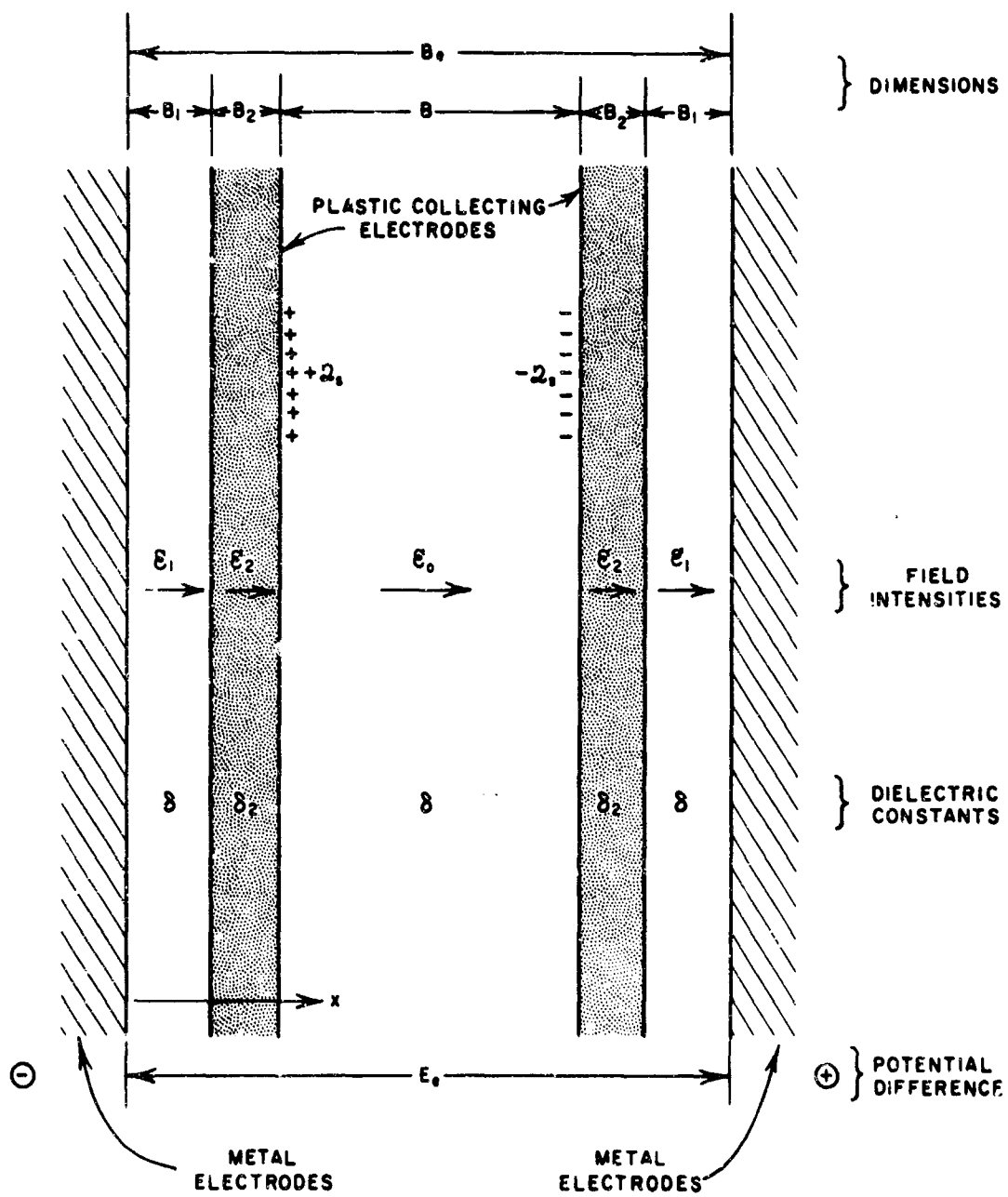
$$\delta = 1$$

$$\delta_2 = 2.55$$

Therefore

$$k_{\epsilon_e} = 1.082$$

$$k_{\epsilon_g} = 0.188$$



TA-4900-675

FIG. D-1 DIAGRAM ILLUSTRATING GEOMETRY OF AND ELECTRICAL CONDITIONS IN MOBILITY CHANNEL

## Appendix E

### CAPACITANCE OF CHARGE ANALYZER

The calibration of the analyzer is given by the factor relating the electrometer reading (a voltage  $E_m$ ) to the total charge under the measuring probe ( $Q_d$ ). The ratio  $Q_d/E_m$ , is a capacitance and can be called the calibration capacitance of the instrument,

$$C_c = Q_d/E_m \quad (E-1)$$

The calibration of the instrument will then involve determining the value of  $C_c$ .

#### Derivation of Basic Capacitance Relationships

In general,  $C_c$  will be affected by the dimensions of the mobility chamber and analyzer probe, the effective dielectric constant of the collection surface, various spacings between components, and the meter and cable capacitances. Their relative effects can be determined by a capacitance analysis of the measuring system. The system is diagrammed in Fig. E-1.

The system is divided into three regions indicated by circled numbers in Fig. E-1. The charge deposit is assumed to be uniform in each region; it can, therefore, be assumed to exist on an infinitesimally thin conductor in each region, but the conductor of one region being insulated from the other. Region 1 is outside of the probe carriage. Region 2 is the shield portion of the probe carriage, and Region 3 is the measurement area. These regions are considered plane-parallel capacitors; the capacitors of one region are connected to those of an adjacent region only where conductors cross the dashed lines. The resulting capacitor diagram is shown in Fig. E-2 for each region with interconnections shown as dashed lines. The signal voltages are measured

at  $E_m$  and  $E'_m$ . Additional capacitances (of the electrometer, slide wire and cables) are associated with these measurements.

If the electrodes and shield are grounded during the measurement, then the capacitances of Regions 1 and 2 do not affect the readings at  $E_m$  and  $E'_m$ . The resulting capacitance diagram, including the effects of the measurement capacitance, is shown in Fig. E-3.

In Fig. E-3,  $C_s$  is the capacitance per unit area of the collection surface when isolated from the rest of the system;  $A_m$  is the area of the probe;  $B_3$  and  $B_4$  are indicated in Fig. E-1; and  $C_m$  is the meter, slide wire and cable capacitance. A total charge  $Q_d$  is contained on the "conductor" marked in bold lines. Note that the two probe systems are isolated and can be considered separately. Since they are also identical in form, only one side need be solved. The circuit to be solved is shown in Fig. E-4, which indicates the charges on the capacitor plates. The equations are

$$E_m = \frac{Q_c}{C_m + (\epsilon \delta A_m / B_4)} \quad (E-2)$$

$$E_m - E_1 = \frac{Q_a}{(\epsilon A_m / B_3)} \quad (E-3)$$

$$E_1 = \frac{Q_b}{C_s A_m} \quad (E-4)$$

In addition, it is known that the probe (the conductor labeled  $E_m$ ) is uncharged, since it is an isolated conductor and is discharged before a measurement is made. Therefore

$$Q_a = -Q_c \quad (E-5)$$

and

$$Q_b - Q_a = Q_d \quad (E-6)$$

The above equations can then be reduced to

$$\mathcal{Q}_a = -E_m [C_m + (\epsilon\delta A_m/B_4)] \quad (\text{E-7})$$

$$\mathcal{Q}_a = (E_m - E_1)(\epsilon\delta A_m/B_3) \quad (\text{E-8})$$

$$\mathcal{Q}_d = E_1 [C_{sm} + (\epsilon\delta A_m/B_3)] - E_m \epsilon\delta A_m/B_3 \quad (\text{E-9})$$

These three equations can be solved for  $\mathcal{Q}_d$  by eliminating  $E_1$  and  $\mathcal{Q}_a$  to yield

$$\mathcal{Q}_d = E_m \left\{ [C_s + (\epsilon\delta/B_3)] [A_m + (C_m B_3/\epsilon\delta) + (B_3 A_m/B_4)] - [\epsilon\delta A_m/B_3] \right\} \quad (\text{E-10})$$

From Equations E-1 and E-10,

$$\begin{aligned} C_c &= [A_m + (C_m B_3/\epsilon\delta) + (B_3 A_m/B_4)] [C_s + (\epsilon\delta/B_3)] - [\epsilon\delta A_m/B_3] \\ &= [A_m C_s] + [(B_3/B_4) A_m C_s] + [\epsilon\delta A_m/B_4] + C_m + [C_m C_s B_3/\epsilon\delta] \end{aligned} \quad (\text{E-11})$$

which can be simplified to

$$C_c = A_m C_s + (B_3/B_4) [1 + (1/\delta_m)] A_m C_s + (1 + \delta_m) C_m \quad (\text{E-12})$$

where

$$\delta_m = C_s B_3/\epsilon\delta \quad (\text{E-13})$$

#### Final Relationship

The capacitance  $C_m$  represents the combined capacitances of the electrometer, interconnecting cables, slide wires, and miscellaneous distributed capacitances. The value of  $C_m$  is difficult to determine without removing the probe portion of the analyzer from the carriage.

However, the capacitance labeled  $C_m + (\epsilon\delta A_m/B_4)$  in Fig. E-4 is the total capacitance,  $C_p$ , between the probe and ground with the electrode plates removed; this can be easily measured. When Equation E-12 is written in terms of  $C_p$ , we obtain

$$C_c = A_m C_s + (1 + \delta_m) C_p \quad . \quad (E-14)$$

#### Application

The factors in Equations E-14 can all be measured:  $C_s$  is determined by coating an electrode with a thin conductive surface of known area and measuring its capacity with a bridge;  $C_p$  is measured on a bridge by removing the electrode plates and measuring the total capacitance between probe electrodes and ground;  $A_m$  and  $B_3$  are fixed by the design geometry. In this fashion, the following values were obtained:

$$\begin{aligned} C_s &= 1.429 \text{ picofarads/sq. in.} \\ C_p &= 83.5 \text{ picofarads} \\ A_m &= 5.72 \text{ sq. in.} \\ B_3 &= 0.125 \text{ in.} \end{aligned}$$

Therefore

$$\begin{aligned} \delta_m &= C_s B_3 / \epsilon \delta = 0.794 \\ A_m C_s &= 8.2 \text{ picofarads} \end{aligned}$$

and, from Equation E-14,  $C_c = 158.0$  picofarads.

An alternative method is to measure the potential recorded by the probe electrode in the presence of a given charge on the mobility channel electrode both in the presence and absence of a large known capacitance,  $C_x$ , in parallel with the probe. For these cases, from Equations E-1 and E-14

$$2_d = F_m C_c = E_m [A_m C_s + (1 + \delta_m) C_p] \quad (E-15)$$

$$\begin{aligned}
Q_d &= E_{mx} C_{cx} = E_{mx} [A C_m C_s + (1 + \delta_m)(C_p + C_x)] \\
&= E_{mx} [A C_m C_s + (1 + \delta_m)C_p + (1 + \delta_m)C_x] \\
&= E_{mx} [C_c + (1 + \delta_m)C_x] \tag{E-16}
\end{aligned}$$

Combining E-15 and E-16 and solving for  $C_p$  or  $C_c$

$$C_p = \left[ \frac{C_x}{(E_m/E_{mx}) - 1} \right] - \left[ \frac{A C_m C_s}{(1 + \delta_m)} \right] \tag{E-17}$$

$$C_c = \frac{(1 + \delta_m)C_x}{(E_m/E_{mx}) - 1} \tag{E-18}$$

For a capacitance  $C_x$  of 970.0 picofarads, it was found that  $(E_m/E_{mx})$  was 11.45 and 11.58 for the left and right electrodes, respectively. Thus, using the previously determined value of  $C_s$  of 1.429 picofarads/sq. in. (and hence  $\delta_m = 0.794$ ), the following values are obtained from Equations E-17 and E-18

Electrode	Capacitance, picofarads	
	$C_p$	$C_c$
left	88.1	166.5
right	86.9	164.5

Since the last term of Equation E-17 is small,  $C_p$  is almost independent of the value of  $C_s$ . Thus, this technique is basically an independent measurement of  $C_p$ . The value calculated for  $C_c$  from Equation E-18 is dependent on  $\delta_m$ , which in turn is based on the same value of  $C_s$  obtained previously.

An average value of 163 picofarads has been assumed in all calculations for converting electrometer reading to charge on the tape being scanned.

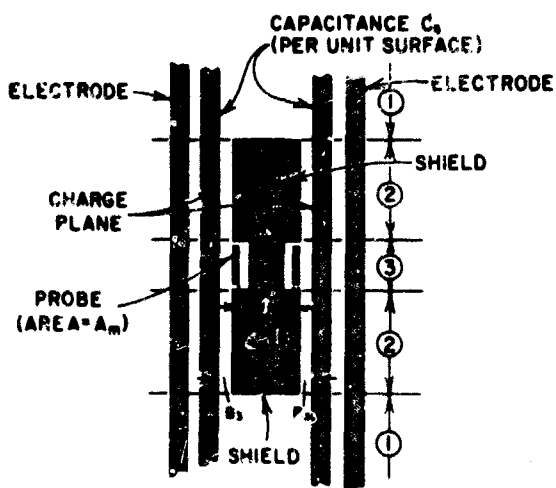


FIG. E-1 DIAGRAM OF PROBE MEASUREMENT SYSTEM

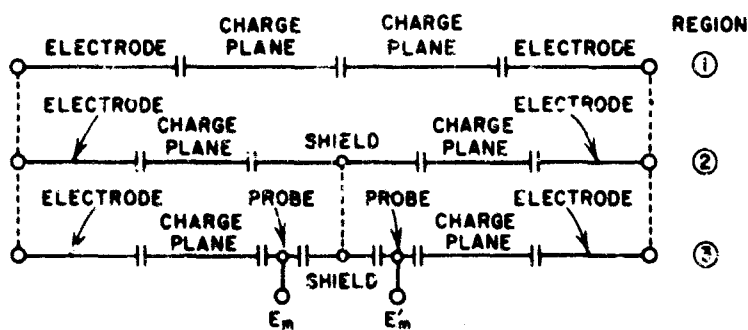


FIG. E-2 GENERALIZED CAPACITANCE DIAGRAM

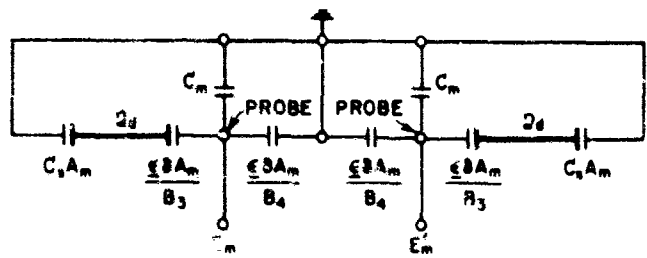


FIG. E-3 MODIFIED CIRCUIT

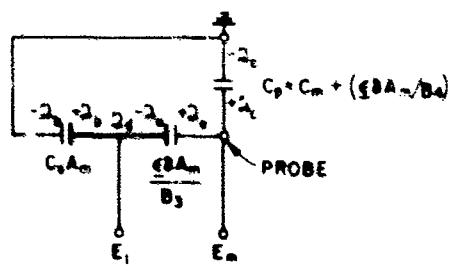


FIG. E-4 FINAL REDUCED CIRCUIT

UNCLASSIFIED

Security Classification

## DOCUMENT CONTROL DATA - R &amp; D

(Security classification of title, body of abstract and indexing annotation must be entered when the overall report is classified)

1. ORIGINATING ACTIVITY (Corporate author) Stanford Research Institute Menlo Park, California 94025		2a. REPORT SECURITY CLASSIFICATION UNCLASSIFIED	
		2b. GROUP N/A	
3. REPORT TITLE  DEVELOPMENT OF AEROSOL CHARGE ANALYZER			
4. DESCRIPTIVE NOTES (Type of report and inclusive dates) Special Technical Report 11 July 1965 - September 1966			
5. AUTHOR(S) (First name, middle initial, last name)  C. E. Lapple      D. E. Blake      G. L. Pressman			
6. REPORT DATE April 1967		7a. TOTAL NO. OF PAGES 146	7b. NO. OF REFS 4
8a. CONTRACT OR GRANT NO. DA-18-035-AMC-122(A)		8a. ORIGINATOR'S REPORT NUMBER(S) SPEC TR-11, PAU-4960	
b. PROJECT NO. Task 1B522301A08101			
c.		8b. OTHER REPORT NO(S) (Any other numbers that may be assigned this report) N/A	
d.			
10. DISTRIBUTION STATEMENT  This document is subject to special export control and each transmittal to a foreign government or foreign nationals may be made only with prior approval of the CO, Edgewood Arsenal, Attn: SMUEA-TS/I-T, Edgewood Arsenal, Maryland 21010			
11. SUPPLEMENTARY NOTES  Dissemination investigations of liquid and solid agents		12. SPONSORING MILITARY ACTIVITY  Edgewood Arsenal Research Laboratories Edgewood Arsenal, Maryland 21010	
13. ABSTRACT  A technique was developed for measuring electrical mobility distribution of an aerosol and average effective size at each mobility level. An aerosol is passed through a purifier and a narrow mobility channel. The purifier removes charged particles from all but a thin central stream that enters the mobility chamber halfway between electrodes. Particles are deposited on an insulating surface according to their mobility. Total charge distribution on the walls was determined by a special scanning probe, mass distribution was determined by chemical or colorimetric analysis. Tests to determine mobility distribution of a uranine aerosol generated by atomizing and evaporating a dilute water solution yielded fairly consistent results. Results were consistent with expected magnitudes; average particle diameter (volume-to-diameter mean) was 0.8 micron, and particle charge levels ranged from 0.05 to 1 volt/micron specific particle surface gradient. Remaining problem areas are listed and suggestions are given for improving the technique and extending its usefulness.			

DD FORM 1473 (PAGE 1)

1 NOV 66  
S/N 0101-807-6001

145

UNCLASSIFIED

Security Classification

14 KEY WORDS	LINK A		LINK B		LINK C	
	ROLE	WT	ROLE	WT	ROLE	WT
Evaluation Interrelationship Mean diameters Material balances Operating procedures Distribution data Aerosol characteristics Measurement techniques Aerosol charge analyzer Aerosol generation system Mobility channel system						